

**DEVELOPMENT OF CONDUCTIVE AND
BIODEGRADABLE NANOFIBROUS YARNS: STUDY
OF ELECTRICAL AND MECHANICAL PROPERTIES**

Puwakdandawe Vishakha Thilini Weerasinghe

(188058V)

Degree of Master of Science

Department of Textile and Clothing Technology

University of Moratuwa

Sri Lanka

January 2020

**DEVELOPMENT OF CONDUCTIVE AND
BIODEGRADABLE NANOFIBROUS YARNS: STUDY
OF ELECTRICAL AND MECHANICAL PROPERTIES**

Puwakdandawe Vishakha Thilini Weerasinghe

(188058V)

Thesis submitted in partial fulfillment of the requirements for the
degree Master of Science in Textile and Clothing Technology

Department of Textile and Clothing Technology

University of Moratuwa

Sri Lanka

January 2020

Declaration

“I declare that this is my own work and this thesis does not incorporate without acknowledgement any material previously submitted for a Degree or Diploma in any other University or institute of higher learning and to the best of my knowledge and belief it does not contain any material previously published or written by another person except where the acknowledgement is made in the text.

Also, I hereby grant to University of Moratuwa the non-exclusive right to reproduce and distribute my thesis, in whole or in part in print, electronic or other medium. I retain the right to use this content in whole or part in future works (such as articles or books).”

Signature:

Date:

“The above candidate has carried out research for the Master’s thesis under my supervision.”

Name of the supervisor:

Signature of supervisor:

Date:

Name of the supervisor:

Signature of supervisor:

Date:

Abstract

Electrically conductive and biodegradable materials are desired for a vast array of applications in wearable and flexible electronic areas to address the growing ecological problem of e-waste. Herein, we report on the design and fabrication of all-organic, conductive and biodegradable yarn using polyaniline (PANi) and polycaprolactone (PCL). The process of PANi incorporation is achieved in two ways; i) electrospinning a blend of PANi and PCL solution ii) in-situ polymerization of PANi on the nanofibrous surface of PCL electrospun fibers. The electrospun PANi incorporated webs are cut into ribbons and twisted to develop twisted yarns. A customized setup was used to produce continuous electrospun yarns. The effect of different degrees of PANi blended into PCL was investigated. Moreover, the effect of an array of aniline concentrations in coated fibers were studied. PCL/PANi blended solution with 2% PANi resulted in nanofibers with resistance of $10 \pm 4 \text{ M}\Omega/\text{cm}$. Fibers coated with 1% aniline concentration resulted in the core-shell fibers with of $50 \pm 8 \text{ k}\Omega/\text{cm}$. Increasing the number of plies of yarn to 3 plies resulted in a 3-fold reduction of the resistance. The twisted plied yarns were incorporated into fabric by stitching or weaving to demonstrate the stability of conductivity over mechanical forces. Both PANi blended and PANi coated yarns were found to be biodegradable in controlled environmental conditions. The use of PANi blended yarn as a biomaterial for tissue engineering and PANi coated yarns as a wearable electrode for capacitive sensors were demonstrated. The electromechanical behavior of PANi coated yarn is expected to provide inspiration for the production of highly sensitive strain sensors. This approach presents an early step on the way to the realization of all organic conductive biodegradable nanofibrous yarns for sustainable smart textiles.

Key words: Conductive polymers, nanofibrous yarns, biodegradable, electrospinning, polyaniline

Dedication

I dedicate my thesis to all my professors and doctors and scientists for the extensive knowledge you share with me. Your unselfish guidance increased my passion for nanotechnology.

Acknowledgement

I wish to acknowledge who supported me in numerous ways to achieve my MSc. First, I am indebted to research supervisor Dr. N.D. Wanasekara, Senior Lecturer, Department of Textile and Clothing Technology, University of Moratuwa for invaluable support, and motivation he readily gave me to accomplish this research. His patience in guiding me, vast knowledge, advice and experience helped me in many ways to conclude my research.

I would like to express appreciation thanks to Dr. (Mrs.) D.G.K. Dissanayake, Senior Lecturer, Department of Textile and Clothing Technology, University of Moratuwa, insightful comments and encouragement from the start to the very end of the days I worked on this thesis and also, magnanimous way of educating me to the world of scientific publication, are very much appreciated.

Besides my supervisors, I am also thankful towards my progress review committee: Dr. Srimala Perera and Dr. T.S.S. Jayawardena for their motivation comments and encouragement in each progress review to make my focus to the strategical research plan.

Also, I wish to express gratitude to Sri Lanka Institute of Nanotechnology (SLINTEC) to give access to advanced laboratory facilities and scientists, Miss. Nadeeka Tissera, Mr. Ruchira Wijesena and Prof. Nalin de Silva who assisted and supported me while dedicating their valuable time.

I also express my sincere gratitude to the academic and nonacademic staff of Department of Textile and Clothing Technology, University of Moratuwa for the continuous support and guidance given throughout my undergraduate and postgraduate life. Furthermore, I thank Nilupuli Rathnayake from the 15th batch and Sasini Weerasinghe from the 13th batch, Department of Textile and Clothing technology for all the support given to accomplish this research without any stress.

The financial support for this research was provided through the SRC Grant (SRC/LT/2018/ 33) offered by the Senate Research Council, University of Moratuwa.

I would like to extend my sincere thanks to SRC for identifying the value of this research and approving the requested budget for this research. I would like to acknowledge Dr. (Mrs.) D.G.K. Dissanayake for appointing me as a research student to conduct this research under the above SRC grant.

Last but not least, it is with a heart laden with gratitude that I thank to my family for the tremendous support given me and who were always there to lift me up during hard times.

Table of contents

	Page
Declaration of the candidate & supervisors	i
Abstract	ii
Dedication	iii
Acknowledgements	iv
Table of contents	vi
List of figures	x
List of tables	xv
List of abbreviations	xvi
List of appendices	
CHAPTER 01	xvii
1. INTRODUCTION	1
1.1 Introduction	1
1.2 Problem statement	2
1.3 Objectives	3
1.4 Chapter framework	
CHAPTER 02	
2. LITERATURE REVIEW	5
2.1 Introduction	5
2.2 Importance of conductive yarns	5
2.3 Problems of existing conductive yarn manufacturing methods	5
2.4 Conductive polymers	6
2.5 Doping of conductive polymers	8
2.6 Polyaniline	10
2.7 Nanofibrous yarns	11
2.8 Electrospinning	11
2.9 Electrospinning yarns	12
2.10 Electrospun conductive yarns	15
2.11 Importance of biodegradability in smart textiles	15
2.12 Biodegradable applications in smart textiles	16

2.13	Electrospinning of biodegradable polymers	16
2.14	Degradation of poly (ϵ -caprolactone)	17
2.15	Electrospinning of conductive biodegradable polymers	17
2.16	Electrospun conductive and biodegradable yarns	18
2.17	Summary	
CHAPTER 03		
3.	METHODOLOGY	20
3.1	Introduction	20
3.2	Materials and reagents	20
3.3	Selection of suitable carrier polymer	21
3.3.1	Preparation of PVA and PCL polymer solution	21
3.3.2	Conventional electrospinning	21
3.3.3	Analyzing fiber mats to select the biodegradable polymer	21
3.4	Preparation of PANi blended yarns	22
3.4.1	Preparation of PANi solution	22
3.4.2	Preparation of PANi/PCL casted films	22
3.4.3	Preparation of PANi/PCL solution	23
3.4.4	Electrospinning by using rotary collector	23
3.4.5	Yarn preparation from nanofibrous web	24
3.4.6	Design and development of collector attachment for production of continuous nanofiber yarns	25
3.4.7	Continuous yarn production by electrospinning	27
3.5	Preparation of PANi coated yarns	27
3.5.1	Dip coating of PANi	27
3.5.2	PANi in-situ polymerization	27
3.5.3	Preparation of twisted yarns	28
3.6	Characterization	28
3.6.1	Fiber Morphology	28
3.6.2	Conductivity measurement	29
3.6.3	Tensile strength	31
3.6.4	DSC Analysis	31
3.6.5	FTIR analysis	31

3.6.6	TGA analysis	31
3.6.7	Conductivity over mechanical deformation	31
3.6.8	Biodegradation of the material under controlled composting conditions	32
3.7	Applications	33
3.7.1	Capacitive sensor	33
3.7.2	Biomaterial	34
	3.7.2.1 Biodegradability	34
	3.7.2.2 Cell cytotoxicity study	35
	3.7.2.3 Cell morphology study	36
3.8	Summary	
CHAPTER 04		
4.	RESULTS AND DISCUSSION	37
4.1	Introduction	37
4.2	Electrospinning of PVA and PCL	37
4.3	PANi blended nanofibrous yarns	41
	4.3.1 Influence of conductivity on electrospinnability	41
	4.3.2 Conductivity measurement	45
	4.3.3 Nanofibrous yarn formation	46
	4.3.4 Continuous yarn formation	48
	4.3.5 Effect of PANi concentration on mechanical properties of yarns	49
	4.3.6 TGA analysis	51
	4.3.7 DSC analysis	53
	4.3.8 FTIR analysis	55
	4.3.9 Optimizing PANi concentration	56
	4.3.10 Electro-mechanical behaviour of electro-conductive yarn	56
	4.3.10.1 Effect of weaving and sewing on electrical resistance of the yarn	56
	4.3.10.2 Effect of strain on electrical resistance of the yarn	58
	4.3.10.3 Effect of twist on electrical resistance of the yarn	59
	4.3.11 Biodegradability	60

4.4	PANi coated nanofibrous yarns	64
4.4.1	Effect of dip coating on PANi on fiber morphology, electrical and mechanical properties	64
4.4.2	Studying PANi in-situ polymerization	65
4.4.2.1	Polymerization of aniline on PCL nanofibers	65
4.4.2.2	Effect of concentration of reaction mixture on fiber morphology	69
4.4.3	Conductivity measurement	71
4.4.4	Nanofibrous yarn formation	74
4.4.5	Effect of aniline concentration on mechanical properties of yarn	75
4.4.6	TGA analysis	77
4.4.7	DSC analysis	79
4.4.8	FTIR analysis	81
4.4.9	Electro-mechanical behaviour of electro-conductive yarn	83
4.4.9.1	Effect of weaving and sewing on electrical resistance of the yarn	83
4.4.9.2	Effect of tensile strain on electrical resistance of the yarn	86
4.4.9.3	Effect of twist on electrical resistance of the yarn	87
4.4.10	Biodegradability	88
4.5	Comparison of PANi blended and coated yarns and potential applications	91
4.5.1	Capacitive sensor	92
4.5.2	Biocompatibility	93
4.5.2.1	Cytotoxic effects of the PANi blended nanofibers	93
4.5.2.2	Cell morphology study	93
4.5.2.3	In-vitro degradability	94
4.6	Summary	96
CHAPTER 05		
5.	CONCLUSIONS AND RECOMMENDATIONS	97
5.1	Introduction	97

5.2	Key conclusions	97
5.3	Key recommendations	99
	Reference list	100
	Appendix A: Arduino code linked with cap sense library	113
	Appendix B: Publications on this study	114

List of figures

Figure	Description	Page
Figure 2.1	Energy band diagram demonstrating band gaps	8
Figure 2.2	Band structure of a conjugated polymer as a function of p-doping level	9
Figure 2.3	Oxidation states of PANi	11
Figure 2.4	Electrospinning basic setup	12
Figure 2.5	Electrospinning continuous yarns using one nozzle	14
Figure 2.6	Electrospinning continuous yarns using two nozzles	14
Figure 3.1	Designed schematic diagram of modified electrospinning unit with rotational drum collector	24
Figure 3.2	Designed schematic diagram of apparatus for twisting single yarns and ply yarn.	25
Figure 3.3	Designed schematic diagram of continuous yarn forming setup	26
Figure 3.4	Schematic diagram of test circuit for measuring resistance with the four-point probe method	29
Figure 3.5	Schematic diagram of test circuit for measuring resistance of fiber ribbons with the two-probe method using multimeter	30
Figure 3.6	Schematic diagram of test circuit for measuring resistance of the yarn with the two-probe using multimeter	30
Figure 3.7	Homemade apparatus for measuring resistance vs strain	32
Figure 3.8	Basic circuit for capacitive sensors	34
Figure 3.9	Well plate with cells that were treated with nanofibers	35
Figure 4.1	SEM image and diameter distribution histogram of (a) PCL nanofibers, (b) PVA nanofibers	38
Figure 4.2	Illustration of hydrogen bonding interaction among PVA by water	38
Figure 4.3	Solutions of (a) emeraldine base (EB) PANi/PCL, (b) emeraldine base (EB) PANi/CSA/PCL, (c) emeraldine salt (ES) PANi (PANi doped by HCl)/CSA/PCL	40

Figure 4.4	Casted films of (a) emeraldine base (EB) PANi/PCL, (b) emeraldine base (EB) PANi/CSA/PCL, (c) emeraldine salt (ES) PANi (PANi doped by HCl)/CSA/PCL	40
Figure 4.5	Demonstrating conductive nanofiber electrospinning process	42
Figure 4.6	A photo of the electrospinning step with rotational drum collector	42
Figure 4.7	Morphology of nanofibers synthesized from different PANi concentrations and PCL. (a) pure PCL, (b) PANi 0.5%, (c) PANi 1%, (d) PANi 2%, (e) PANi 3%	44
Figure 4.8	(a) The four probe V - I characteristics of PANi blended electrospun mats, (b) PANi concentration vs conductivity measured using four-probe method	45
Figure 4.9	PANi 2%(a) Twisting single yarns, (b) twisting ply yarns, (c) PCL/PANi 1-ply yarn, (d) PCL/PANi 2-ply yarn, (d) PCL/PANi 3-ply yarn	47
Figure 4.10	Effect of number of plies on resistance	48
Figure 4.11	(a) Developed continuous yarn manufacturing unit, (b) 3D fibrous cone and twisted yarn	49
Figure 4.12	(a) The stress–strain curves of Pure PCL, PANi 0.5%, PANi 1%, PANi 2%, (b) effect of PANi concentration on energy at break value of yarns, (c) effect of PANi concentration on modulus of yarns	51
Figure 4.13	TGA profiles of pure PCL and conductive PANi/PCL yarns with different PCL to PANI ratio	53
Figure 4.14	DSC profiles of pure PCL and conductive PANi/PCL yarns with different PCL to PANI ratio	54
Figure 4.15	FTIR spectra of pure PCL and PANi 2%	55
Figure 4.16	PCL/PANi 2% blended nanofibrous yarns. (a) Image of yarn stitched on a nylon fabric, (b) microscopic image of yarn stitched on the nylon fabric	57

Figure 4.17	Fabric woven with PANi 2% blended nanofibrous yarns and 2-ply nylon yarns. (a) Conductivity measuring of unfolded fabric, (b) conductivity measuring of folded fabric, (c) microscopic image the fabric, (d) demonstrating yarn short circuiting by folding, (e) illustrating resistance change by number of folding cycles	58
Figure 4.18	Effect of tensile strain on electrical resistance of PCL/PANi 2% blended yarn	59
Figure 4.19	PANi 2% nanofibrous fiber ribbons (a) as made, (b) twisted, (c) effect of twist on electrical resistance	60
Figure 4.20	Physical appearance of different stages of biodegradation of cellulose filter paper, PCL, PCL/PANi, and polyethylene	61
Figure 4.21	Residual weight percentages vs number of days in each stage of biodegradation	62
Figure 4.22	SEM images of (a) PCL before and (b) after degradation in soil and (c) magnified SEM image of after degradation in soil. (d) PCL/PANi blended fibers before and (e) after degradation in soil. (f) Magnified SEM image of after degradation in soil	63
Figure 4.23	(a and b) SEM image and its magnified image of 10% PANi dip coated PCL nanofibers. (c) Stress- strain curve of PCL pure and PANi 10% dip coated nanofibrous yarns	64
Figure 4.24	(a) Schematic of the apparatus for producing of continuous PCL twisted yarns. (a') The 3D nanofibrous cone drawing from collector. (b and c) SEM image of collected PCL nanofibrous twisted yarn and magnified image of aligned nanofibers	66
Figure 4.25	Sketch illustration of Fabrication of PANi decorated PCL nano-fibrous yarns	66
Figure 4.26	Color change of aniline reaction mixture by adding APS after (a) 60 s, (b) 90 s, (c) 120 s, (d) 150 s, (e) 180 s, (f) 220 s, (g) 260 s, (h) 10 min.	68
Figure 4.27	SEM images of (a) Pure PCL, (b) aniline 0.5%, (c) aniline 1% (d) aniline 2%	70

Figure 4.28	Resistance per unit length verses used aniline concentration in reaction mixture	71
Figure 4.29	(a) The four probe V - I characteristics of PANi coated electrospun mats, (b) aniline concentration vs log value of conductivity measured from four probe	73
Figure 4.30	SEM images of (a) 1- ply yarn, (b) 2 – ply yarn and (c) 3 – ply yarn	74
Figure 4.31	Effect of number of plies on resistance	75
Figure 4.32	(a) The stress–strain curves of Pure PCL, aniline 0.5%, aniline 1%, aniline 2%, (b) effect of aniline concentration on energy at break value of yarns, (c) effect of aniline concentration on modulus of yarns	77
Figure 4.33	TGA profiles of pure PCL, aniline 0.5%, aniline 1%, aniline 2%	79
Figure 4.34	DSC profiles of pure PCL, aniline 0.5%, aniline 1%, aniline 2%	80
Figure 4.35	FTIR spectra of pure PCL and aniline 1%	81
Figure 4.36	Aniline 1 % coated nanofibrous yarns. (a) Image of yarn stitched on a nylon fabric, (b) microscopic image of yarn stitched on the nylon fabric	83
Figure 4.37	Fabric woven with aniline 1% coated nanofibrous yarns and 2-ply nylon yarns. (a) Conductivity measuring of unfolded fabric, (b) conductivity measuring of folded fabric, (c) microscopic image the fabric, (d) SEM image of the fabric (e) demonstrating yarn short circuiting by folding, (f) illustrating resistance change by number of folding cycles	85
Figure 4.38	Effect of tensile strain on electrical resistance of yarn	86
Figure 4.39	Time-dependent normalized resistance change of the yarn under maximum strains of 20%	87
Figure 4.40	Aniline 1 % nanofibrous fiber ribbons (a) as made, (b) twisted, (c) effect of twist on electrical resistance	88
Figure 4.41	Residual weight percentage versus number of days in each stage of biodegradation	89
Figure 4.42	Physical appearance of different stages of biodegradation of cellulose filter paper, PCL, PCL/PANi and polyethylene	89

Figure 4.43	SEM images of PCL nanofiber (a) before degradation and (b-c) after degradation in soil. PANi/PCL nanofibers (d) before degradation and (e-f) after degradation in soil	90
Figure 4.44	Illustration of the electrical conductivity nature for the prepared PANi coated PANi /PCL yarns with application of flexible capacitive sensor for operation of LED (a) ON (c) OFF by touching	92
Figure 4.45	In-vitro cytotoxicity effects of the PCL and PANi/PCL electrospun nanofibers on Vero cells (green monkey kidney)	93
Figure 4.46	SEM images of (a) Vero cells seeded PCL nanofibers and (b) PCL/PANi nanofibers	94
Figure 4.47	Degradation profile of the PCL, and PANi blended PCL electrospun nanofibers	95
Figure 4.48	SEM images of the (a) PANi/PCL electrospun nanofibers after 20 days soaking in PBS and (b) magnified SEM image	95

List of tables

Table	Description	Page
Table 3.1	The weight of PCL and PANi taken for preparing solutions and volume ratios of each solution in solution mixture	23
Table 3.2	Amounts of anile and APS taken for solution mixture	28
Table 4.1	Effect of different dopant on electrospinnability and resistance	41
Table 4.2	Measuring resistivity by different methods	46
Table 4.3	TGA data compilation for the tested fibers, including the first peak weight loss attributed to HCL, second onset and weight loss attributed to PANi, third onset and weight loss attributed to PCL and residual weight	52
Table 4.4	Melting temperature and melting enthalpy of pure PCL and conductive PANi/PCL yarns with different PCL to PANI ratio	54
Table 4.5	Characterization peaks of PCL and PANi 2%	55
Table 4.6	Volume of aniline in aniline/HCl mixture and the weight of APS in APS/HCl mixture	66
Table 4.7	Measuring resistivity by different methods	73
Table 4.8	TGA data compilation for the tested fibers, including weight loss attributed to HCL and water, second third onset and weight loss attributed to PCL and residual weight	88
Table 4.9	Melting temperature and melting enthalpy of pure PCL, aniline 0.5%, aniline 1%, aniline 2%	81
Table 4.10	Characterization peaks of PCL and PANi 2% for aniline 1% nanofibers	82
Table 5.1	Summary of important results of the study	98

List of abbreviations

Abbreviation Description

PANi	Polyaniline
PCL	Polycaprolactone
CBNY	Conductive and biodegradable nanofibrous yarn
NY	Nanofiber yarn
SEM	Scanning electron microscope
FTIR	Fourier transform infrared
DSC	Differential scanning calorimetry
TGA	Thermogravimetric
PBS	Phosphate-buffered saline
ASTM	American Society for Testing and Material

List of appendices

Appendix	Description	Page
Appendix A	Arduino code linked with cap sense library	113
Appendix B	Publications on this study	114

CHAPTER 01

1. INTRODUCTION

1.1 Introduction

Smart textiles have attracted great fascinate in an array of fields such as healthcare, public safety, military, space exploration, consumer fitness, and sport. Antennas [1], sensors [2] and electromagnetic interference (EMI) shielding devices [3] are developed on textile surfaces to achieve smartness. Nowadays, most commercial applications of smart textiles are fabricated by integrating rigid conventional electronic hardware units into clothes. However, these devices limit the most essential and desired properties of textiles such as comfortability, flexibility, and lightweight. Therefore, the field of wearable electronics is being revolutionized by integrating electronic functionalities directly onto fabrics, yarns or fibers. Conductive yarn is an important component of electronic-textiles which can be utilized in the form 3D or 2D electronic devices as electrodes or connectors by weaving and/or knitting. Generally, conductive yarns are manufactured by embedding or coating conductive components such as carbon, silver, gold, nickel, copper, and conductive polymers.

Yarn properties can be considerably increased with the reduction of fiber diameter, and therefore, nanofibers are a promising approach to produce continuous yarns. Among the several methods of manufacturing nanofibers, such as self-assembly, electrospinning, thermal-induced phase separation and template synthesis, electrospinning is the most trending method with the feasibility of mass production of continuous nanofibers from different polymers, and the ability to control the fiber diameter to produce ultrathin nonaligned or aligned fiber webs [4, 5]. Different types of fiber assemblies such as thin films and continuous electrospun yarns have been prepared from electrospinning by changing the parameters and modifying the electrospinning setup.

Biodegradable polymers are widely employed as biomaterials in medical devices for applications including tissue scaffolds and carriers for controlling drug delivery. Furthermore, biodegradable polymers can be implicated in areas such as consumer

electronics and environmental sensors. Since the lifetime of electronic is becoming shorter, the use of biodegradable conductive materials consisting of biodegradable polymers would be a solution for the global issue of rising electronic waste (E-waste). Therefore, it is important to develop nanofibrous conductive yarns that are biodegradable and investigate mechanical and electronic properties of such yarns.

1.2 Problem statement

Although polymers like nylon and para-aramids are very strong, they are electrically insulating and non-conductive. The manufacturing methods for conductive yarns and fabrics used in the industry today are based on applying a conductive coating/printing, incorporating metallic wires as conductors twisted into a yarn and use metalized fibers or incorporate metal nanoparticles. Even though these composite yarns have superior conductivity, there are some drawbacks due to chemical corrosion, sloughing of deposition, stiff-feeling and easy decay [6]. Therefore, the use of conductive polymers is one of the best solutions for producing conductive yarns for E-textiles. Conductive polymeric yarns can be developed to withstand stretch-recovery, handle and drape and have properties close to those of conventional textiles.

Although e-textiles provide an excellent prospect as an emerging technology, it may lead to harmful environmental impacts. One of the major concerns is the disposal of e-textiles at the end of the useful lifetime. Most likely, problems may occur at the end of life (disposal and recycling) when environmental concerns are not taken into consideration during designing, development and mass production stages. Thus, using biodegradable polymers could eliminate waste streams and practical difficulties associated with disposal, reuse and recycle.

Although some published researches provide evidences of conductive nanofibrous yarns [7, 8] and, conductive and biodegradable nanofibrous mats [9], there are hardly accessible literature regarding the conductive and biodegradable nanofibrous yarn (CBNY). Nevertheless, it is increasingly becoming important to develop a conductive and biodegradable nanofibrous yarn for biomedical applications as well as e-textile applications and discover the mechanical and electrical properties of such yarns.

This study aimed at developing conductive and biodegradable nanofibrous yarn by electrospinning method. The developed yarns were comprehensively characterized to investigate and evaluate the mechanical and conductive properties.

1.3 Objectives

The main objectives of the research are as follows,

- To identify a method to develop a conductive and biodegradable polymer solution, which is electrospinnable.
- To investigate parameters which could influence the transformation of polymer solution into nanofibers through electrospinning.
- To establish a method to develop a nanofibrous yarn.
- To evaluate electrical and mechanical properties of developed yarn.

1.4 Chapter framework

This thesis comprised of five chapters in total, describing the research study in detail. In this introductory chapter the significance of the research, summary of the background, research problem and objectives were discussed.

Chapter 2 identifies and appraises the literature in understanding existing conductive textiles and limitations, conductive polymers and electrospinning, the importance of biodegradability in e-textiles. This chapter further identifies existing conductive and biodegradable composites and their applications, and research gap between existing reported studies and the study reported in this thesis.

Chapter 3 is dedicated to describe the research methodology in detail. The research methodology consists of both quantitative and qualitative studies. The experimental plan was divided into three major parts for polyaniline blended yarns, polyaniline coated yarns and their applications.

Chapter 4 of the thesis discusses the corresponding research results. This chapter was divided into four major parts to discuss, selecting polymers, polyaniline blended yarns, polyaniline coated yarns and, comparison of two types of yarns along with end applications.

Chapter 5 discussed the conclusions and recommendations of the research, derived from results and discussion in Chapter 4.

CHAPTER 02

2. LITERATURE REVIEW

2.1 Introduction

This chapter reviews published literature related to the existing conductive yarns and conductive polymers. Then, properties of nanofibers, basics of electrospinning and electrospinning of conductive yarns are discussed. Further, biodegradability aspect in smart textiles and conductive biodegradable nanofibrous applications are explored. Finally, PANi (polyaniline) and PCL (Polycaprolactone) as materials to develop conductive biodegradable yarns is reviewed.

2.2 Importance of conductive yarns

At present, innovations in textile field are more extensive and go beyond the applications of conventional textiles. Among them, conductive textiles have acquired a great attraction by demonstrating potential applications such as detectors and sensors, electro-energy, tissue engineering, and drug delivery and textiles for construction, mining, electronic, and automotive industries [10, 11]. Conductive yarns have been utilized for connecting circuits and embroidering circuits in wearable electronics [12]. The possibility of introducing conductive electrodes by weaving and knitting conductive yarns has been explored for home healthcare and long-term monitoring [13]. Moreover, scaffolds for tissue engineering applications have been produced by knitted conductive yarns [14].

2.3 Problems of existing conductive yarn manufacturing methods

The manufacturing methods for conductive yarns and fabrics used in the industry today are based on applying a conductive coating/printing, incorporating metallic wires as conductors twisted into a yarn, and use of inherently conductive polymers or metalized fibers [11]. These conductive materials which are used as hosts for electronic components in textile applications should not only be flexible but also comfortable since it is in close contact with the human body [15].

The problems of metal wires are low elasticity and low strain-at-break values [16]. Metal coated fibers and fabrics are less durable, can be cracked or corroded easily [7]. Therefore they are susceptible to a change in resistance, when it is subjected to stress and deformation due to body movements [17]. Integrated microdevice is one of the new domains, springing up from flexible electronics [18, 19], but the comfort problems emerge as wires and hard materials inside the clothing result in rigidity. Furthermore, the desirable properties of the yarn may be lost owing to yarn bending and straining during knitting and weaving by commercial knitting and weaving machines, which may lead to device failure [20].

Diverse methods have been utilized to produce a metallic layer on the surface of the fabric using electric plating, chemical electroless-plating, sputtering, chemical vapor deposition(CVD) and physical vapor deposition(PVD) [21]. The electroplating processes are not appropriate for non-conductive textile materials, since they require a conductive substrate. Nevertheless, CVD and sputtering methods require high temperature treatment, where textiles are impossible to withstand [22]. Moreover, PVD processes require huge energy and high vacuum conditions, which are of high cost [23]. Among various processes, electroless-plating is a versatile process, because it provides a uniform coating, low cost and can be applied over non-conductive substrate. Copper, Nickel, Silver, and other conductive metals make textile surfaces electrically conductive by electroless plating. The metal was deposited on the substrate without passing electric current [24].

2.4 Conductive polymers

The use of conductive polymers is one of the possible solutions for problems mentioned above, because low strength, processability, and poor flexibility can be overcome by using conductive polymer on textile substrates [26]. Conductive polymers are also a component of the new generation of “smart” biomaterials which can deliver stimulation to cells through electrical signals [27]. Thus, it will innovated the world of tissue engineering with its tremendous properties which are high conductivity/weight ratio, biocompatibility, biodegradability, and porous [28-31]. Poyacetylene (PA), Polyaniline (PANi), Polypyrrole (PPy), Polythiophene (PTs), Poly

(3, 4 – ethylene – dioxythiophene, PEDOT), Poly (phenyl vinylene, PPV) are examples for conductive polymers [32].

Pure conductive polymers show conductivity levels in between metals and semiconductors (10^{-5} S cm^{-1}). However, doped polymers display conductivity in between 100 – 10^5 S cm^{-1} [25-27]. Therefore, conductive polymers exhibit performance that can be a substitute for both metallic conductors and semiconductors [28].

The band gap between insulators, conductors, and semiconductors is demonstrated in Figure 2.1. Most conventional polymers consist full valence bands and empty conduction bands. These two types of bands are differentiated from each other by a wide energy gap. Nevertheless, conjugated polymers have narrow band gaps between conduction and valence bands which lead to better conductivity. Moreover, structural aspects of a linear π -conjugated system. The alternation of bond length, chain length, planarity, and the existence of electron donor or electron-acceptor and the resonance stabilization energy of the aromatic cycles affect the HOMO–LUMO gap (band gap). Similarly, as in the doping of semiconductors, doping of conductive polymers can vary their band structures by adding electrons to the conduction band (n-doping) or taking electrons from the valence band (p-doping) [29-31].

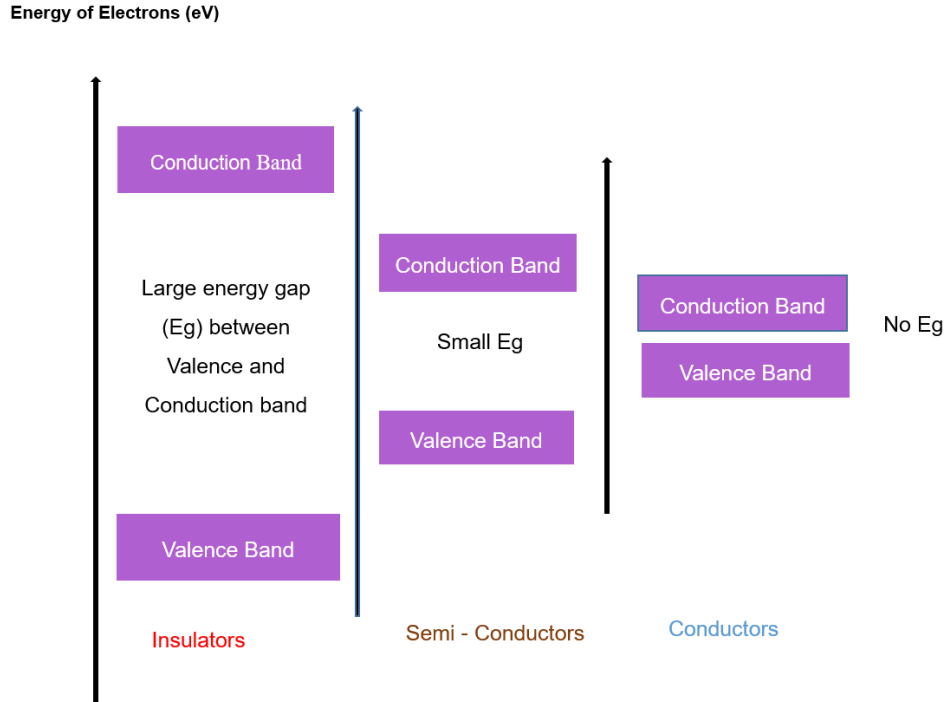


Figure 2.1: Energy band diagram demonstrating band gaps [32]

2.5 Doping of conductive polymers

The added and removed electrons in the polymer chain are delocalized as polarons, bipolarons or solitons as shown in Figure 2.2. The polaron is formed by removing an electron from the top of the valence band of a conjugated polymer resulting in a partially filled radical cation. In the opposite way, radical anion polaron is created by the addition of an electron to the bottom of the conductive band. The creation of polaron causes the reduction of the band gap between conduction and valence. A polaron carries both spin ($1/2$) and charge (+). Absence of a second electron from a chain already having a polaron result in the formation of a bipolaron (spinless, charge = ++) [35, 39, 40].

Another charge defect is the soliton. Three types of solitons are available as neutral soliton, positive soliton, and negative soliton. However, solitons do not form in conjugated polymers such as polythiophene, polypyrrole, and PANi that have non-degenerate ground states [39-42].

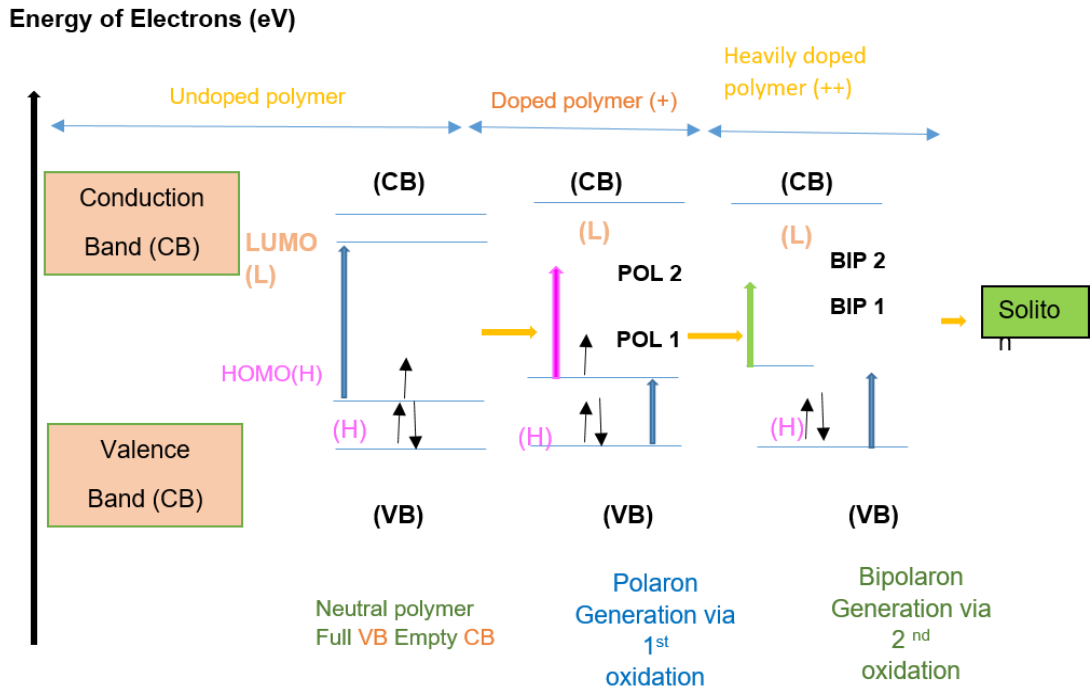


Figure 2.2: Band structure of a conjugate polymer as a function of p-doping level [33]

When electrical potential is implemented, the dopants start disrupting the stable backbone by moving in or out of the polymer (depending on the polarity). This facilitates passing the charge through the polymer chain [34-36].

Therefore, in the doping process of a polymer, charge carriers (polarons and bipolarons) are introduced to yield conductivity [37, 38]. As in the same way in semiconductor, polymer chain can be positively charged by p-doping and negatively charged by n-doping by oxidizing and reducing the polymer, respectively [37, 39-41].

The conductivity of the dopant and the amount of dopant used are in a proportional relationship [42]. The conductivity further is affected by the dopant type. However, this changes the bulk structural and surface properties (e.g. porosity, volume, color and tensile strength) of the polymer [38, 41, 43-45]. Dopants can be divided into two categories on the basis of the molecular size which are large dopants (e.g. sodium polystyrene sulfonate (PSS), Camphor Sulfonic Acid (CSA)) and small dopants (e.g. H^+ , Cl^-) [37, 38, 46, 47]. Large dopants are more interacted with the polymer backbone and will not de-dope with time and provides greater electrochemical stability [46-48].

On the other hand, small dopants exhibit cycling between doping and de-doping by re-entering and leaving the dopant granting the basis of the drug release applications [38, 49].

2.6 Polyaniline

PANi is a mixed oxidation state polymer (Figure 2.3) consisting of reduced benzoid units and oxidized quinoid units. These 2 units can be converted into each other by a redox reaction. Based on the oxidation stage PANi has different forms. The fully oxidized form is pernigraniline base, the half-oxidized form is emeraldine base and the fully reduced state is leucoemeraldine base. Among them, emeraldine, is the most stable and conductive [47, 49]. The polymer chain of PANi contains strongly localized σ -bond and less strongly localized p -bond [58]. The overlapped p -orbitals are allowing the electrons to be more easily delocalized and move freely between the atoms [51, 55, 60, 61]. Organic (CSA) or non-organic (hydrochloric, HCl) acids are used as a final key to the [50, 51, 56] doping.

PANI has many positive impacts such as environmental stability, low cost, ease of synthesis, and the ability to be electrically switched between its resistive and conductive states [27, 50, 62-64]. However, its utilization in biological applications is bound by its lack of flexibility, low processibility, and non-biodegradability, also can cause chronic inflammation during implantation [62, 65, 66]. PANI has been investigated for neural probes, biosensors, tissue engineering applications and controlled drug delivery [56]. Some of these applications are based on PANi integrated yarns. For instance, PANi in-situ polymerized conductive yarns from ultra-high molecular weight polyethylene (UHMWPE) [67] and PANi coated polyethylene terephthalate (PET) [7] were reported.

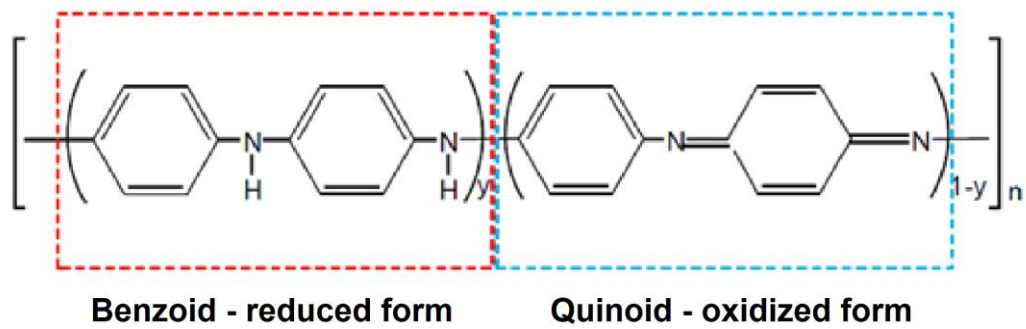


Figure 2.3: Oxidation states of PANi [50]

2.7 Nanofibrous yarns

Although conductive polymeric fibers can be prepared in microscale, particular interest towards nanofibrous systems has been drawn due to transport and structural properties of nanofibre membranes. Due to its porous structure nanofiber mats have the capability of trapping airborne particles and also can be used as a highly efficient filter, because the surface area of fibers is greatly increased when it is converted from solid materials to nanofibers [69]. Likewise, properties can be considerably increased with the reduction of fiber diameter, therefore nanofibers are an attractive approach to produce continuous yarns [70]. Numerous methods have been used to produce polymer nanofibers for example self-assembly, phase separation, bacterial cellulose, templating, drawing, extraction, vapor phase polymerization, kinetically controlled electrospinning [8].

2.8 Electrospinning

Among all methods of engineering nanofibers, electrospinning is one of the most versatile methods. An array of different types of fiber assemblies has been made from electrospinning by varying the parameters and processes. An array of products can be produced with great performance and results in different types of fiber assembly applications. These fiber assemblies include aligned fiber mats, nonwoven fiber mesh, patterned fiber mesh, sub-micron spring, random three-dimensional structures and convoluted fiber [51]. Electrospinning can be known as one of the most flexible

processes to produce continuous nanofibers from a wide range of materials. The electrospinning was first performed in 1990s, the first patent of the electrospinning was filed by John Francis Cooley with the concept of inventing an apparatus for dispersing a fluid electrically [52]. Then it was upgraded up to a novel electrospinning apparatus. The simplest electrospinning unit includes a syringe pump with solution storage and feeding systems, a syringe with a metal needle as the spinneret, a metal plate collector and high voltage DC power supply [53] as shown in Figure 2.4.

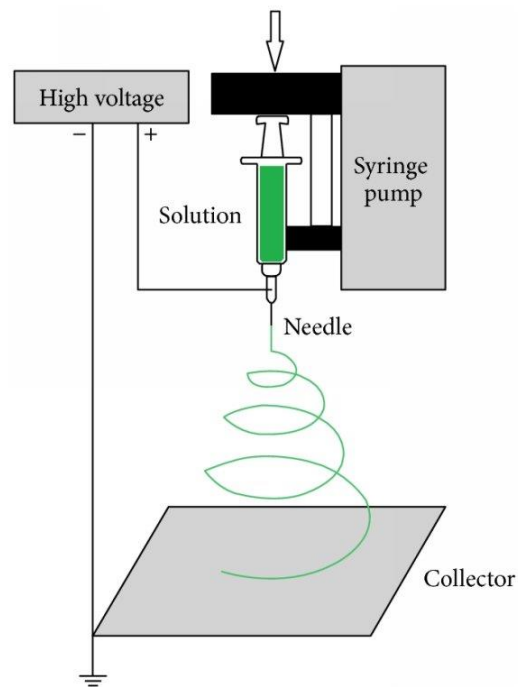


Figure 2.4: Electrospinning basic setup [73]

2.9 Electrospinning yarns

The basic set up of electrospinning produces a fiber mat with randomly oriented fibers [70, 74], but challenges do occur in its weakness in mechanical properties during handling in applications such as bio-scaffolds. A complicated fibrous architecture can be built, by interlocking the fibers in the bundle which are the basic building blocks of yarn and also helps to improve mechanical properties. Several examples exist in the literature where functional nanofibrous yarns have been produced utilizing electrospinning as a tool. Nanofibrous yarns have been manufactured by cutting and strip twisting non-aligned or aligned Polyvinylidene fluoride (PVDF) electrospun

nanofibrous stripes because of the easy control toward fibrous orientation, twist level and fiber uniformity [75, 76]. Aligned nanofiber webs have been produced by altering a collector to a rotating drum or a frame or a pair of split electrodes [74].

Recently, significant efforts have been taken to prepare short twisted bundles or twisted continuous yarns. To prepare a yarn, giving a twist to the nanofiber bundle around the longitudinal axis of the yarn is essential, in addition to the spinning process. However, by utilizing different mechanical collection devices and/or the deliberate manipulation of the electric field, a moving collector or spinneret systems, processing parameters, one can collect non-continuous nanofiber bundles or twisted yarns rather than mats [77]. Several methods have been reported to produce direct continuous yarns. Manipulation of the electric field has been employed to redirect the deposited nanofibrous to a winding roller [78], collecting nanofibrous into the water reservoir and drawn to form a yarn [79]. Producing continuous twisted yarn from well-aligned nanofibers by using water vortex [6]. Another method utilizes needles placed face-to-face. Positively and negatively charged fibers are attracted and discharged. Accumulated fiber bundle should be pulled up by the take-up roller for winding, but fibers were not aligned [5, 80].

Recently, a novel setup has been introduced to produce aligned continuous nanofibers twisted yarn as shown in Figure 2.5. The collecting system was replaced by a slowly rotating funnel. The electrically grounded funnel was set up as open-on-top, fibers are assembled on an intermediate funnel mouth plane forming a web. The web was drawn by the winding roller right up to the funnel to make fibers align with each other and reduce the average diameter of the yarn. Twisting was imparted due to the rotation of the funnel [54].

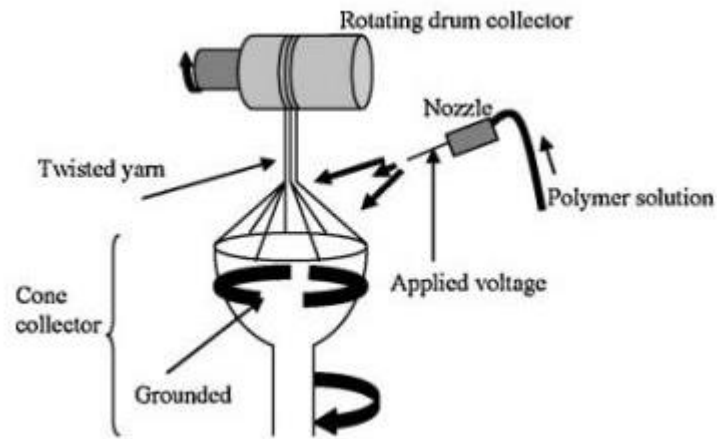


Figure 2.5: Electrospinning continuous yarns using one nozzle [54]

Differently charged nozzles could also be used to eject a polymer solution from two directions on to the open plane of the funnel to create a hollow nanofibers cone [55] as shown in Figure 2.6. The method is efficient than the previously mentioned [54, 56]. The twist can be controlled by the rotation of the funnel and winding roller in both methods.

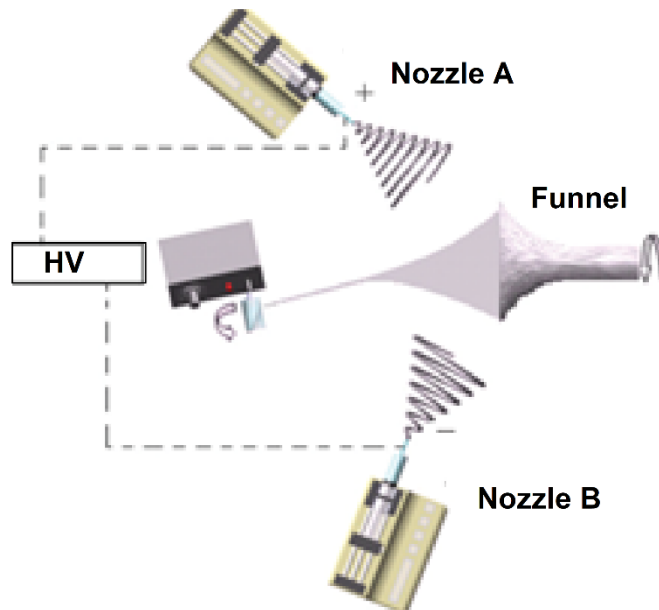


Figure 2.6: Electrospinning continuous yarns using two nozzles [55]

2.10 Electrospinning continuous conductive yarns

Remarkable progress in nanofibrous yarns with various features has been reported. Smart fabric finishes by nanofibrous twisted yarn were prepared to have functionalities such as piezoelectricity, electrical conductivity, enhanced fluorescence [57]. Superparamagnetic nanofiber yarns were prepared by using polymers with iron oxide [58], and core-shell structured carbon nanofibrous yarn with polypyrrole and graphene [59].

Polyacrylonitrile (PAN) was mixed with different graphene ratios to prepare nanofibrous yarns [60]. PAN was doped by single-walled carbon nanotubes to prepare a conductive nanofibrous yarn [61]. PANI/PAN uniaxially aligned coaxial nanofiber yarns were produced for smart wearable sensors [62].

2.11 Importance of biodegradability in smart textiles

One of the ways to accomplish sustainable development is sustainable production, which can be described as using a system to manufacture product and services that will not pollute the environment. This can be achieved by optimizing energy and material that are used for production, packaging, and transport by developing materials with durable, reuse, repairable and biodegradable properties [88].

Nowadays, the usage of fabrics goes beyond the purpose of using conventional fabrics, therefore it has multifunctional purposes such as environmental protection, fashion, chemical flame protection, and other functional properties. Smartness is the quick response to an external stimulus such as thermal, mechanical, magnetic and chemical [89]. E-textile innovations are enabling technologies incorporated with electronic integrated textile materials based components such as sensors, actuators, embroidered, woven or printed circuits [90, 91]. Although e-textiles provide smart prospect as an emerging technology, on the flip side, it may prompt a harmful environmental impact [92]. One of the major concerns is the disposal of e-textiles at the end of the useful lifetime. It reveals that there may be problems in disposal and recycling if it is designed, developed and mass-produced without considering the end of life fate. E-textiles and other electronic devices with similar properties have affected the global

issue of electronic waste (E-waste) [93]. E-waste usually consists of various harmful substances which can be harmful to both the environment and human beings. Moreover, e-waste consists of non-renewable materials such as rare earth elements and precious metals which can result in large environmental footprint.

Electronic fibers, yarns, bonding, contacting elements and electronically active textile materials are manufactured by coating or plating metals such as silver, copper, stainless steel and gold [18, 94]. Silver-coated nylon yarns used as sensors for wearable electrocardiogram monitors [95]. PEDOT coated polypropylene fibers, metallic nanolayers with lithium fluoride/aluminum were reported [96]. The polymers which reported have problems in disposal due to non-biodegradability. Waste prevention in the design stage is an initial strategy than recycling or end of life treatments [97]. Therefore one of the solutions to prevent the adverse impact of e-waste by e-textiles is utilizing biodegradable materials as taking precaution during the designing stage.

2.12 Biodegradable applications in smart textiles

Biodegradable materials and their applications are widely discussed in the literature. Thermoresponsive hydrogel coated nonwoven material was fabricated for skin application using biodegradable materials poly (ϵ -caprolactone) (PCL) with hexamethylene diisocyanate (HMDI) and poly (ethylene glycol) (PEG) to keep topical skin area breathable, clean and comfortable [63]. Biodegradable elastic shape memory polymers are used for medical applications such as wound closure which can be loosely sewing and tightening with the temperature rising [64]. Chitosan, graphene, and glucose oxide sensors are reported to detect glucose [65]. Also chitosan-based sensor applications are reported to be used as a heavy metal iron sensors, urea sensors, and humidity sensors. Biodegradability is found to be an essential factor for the applications such as drug delivery systems, surgical structure, and implants, porous scaffolds for tissue engineering, surgical structures and implants [66].

2.13 Electrospinning of biodegradable polymers

Electrospun fiber carriers were prepared for drug delivery from electrospun poly (ethylene-co-vinyl acetate), poly (lactic acid), PDLLA electrospun fibers containing

Mefoxin [67]. Non-woven poly (ϵ -caprolactone) (PCL), microporous scaffolds were prepared by electrospun fibers. Mesenchymal stem cells (MSCs) were cultured, expanded and seeded on PCL scaffolds of nanofibrous mat [68]. Polycaprolactone and ethyl ethylene phosphate (EEP) electrospun nanofibrous fibers were reported for the sustained release of proteins [69]. PVA and cellulose acetate were electrospun to synthesize blended electrospun fiber mats [70]. Biodegradable polyurethane can undergo enzymatic and hydraulic degradation in vivo and support the in-growth of cells [71].

Biodegradable electrospun nanofibrous yarns are also reported to be prepared as three dimensional (3D) macroporous scaffold from poly(L-lactic acid)/polycaprolactone (PLLA/PCL) aligned electrospun nanofibrous yarns for bone tissue engineering [72].

2.14 Degradation of poly (ϵ -caprolactone)

Polycaprolactone (PCL), a biodegradable synthetic aliphatic PCL synthesized from a petroleum-based monomer [73]. The melting point and glass transition temperature of PCL are 60 °C to 65 °C and -65 °C to -60 °C, respectively [74].

PCL has great potential in industry as a sustainable substitute for plastic. On the other hand, it is thermostable and biocompatible for use in medical applications including wound dressing, tissue engineering, and drug release [75, 76]. Degradation of PCL may take place in various ecosystems such as water, soil, and compost which caused by the action of aerobic and anaerobic microorganisms [77].

Most of the PCL-degrading fungi can be found in genera *Penicillium* and *Aspergillus* [78, 79], and most PCL-degrading bacteria are genus *Clostridium*, *Pseudomonas*, and *Streptomyces* [80-82]. The micro-organisms have ability to enzymatically degrade polymers into oligomers with low molecular weight, dimers and monomers acts as an influential tool for treatment and recycling of biodegradable wastes [83].

2.15 Electrospinning of conductive biodegradable polymers

Electrospinning is a comparatively simple and fruitful method to prepare nonwoven fiber mats with nanometer range diameters [84, 85]. Varieties of synthetic and natural

biodegradable porous nanofiber-based scaffolds have been electrospun for tissue engineering applications such as gelatin [86], chitosan [87], polylactide [88, 89] and other biomaterials [90, 91]. Many studies have introduced electrical signal can modulate cell differentiation, adhesion, and proliferation [92]. Conductive nanofibrous scaffolds construct a microenvironment that can regulate the behavior of cells [93]. Therefore conductive polymers containing electrospun nanofibers, such as polyaniline (PANi) [94] and polypyrrole (Ppy) [95], have attracted much attention as porous scaffolds for tissue engineering applications. The conductivity was achieved by in-situ polymerization of conductive polymers on non-conductive biodegradable fiber surfaces, blending conductive polymer with a non-conductive polymer to prepare electrospinnable solution or coating conductive polymer solution on non-conductive fiber surface [96, 97].

Poly (L-lactide-co- ϵ -caprolactone) (PLCL) is a product of combination PLA and PCL in different ratios. These two polymers are popular biodegradable polymers and dissolve in 1, 1, 1, 3, 3, 3-hexafluoro-2-propanol (HFIP) [98]. Ppy and PANi/Ppy were dissolved in HFIP and added to a mixture of PCL and gelatin to prepare membrane for cardiac tissue scaffolds [99]. Poly(3-hexylthiophene) (PHT) and Poly(lactide-co-glycolide) (PLGA) mixture was electrospun into aligned nanofibers which have the ability of proliferation and adhesion of Schwann cells and scaffold for neural regeneration [9]. Poly (lactic-co-glycolic acid) (PLGA) was dissolved in HFIP and electrospun to a fiber mat, then it was dipped in a Ppy solution and ultra-sonicated to make it saturate from Ppy [100]. PANi/PCL blend which was dissolved in HFIP is an example of conductive polymer blended biodegradable nanofibers [101]. Aniline pentamer used as a model of PANi and grafted on gelatin/PLLA nanofiber mat for bone tissue engineering [102].

2.16 Electrospun conductive and biodegradable yarns

There has been a little research conducted on integrating biodegradable polymers in conductive yarns. Conductive nanofiber yarns were synthesized from PCL/Carbon nanotubes/silk fibroin (SF) and woven into conductive nanofiber network. This was engineered into a 3D scaffold by mimicking Cardiac Anisotropy to cardiac tissue

regeneration. Although PCL was used to prepare nanofibers, the yarns were not claimed as biodegradable [14].

PCL/PANi /SF nanofiber yarn with a core-shell structure was synthesized to mimic the native skeletal muscle tissue. The nanofiber core yarn was covered by hydrogel shell, but this yarn was not reported as a conductive yarn and conductivity of the material was studied [103].

2.17 Summary

This chapter sought to review the literature that supports the immediate requirement for the development of conductive and biodegradable nanofibrous yarn, in order to realize the contributions and limitations of current research in this area. The literature study has allowed the development of an experimental framework to guide the studies.

Many researches have been reported about manufacturing conductive and biodegradable nanofibrous, but these composites were only studied as for biomedical applications in tissue engineering, drug delivery, etc. Moreover, still there is a requirement to study conductive and biodegradable nanofiber yarns not only for biomedical applications but also for consumer wearable electronics.

Most of the conductive nanofibrous electrospun yarns have been produced with the addition of conductive fillers such as metal oxides, CNT, graphene and etc. However, a conductive nanofibrous electrospun yarn has been reported rarely without addition of any fillers. Therefore, in this study PANi, an organic material was selected to dope the conductivity to the yarn which was mostly reported in conductive and biodegradable nanofibers.

Across the literature, PCL is a popular biodegradable polymer. Hence, it was selected in preparing PANi in-situ polymerized PANi/PCL nanofiber yarns and PANi/PCL blended nanofiber yarns.

CHAPTER 03

3. METHODOLOGY

3.1 Introduction

This chapter discusses the experimental work carried out for the synthesis and spinning of electrospun nanofibrous yarns. This research is aimed at the development of conductive and biodegradable nanofibrous yarn and investigating mechanical and electrical properties of the newly developed yarn. Objectives of the research are;

1. To identify a method to develop a conductive and biodegradable polymer solution which is electrospinnable.
2. To investigate parameters which could influence the transformation of polymer solution into nanofibers through electrospinning.
3. To establish a method to develop a nanofibrous yarn.
4. To evaluate electrical and mechanical properties of developed yarn.

To achieve these objectives a quantitative methods were followed. The experimental procedure followed in developing conductive and biodegradable nanofibrous yarns is explained in detail in the below sections;

3.2 Materials and reagents

Dimethylformamide (DMF, ACS reagent, $\geq 99.8\%$), chloroform (CHCl_3 , 99.8% purity), Aniline (ACS reagent, $\geq 99.5\%$) and polycaprolactone (PCL, average Mn 80,000), camphor sulfonic acid (CSA) were supplied from Sigma Aldrich. Ammonium persulphate (ammonium peroxydisulphate, APS) was purchased from Research-Lab Fine Chem Industries. hydrochloric acid (HCl, extrapure AR 37%) was purchased from Sisco Research Laboratories Pvt. HCl doped polyaniline (average Mw $>15,000$, 60 wt.% polyaniline on carbon black) and polyvinyl alcohol (PVA, Mw $\sim 130,000$, ign. residue $\leq 0.5\%$) were obtained by Sri Lankan Institute of Nanotechnology.

3.3 Selection of suitable carrier polymer

According to the literature, polyaniline is popular for producing conductive and biodegradable composites. Since it is difficult to electrospinning it alone, a carrier polymer should be utilized. Polycaprolactone (PCL) and polyvinyl alcohol (PVA) were selected as biodegradable carrier polymers. Both PCL and PVA were electrospun to identify feasible concentrations and parameters for electrospinning.

3.3.1 Preparation of PVA and PCL polymer solution

PVA and PCL were selected since they are feasible to electrospin easily and biodegradable. To obtain 10% (w/v) PVA solution, 0.5 g of PVA powder was dissolved in 5 ml of deionized water at 90 °C which was stirred on a hotplate for 1h until the solution became clear and uniform. To obtain 10% (w/v) PCL solution 0.5 g of PCL powder was dissolved in 4ml of CHCl₃ using indirect sonication (DAIHAN WUC, DIGITAL ULTRASONIC CLEANER) for 10 min and 1ml of DMF was added. Then the solution was mixed employing direct hand sonicator (Hielscher's Ultrasonic Tissue Homogenizers)) for 5min until the solution became clear and uniform.

3.3.2 Conventional electrospinning

PVA solution was loaded into a 20 mL syringe with a stainless steel needle of 18 gauge for electrospinning. The flow rate was set to 8 μ L/min, and the syringe diameter was set to 16 mm on the syringe pump (New Era Pump systems Inc., Farmingdale, NY). An aluminum foil was attached to the plane collector to assemble the fiber web. The voltage of the high voltage power supply unit was set as 24 kV DC power supply and the distance between the needle tip and the collector was 15 cm. The solution was electrospun for two hour and the fiber mat was peeled off from collector. PCL solution was also electrospun by using the same parameters except using a power supply of 23kV at 27 °C of temperature and 50% of relative humidity.

3.3.3 Analyzing fiber mats to select the biodegradable polymer

The surface morphology of obtained nanofibers of PVA and PCL was analyzed using field emission scanning electron microscope (FSEM), Hitachi SU6600 Analytical

Variable Pressure FE-SEM. Prior to SEM imaging, to make the sample surface conductive, the sample was coated with a gold layer (~1 nm) from Hitachi sputter coater device. PVA electrospun mats are water soluble. Although it can be made water insoluble by crosslinking, tensile and physical properties of the fiber mat can be changed due to bonding of polymer chains. On the other hand, moisture sensitivity and high water absorption rate of PVA, result in reduction in mechanical properties. Also, water absorption limits its applicability as a conductive material, hence the conductivity can be varied from moisture. In addition to these factors by considering fiber morphology and fiber diameter, PCL was selected as the carrier polymer which is commonly used as a biodegradable alternative for plastics.

3.4 Preparation of PANi blended yarns

3.4.1 Preparation of PANi solution

To dissolve PANi (emeraldine base) in DMF 10% (w/v), the solvent was heated up to 60 °C and the PANi was added, then the solution was sonicated by using a direct sonication probe for 15 min. To enhance the conductivity camphor sulfonic acid (CSA) was added (PANi: CSA=1:1) and sonicated for 5 min. Simultaneously, PANi (emeraldine base) was replaced with HCl doped PANi and the same procedure was used to obtain a homogeneous solution. The conductivity of PANi/PCL casted films prepared by both solutions was compared to select the most suitable solution with high conductivity.

3.4.2 Preparation of PANi/PCL casted films

Three solutions were prepared as PANi (emeraldine base), PANi (emeraldine base)/CSA, HCl doped PANi/CSA. Each solution were mixed with 4 ml of 10% (w/v) PCL solutions. Polymer solutions were casted on glass slides and heated at 150 °C. Then sheath resistance of the film was measured using the four-probe method using Keithley 2450 Source Meter SMU Instrument.

3.4.3 Preparation of PANi/PCL solution

PCL/PANi solutions were prepared by dissolving PCL in CHCl_3 and PANi in DMF and mixing them together. The two solutions were mixed as PCL: PANi = 4:1 in volume ratio. The solvent and material contents of PANi and PCL solutions are given in Table 3.1. The samples prepared by these solutions will be referred in the thesis by sample names in the table.

Table 3.1: The weight of PCL and PANi taken for preparing solutions and volume ratios of each solution in solution mixtures

Sample name	PCL weight in 4 ml CHCl_3 (g)	PANi weight in 1ml DMF (g)	Solution volume ratio(PCL: PANi)
PCL Pure	0.500	0.000	4:1
PANi 0.5%	0.475	0.025	4:1
PANi 1%	0.450	0.050	4:1
PANi 2%	0.400	0.100	4:1

3.4.4 Electrospinning by using rotary collector

The stationary collector used in the conventional spinning process is not compatible to spin highly conductive solutions. Therefore, the electrospinning setup was customized by replacing the collector by a rotational drum as shown in Figure 3.1. The drum covered by an aluminium foil (70 mm in height; outer diameter: 40 mm) was fitted horizontally by a steel rod to the motor. The motor (DC 24V MOTOR DME44B-133 D.C. 3600 RPM) was powered by a 0-12 V DC power supply unit. Arduino Pulse with modulator (PWM), L298N DUAL H-BRIDGE MOTOR17 CONTROLLER and potentiometer employed for controlling the speed of the motor. The rotation speed of the motor can be controlled to be in between 100-500 rpm. The electrically grounded drum was assembled as open-on-top, fibers are assembled from the ejected charged

polymer solution on the curved surface of the cylinder and forming a web. Instead, voltage and distance between needle and collector, other parameters of electrospinning set up were set as same as conventional electrospinning of PCL in section 3.3.2. The voltage of the DC power supply was 24 kV, the distance between the needle and collector was 10 cm, temperature was 27 °C and relative humidity was 50%.

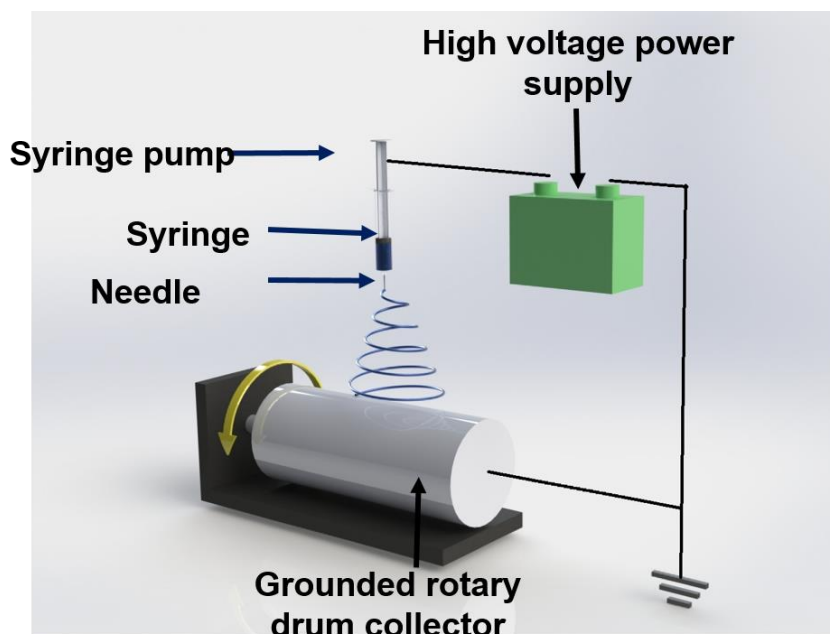


Figure 3.1: Designed schematic diagram of modified electrospinning unit with rotational drum collector

3.4.5 Yarn preparation from nanofibrous web

Prior to preparing the continuous nanofibrous yarn, twisted short-length yarns were prepared from twisting fiber bundles, and for that nanofiber mat was cut into stripes with dimensions of 5cm x 0.5cm. One end of the stripe was clipped to be stationary and the other end was rotated and clipped. A custom-made twisting device was prepared as in Figure 3.2. To obtain uniform yarn 30 S twist per inch was applied to a stripe. The self-twist principle was applied to make the yarn to achieve mechanical stability to avoid automatic untwisting. The simplest self-twist spinner gives S and S twist into each of the two strands as shown in Figure 3.2 (a). The two strands are then immediately converged and allowed to Z self-twist as shown in Figure 3.2 (b), the

twisted yarn exhibited 20 twists per inch, after which the self-twist yarn is wound onto a take-up package. Similarly, three single-ply yarns were twisted into 3-ply yarn by giving Z twist with 10 twists per inch.

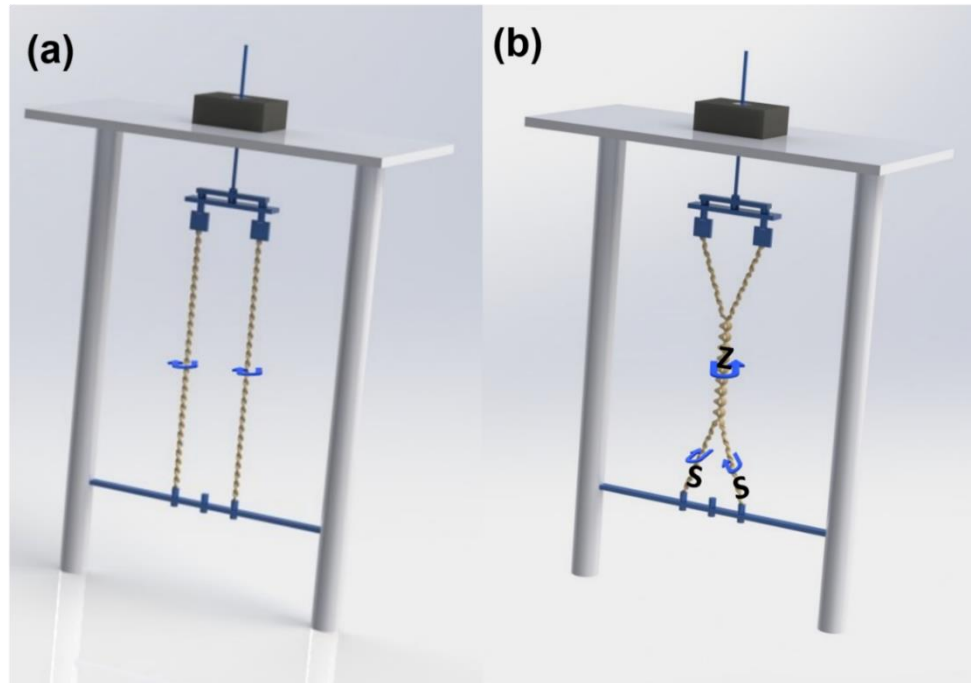


Figure 3.2: Designed schematic diagram apparatus of twisting single yarns and ply yarn.

3.4.6 Design and development of collector attachment for production of continuous

As the first step, a schematic diagram was designed as shown in Figure 3.3. The purpose of this is to build an attachment to the electrospinning unit to prepare nanofibrous yarns, which includes two syringe pumps, a stainless-steel funnel collector, and the winder as illustrated schematically in Figure 3.3. Two needles fitted with 20ml plastic syringes were fixed to two syringe pumps to inject the solution at a predefined flow rate. Two needle nozzles were connected to the two positive electrodes which were powered by DC high voltage power supply unit (MATSUDA Precision 0-30kV). The winding speed of the winder will be designed to be 2 rpm. The funnel collector (40 mm in length; outer diameter: 66 mm) was fitted horizontally by

a steel rod to the motor. The motor (DC 24V MOTOR DME44B- 133 D.C. 3600 RPM) was powered by 0-12V DC power supply unit. Arduino Pulse with modulator (PWM), L298N DUAL H-BRIDGE MOTOR CONTROLLER and potentiometer employed for controlling the speed of the motor. The rotation speed of the motor can be controlled to be between 100-500 rpm. The electrically grounded funnel was assembled as open-on-top, fibers are assembled from the ejected charged polymer solution on the funnel mouth plane and forming a web. Once the cone formed, a nanofibre yarn can be drawn to a winding roller utilizing a plastic rod. The web was drawn by the winding roller right up to the funnel to make fibers align with each other and reduce the average diameter of the yarn. Twisting is imparted from the rotation of the funnel.

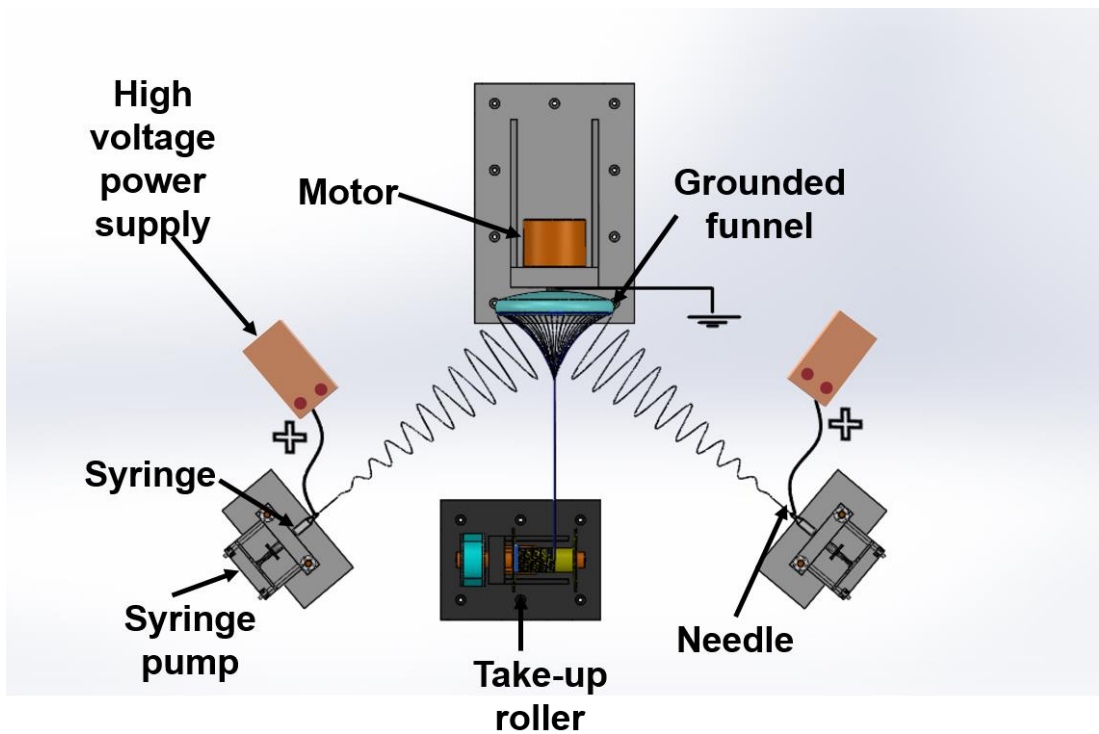


Figure 3.3: Designed schematic diagram of continuous yarn forming setup

3.4.7 Continuous yarn production by electrospinning

The developed electrospinning apparatus can be used for the fabrication of twisted continuous yarns. The setup was comprised of two oppositely charged nozzles injected by two syringe pumps at the rate of $8\mu\text{l}/\text{min}$ and 24kV of oppositely charged voltages were applied onto two needles which were angled 30° from middle axis between two

pumps. Temperature and relative humidity were kept as 27 °C and 50%, respectively. Accumulated fiber bundle can be pulled from a plastic rod. The horizontal distance was kept as 20 cm between two pumps, 15 cm distance was kept between the center of two pumps and the funnel. The solution was electrospun for ½ an hour to obtain 1 m of continuous yarn.

3.5 Preparation of PANi coated yarns

In this method, PANi/PCL conductive nanofibrous yarns were prepared by a two-step method. First, pure PCL was prepared as in section 3.3.1. In order to obtain align nanofibers, the solution was electrospun using the set up with a rotational drum collector demonstrated in Figure 3.1. The electrospinning parameters were set as same as section 3.4.3. Then the electrospun mat was peeled off and cut into ribbons.

3.5.1 Dip coating of PANi

The PCL nanofiber ribbons were wound into nylon mesh and dipped into different concentrations of HCl doped PANi/CSA solutions as in section 3.4.1. The solutions concentrations were taken as 10%, 20%, and 30% (w/v). The PCL nanofiber ribbons were dipped in the PANi solutions for 2 min with stirring. After removing from the PANi solution, the ribbons were mangled by passing it between pair of squeezing rollers. Then rinsed with distilled water to remove loosely bound PANI precipitate particles. Then the PANi coated fiber mats were dried at vacuum condition for 8 hrs.

3.5.2 PANi in-situ polymerization

The PCL nanofiber ribbons 0.1g was immersed in 50ml aniline/HCl solution and shaken the container using a mechanical shaker (Digital RJH5005 12-Stand Orbital Mechanical Shaker) with 100 rpm at room temperature for 30min. Next, 50 ml of $(\text{NH}_4)_2\text{S}_2\text{O}_8$ (APS)/HCl mixture was added dropwise and shaken in the same conditions for 30min. Initially, the ribbons were washed with HCl, deionized water, ethanol and dried in a vacuum oven at 30 °C for 4hours. APS and aniline were mixed to HCl as per in Table 3.2. The fiber mats and yarns coated with these reaction mixtures will be referred by sample names given in Table 3.2.

Table 3.2: Amounts of anile and APS taken for solution mixture

Sample name	Aniline volume per 50ml of HCl (μ l), concentration of HCL (M)	APS weight per 50ml of HCl (g), concentration of HCL (M)
0.5% aniline	250, 0.5	0.775, 0.5
1% aniline	500, 1.0	1.550, 1.0
2% aniline	1000, 2.0	3.100, 2.0

3.5.3 Preparation of twisted yarns

Twisted yarns were prepared from PANi in-situ polymerized conductive nanofibrous webs. The same apparatus used in Figure 3.2. 2-ply and 3-ply yarns were plied from single-ply yarn and characterized for conductive and mechanical properties.

In addition, continuous nanofibrous yarns were electrospun from modified electrospinning set up as shown in Figure 3.3. In order to achieve conductivity, these yarns were also decorated by in-situ polymerization of aniline

3.6 Characterization

All the produced nanofibrous mats and yarns were tested for the various material, mechanical and conductive properties. The properties tested were as follows.

3.6.1 Fiber morphology

The surface morphology of obtained nanofibers of different concentrations of PANi blended and PANi coated fiber mats and yarns were analyzed using field emission scanning electron microscope (FESEM), Hitachi SU6600 Analytical Variable Pressure FESEM. Prior to SEM imaging, to make the sample surface conductive, the sample was coated with a gold layer (\sim 1 nm) from Hitachi sputter coater device.

3.6.2 Conductivity measurement

The electrical properties of the electrospun nanofibers mats were measured on the four-point probe technique using Keithley 2456 Source Meter SMU Instrument (Tektronix, USA). The samples were prepared with dimensions of $2 \times 2 \text{ cm}^2$ were conditioned in $35 \pm 5\%$ relative humidity and $25 \pm 1^\circ\text{C}$ for 24hrs. The required thickness of web was measured by thickness gauge (Sylvac $\mu\text{s}229$, Swiss) The voltage and current measurements taken by four probe method (Figure 3.4) were converted to conductivity using below Equation (1) [104]:

$$\sigma = \frac{\ln(2)}{\pi w} \left(\frac{I}{V} \right) \quad (1)$$

where, σ , I , V , and w and are the electrical conductivity (Smm^{-1}), current (A), voltage (V), and nanofibrous mats thickness (mm) respectively. The thickness between two probes is $s = 1\text{mm}$. Although this method is used for even conductive metal surfaces such as stainless steel, aluminum, titanium, nickel and conductive ink surfaces based on carbon, metal or graphene, it is not ideal for network surfaces such as nanofibrous surfaces. Therefore, the conductivity is calculated using linear resistance.

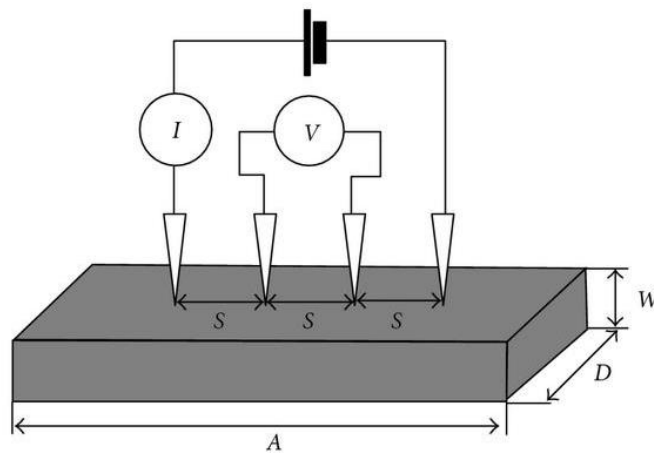


Figure 3.4: Schematic diagram of test circuit for measuring resistance with the four-point probe method

The yarn resistance R (Ω) along the yarn length was measured by the two probes method using (Fluke 289 True-RMS Data Logging Multimeter). One method used to measure resistivity as in Figure 3.5, a yarn or a ribbon was kept on the glass substrate, where conductive aluminum tapes were stuck in 1cm distance. In the other method conductive yarn was released from one end and wound from other end as the schematic arrangement in Figure 3.6. Both methods, one probe was kept stationary and movable probe was dragged along the yarn length with increasing the distance between two probes by 1 cm.

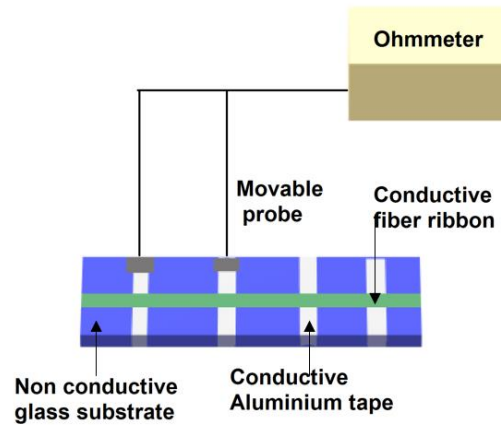


Figure 3.5: Schematic diagram of test circuit for measuring resistance of fiber ribbons with the two-probe method using multimeter

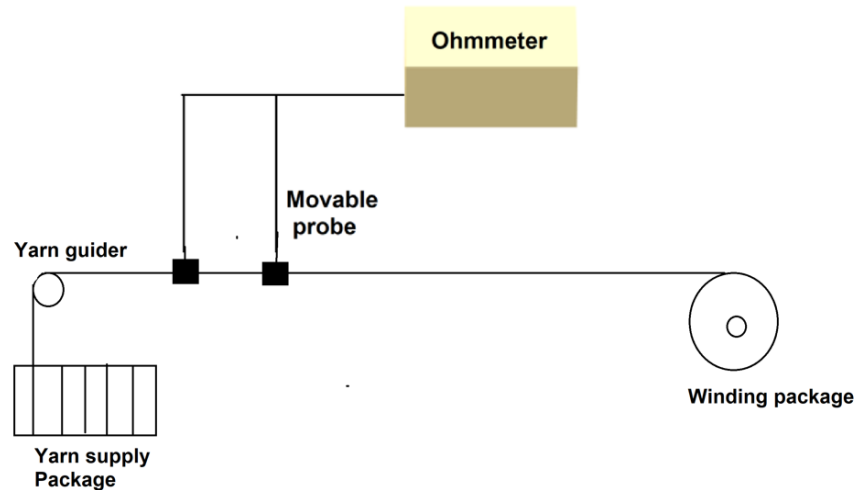


Figure 3.6: Schematic diagram of test circuit for measuring resistance of the yarn with the two-probe method using multimeter

3.6.3 Tensile strength

These tests were used to determine the tensile strength, modulus, and energy at break of the yarn. These measurements were taken from the Instron single yarn strength tester by following ASTM D2256 Tensile Properties of Yarns test method.

3.6.4 DSC analysis

Differential scanning calorimetry (DSC) data was performed by using Q2000 DSC from TA Instruments, New Castle DE. DSC measurements were performed respectively, with a scan rate of 10 °C/min under 50 ml/min flow rate of air atmosphere using Alumina pans and heated up to 400 °C.

3.6.5 FTIR analysis

Fourier transform infrared spectroscopy (Bruker FT-IR Vertex 80) was performed to investigate the functional groups on the surface of the samples. The yarn samples were placed on top of the diamond crystal which was inside the ATR chamber. The maximum contact between the sample and crystal was ensured by the special tightening unit of the instrument. The FTIR spectra were recorded with a resolution of 4 cm⁻¹ between 4000 cm⁻¹ to 600 cm⁻¹, the sample scan time was set as 64.

3.6.6 TGA analysis

TGA (Thermogravimetric) analysis was performed in a nitrogen atmosphere using an STD Q600 analyzer. Small pieces of yarn samples, with a weight of 10-15 mg was compressed into an alumina pan that was heated from room temperature to 1000 °C at a heating rate of 20 °C/min. The percentage of weight loss and ash content were studied from TGA curves.

3.6.7 Conductivity over mechanical deformation

The effect of stretching on resistance was measured at variable percentages of displacements from the initial length of the yarn. The strain was applied from 0-400% using homemade apparatus as in Figure 3.7. The yarn was clamped in 4 cm distance

and a constant load was supplied with a known constant rate. Therefore, strain could be calculated with respect to time. The resistance of the yarn was also measured and saved with respect to time using a multimeter (Fluke 289 True-RMS Data Logging Multimeter). At the end, data was presented as a plot of resistance versus strain. Then the behavior of resistance of the device for 8 stretch and recovery cycles for 20% strain was studied by measuring the resistance of the device with respect to time.

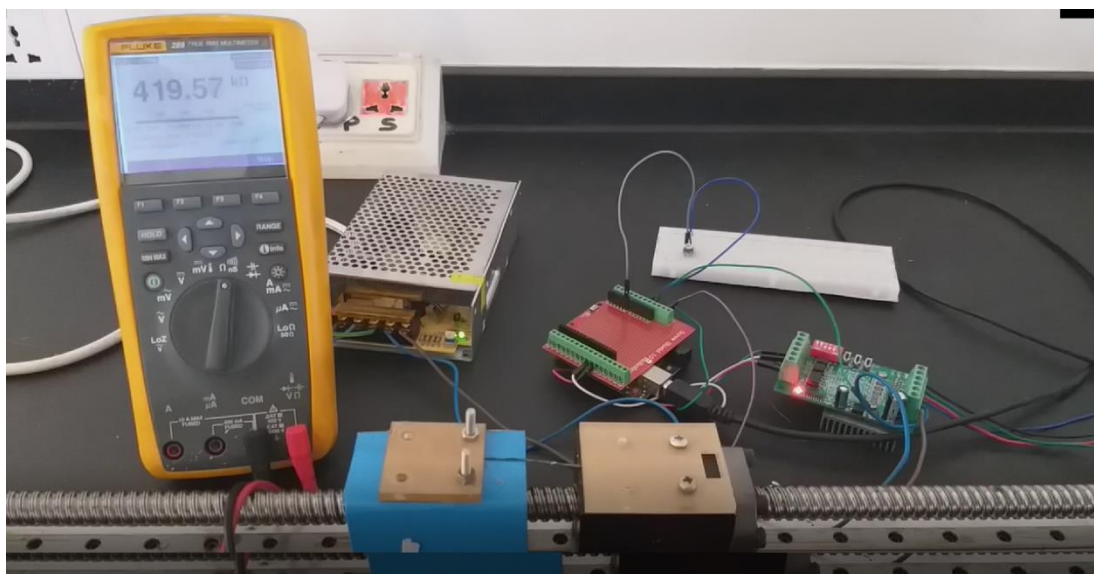


Figure 3.7: Homemade apparatus for measuring resistance vs strain

Simultaneously, to check the ability to sew and weave the yarn into different shapes of devices with different patterns, the PANi/PCL yarns were sewn on nylon fabric and woven with nylon yarns. The resistance of the fabric was measured for 10 folding and unfolding cycles. The resistance of the yarn for a constant length of the yarn with respect to number of twists was also studied.

3.6.8 Biodegradation of the material under controlled composting conditions

Biodegradability of PCL and PANi/PCL blended and coated films were tested according to ASTM 5338 standard. The biodegradability was compared with respect to cellulose filter papers as the positive control and polyethylene plastic sheets as the negative control. The samples were recovered from compost soil, then the weight was measured and the change of physical appearance was recorded. The test specimens

were prepared with the dimensions of 25x25 mm² pieces. Water was added to the soil until the overall moisture content becomes 50%. The samples were observed weekly and excess liquid was added to maintain constant moisture content. The samples were kept at a temperature of 58 ± 2 °C. Further, the samples were shaken weekly to maintain uniformity. The sample containers were filled 75% of the maximum content of specimen and soil [105].

Further, the morphology of degraded PANi coated and blended nanofiber mats were observed using SEM images.

3.7 Applications

3.7.1 Capacitive sensor

The PANi coated PCL yarn was sewn into a conductive switch to construct fabric electrode for capacitive sensing. To achieve capacitive sensor functionality, delay in output pulse compared to input pulse due to touching should be calculated. This was done through Cap Sense library and the circuit was built from Arduino board (Arduino Uno) and some basic electronic components as shown in Figure 3.8. A resistor of 5 M Ω was connected to breadboard. Two wires from two sides of the resistor were connected to pin 2 and 4 of the Arduino board. A wire from the fabric electrode was also connected to a side of the resistor which was connected to the pin 2. In order to observe the output signal, a LED bulb was connected to the breadboard. Wires that come from the two ends of the LED was connected to pin 12, and 13 of Arduino board. The code given in Appendix A was uploaded and compiled to the Arduino and demonstrated the operation of capacitive sensor. The Arduino code linked with Cap Sense library was attached in Appendix A.

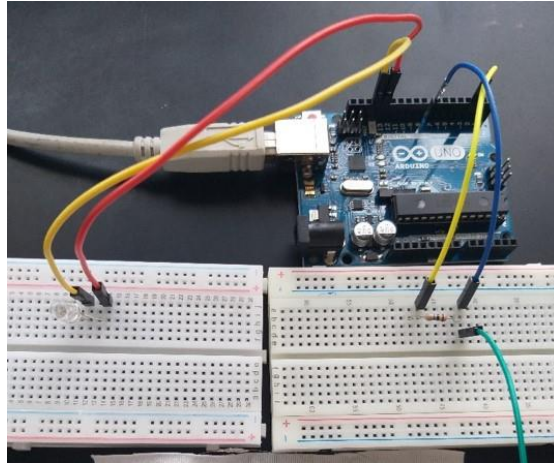


Figure 3.8: Basic circuit for capacitive sensors

3.7.2 Biomaterial

3D macroporous nanofiber scaffolds fabricated from electrospun yarn provide structural support for growth and guide for cell formation in tissue engineering [72]. According to literature, conductive polymers such as polypyrrole (PPy) and polyaniline (PANi) are the most promising because of their unique conductive properties that influence cell attachment, proliferation, migration, and differentiation [106, 107]. Therefore produced CBNYs may be promising as a biomaterial to develop conductive 3D macroporous nanofiber scaffolds. This can be evaluated by a study of in-vitro degradability, cell viability, and cell morphology.

3.7.2.1 Biodegradability

Biodegradation of tissue scaffolds is an advantage to enable tissue regeneration and inhibit surgical removal of the scaffolds. The morphology change and gravimetric measurements of in-vitro degradability of pure PCL, PANi coated and PCL/PANi blend were investigated. This was conducted by soaking the nanofiber ribbons in phosphate-buffered saline (PBS; pH 7.4) at 37 °C. After every five days, the samples were retrieved, washed with distilled water and dried utilizing freeze-drying system prior to weight measurement. Then the mass loss percentages of the weighed samples were calculated with respect to the initial weight. In addition, the morphology of in-

in vitro degraded nanofibers was observed by SEM images. The nanofiber samples, which were soaked in PBS solution for 20 days at 37 °C were taken for SEM analysis.

3.7.2.2 Cell cytotoxicity study

Vero cells (green monkey kidney cell line) were treated with the PCL and PANI/PCL electrospun nanofibers to determine their toxic effect using the MTT assay.

Vero cells monolayer was seeded in a three 96-well flat-bottom microtiter plate at a density of 2×10^5 cells/well and allowed to adhere for 24 hours at 37 °C in a 5% CO₂ [108] incubator. After 24 hours of incubation, the culture medium (DMEM) was removed and washed with sterile PBS. Cells were then treated with nanofibers as in Figure 3.9. The treated cells were incubated for 24 h at 37 °C with 5% CO₂ incubator. After 24 hours of incubation, 100 µl of MTT working solution (5 mg/ml in phosphate buffer solution) was added to each well and the plate will be incubated for 2.5 hours at 37 °C in a CO₂ incubator. The experiment was performed in triplicate. The medium was then aspirated, and the formed formazan crystals will be solubilized by adding 100 µl of MTT solvent per well and shake for 15 min. Finally, the intensity of the dissolved formazan crystals (purple colour) were quantified using the ELISA plate reader at 570 nm.

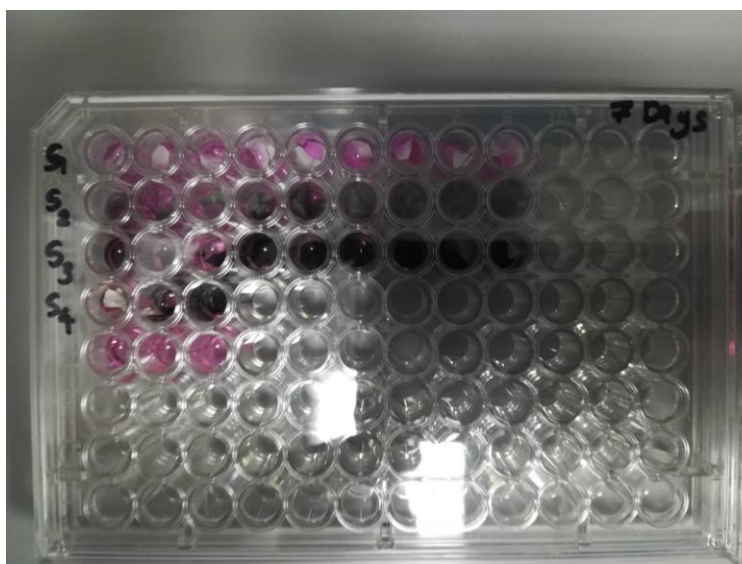


Figure 3.9: Well plate with cells that were treated with nanofibers

3.7.2.3 Cell morphology study

The morphologies of the vero cells adhering to the PCL. PANI /PCL nanofibers were observed using SEM. Briefly, well plates are pre-coated with PCL and PCL/PANi nanofibers, and vero cells (green monkey kidney cell line) were seeded at a density of 2×10^5 cells/well. After 24 hours, the nanofibers were immersed in 3% glutaraldehyde diluted from 0.1M PBS at room temperature for 2 hrs. Then the samples were rinsed with 0.1 M PBS (pH = 7.2). Then samples were dehydrated in graded ethanol solution in water as 30%, 50%, 70%, 80%, 90% and, 100%. The samples were kept in each solutions for 15 mins. Then, dried samples were mounted to SEM stub and analyzed.

3.8 Summary

This chapter reported the links between gaps identified from the literature and converted them into a strategic research plan. The novel modification method inspired from the literature was detailed further to prove it quantitatively using characterization techniques such as SEM, TGA, DSC and FTIR. Conductivity tests and tensile tests were used to analyze the accomplishment of usage for different applications.

CHAPTER 04

4. RESULTS AND DISCUSSION

4.1 Introduction

This chapter discusses the results obtained in line with the methodology. The flow of the chapter is organized in four phases. Firstly, the selection of carrier polymer and the conductive polymer is discussed by stating the reasons. Then, the investigation of PANi blended CBNYs and PANi coated CBNYs have been discussed separately. The yarns were analyzed quantitatively using results obtained from SEM, instron tensile tester, TGA, DSC, FTIR, multimeter and Keithley 2400 Source Meter SMU Instruments. The concentration of PANi was optimized in order to obtain a yarn with good conductive and mechanical properties. As the final part, a comparison of PANi blended CBNY and PANi coated CBNY is discussed along with the end applications.

4.2 Electrospinning of PVA and PCL

PCL and PVA were electrospun and analyzed using the SEM images shown in Figure 4.1. According to the fiber morphology, PCL and PVA fibers have an average diameter of 439 nm and 353 nm respectively for 50 number of fibers. The electrospinning parameters were kept as high voltage of 24kV, distance of 15 cm between needle to collector, flow rate of 8 μ l/min, temperature of 27 °C and 50% of relative humidity. Although PVA has shown low fiber diameter when compared with PCL, PVA has fused fiber morphology while electrospun fiber mat of PCL has individual, uniform fiber morphology with porous structure. On the other hand, PVA is a water-soluble polymer, and therefore water solubility of electrospun PVA mats limit their applications [109] and obviously, not appropriate for usage in textiles. PVA has OH groups that cause strong hydrogen bonds with water resulting in fusing between polymer chains as [110] illustrated in Figure 4.2. Moreover, owing to moisture absorption property, conductivity of PVA blended nanofibers can be varied. Although it opens the pathway to humidity sensors [111], it limits the usage of conductive PVA

fibers for other electronic applications as a substitution for conductive metal wires. Considering all facts, PCL was selected as the carrier polymer for further studies.

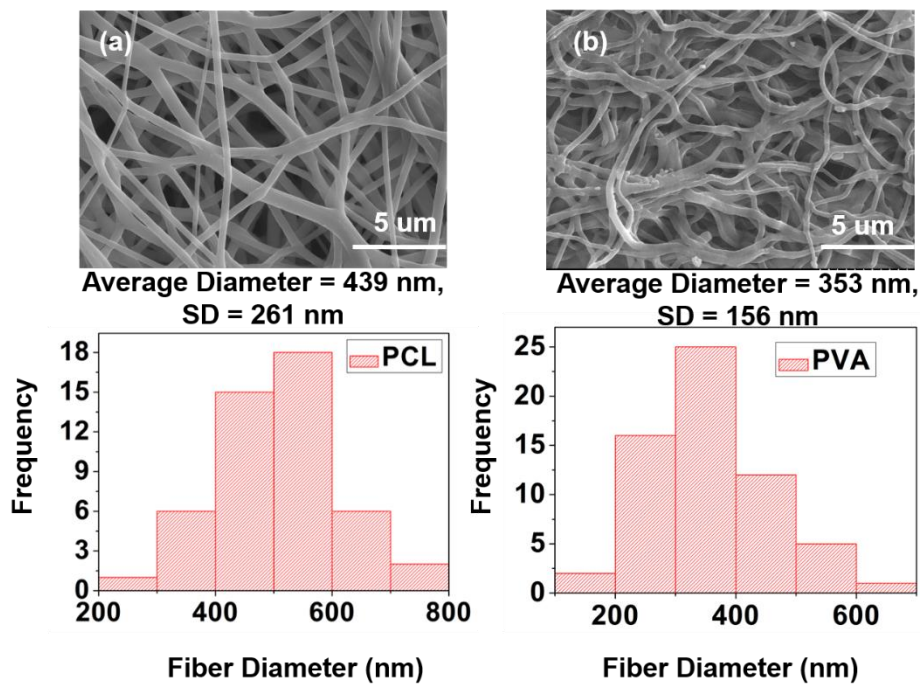


Figure 4.1: SEM image and diameter distribution histogram of (a) PCL nanofibers, (b) PVA nanofibers

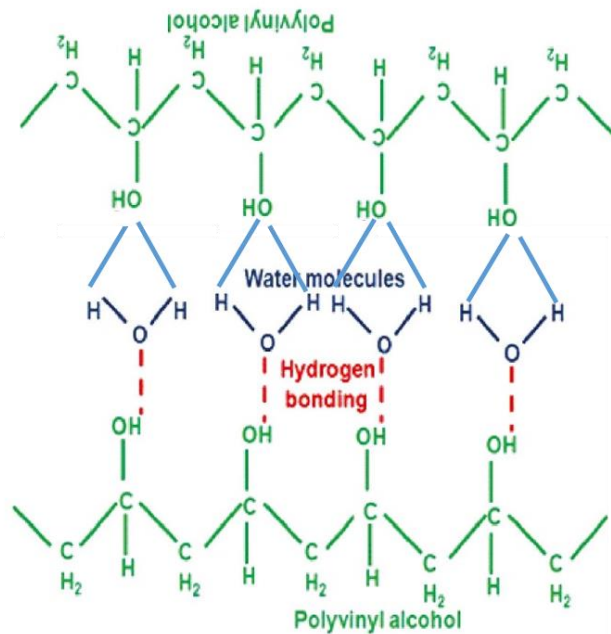


Figure 4.2: Illustration of hydrogen bonding interaction among PVA by water [110].

4.2.1 Enhancing conductivity of PANi by acid doping

The most stable oxidation state at room temperature of PANi is the form of emeraldine. Emeraldine form has two stages as emeraldine base (EB) and emeraldine salt (ES). The emeraldine base solution was blue in color and the polymer film casted based on EB was not conductive. Since the EB is a neutral form with a conductivity of less than 10^{-10} S/cm [112], the blended solution of PANi with an insulating material as PCL should also be non-conductive. Moreover, polyaniline consists of two kinds of rings, benzenoid and quinoid, and this quinoid has conjugate bonds while benzenoid is non-conductive [113]. Hence, a dopant has the ability to transport charge between chains by protonating the polymer chain.

In this research there were, three solutions taken; (i) Emeraldine base PANi, (ii) Emeraldine base PANi doped with CSA, (iii) Emeraldine salt PANi, produced by doping with HCl in polymerization stage was again doped by CSA (Figure 4.3). Then each of the above the PCL/PANi solutions were prepared by dissolving PANi in 1 ml DMF with a concentration of 10% (w/v) and mixed with 4 ml of 10% (w/v) PCL solutions. Then casted as shown in Figure 4.4.

The color of the solution was varied according to the form of emeraldine. The EB acquires blue color while ES acquires green color. The greenish color of the solution was increased due to the amount and stability of the dopant. As demonstrated in Figure 4.3 color change from blue to green can be observed in the following order: EB > ES (CSA doped) > ES (HCl and CSA doped). The resistivity of films also decreased accordingly and the film prepared by adding CSA to HCl doped PANi shows the lowest resistivity meaning the highest conductivity. Here, an interesting secondary doping effect [114] can be observed in this case, with the organic acid, camphorsulfonic acid (CSA) which increased the conductivity by protonating all the imine sites.

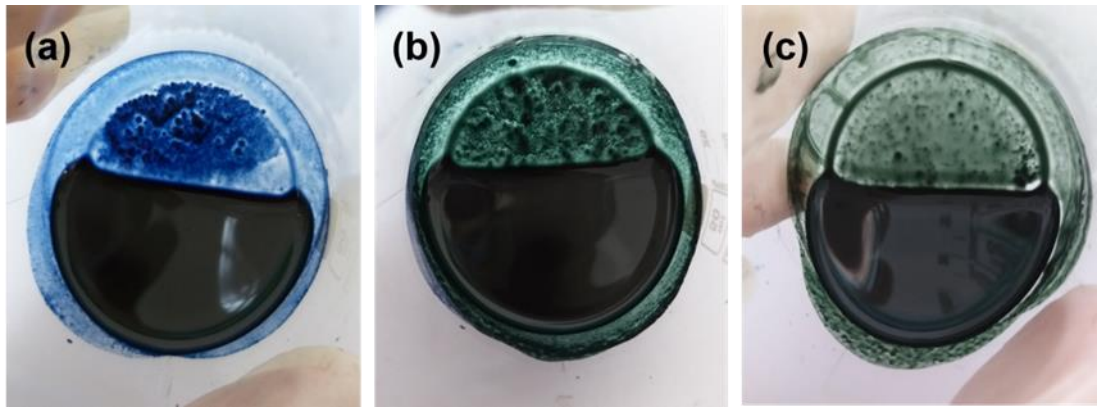


Figure 4.3: Solutions of (a) emeraldine base (EB) PANi/PCL, (b) emeraldine base (EB) PANi/CSA/PCL, (c) emeraldine salt (ES) PANi (PANi doped by HCl/CSA/PCL

Moreover, treatment of organic acid increased the solubility of PANi. Nevertheless, there is a big disadvantage of using smaller molecule acids for doping PANi, because the evaporation of acid can cause conductivity depression of PANi. Non-volatile acids such as camphor sulfuric acid (CSA) and dodecylbenzylsulfonic acid should be used to overcome this issue [115]. Thus the HCl doped PANi was secondary doped with CSA to obtain good conductivity.

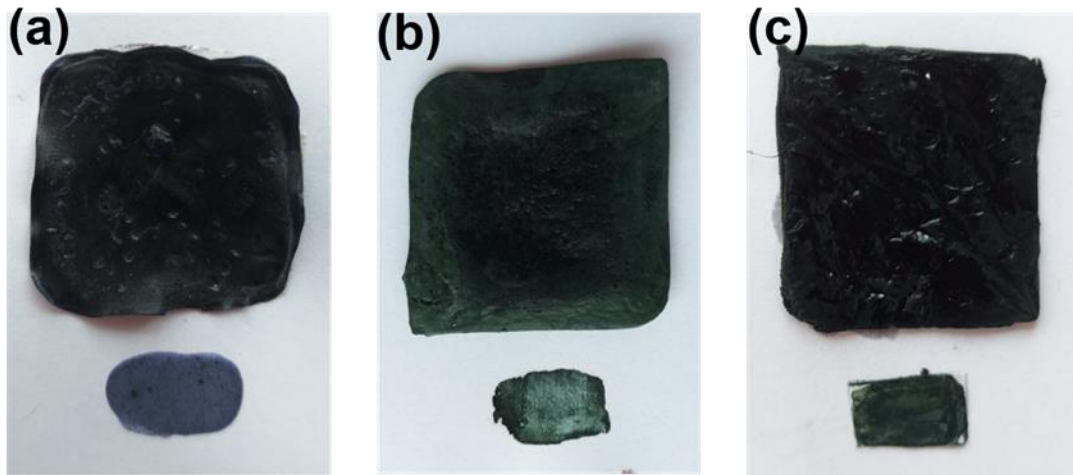


Figure 4.4: Casted films of (a) emeraldine base (EB) PANi/PCL, (b) emeraldine base (EB) PANi/CSA/PCL, (c) emeraldine salt (ES) PANi (PANi doped by HCl/CSA/PCL

Table 4.1 Effect of different dopant on electrospinnability and resistance

Weight of PCL and PANi	Dopant	Ability of electrospinning	Sheath resistance(MΩcm)
0.450, 0.05	No	Yes	-
0.450, 0.05	CSA	Yes	50
0.450, 0.05	CSA for HCl doped PANi	Yes	20

4.3 PANi blended nanofibrous yarns

4.3.1 Influence of conductivity on electrospinnability

PANi blended fiber mats can be prepared from a rotary drum collector. If a screen collector was used, the fibers would not deposit on the screen collector. As shown in Figure 4.5, the conductivity of polymer jet has resulted in growing of fiber bundle towards the needle (anode) and fiber bundle has formed in between needle and collector. Further spinning process was disturbed by the fiber bundle in between collector and needle. This problem was overcome by replacing the screen collector by rotational collector. The fibers, which grow towards the anode, were wrapped over the drum. Furthermore, the alignment of fibers can be adjusted by varying the rotational speed of the rotational drum. Figure 4.6 illustrates the developed setup to produce aligned and conductive nanofibers.

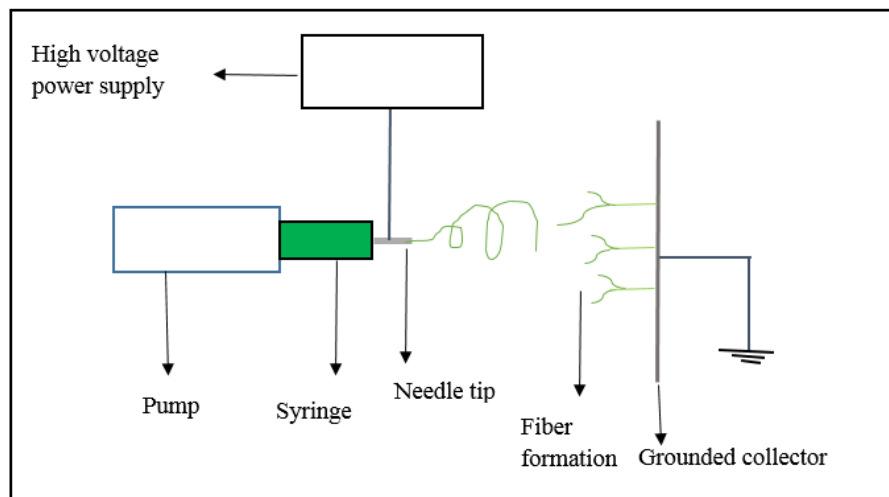


Figure 4.5: Demonstrating conductive nanofiber electrospinning process



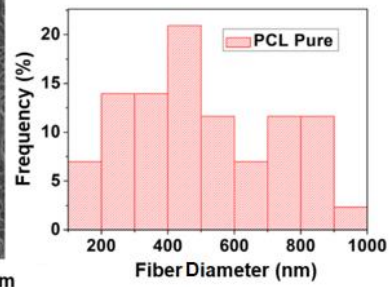
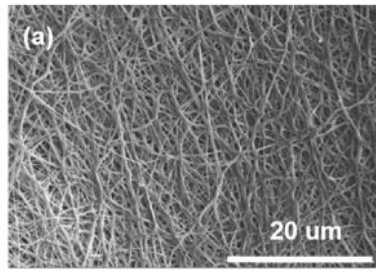
Figure 4.6: A photo of the electrospinning setup with rotational drum collector.

Nanofibers were electrospun from pure PCL (PCL Pure) and the other three sets of PCL/PANi-CSA blended polymer mixtures. The electrospinning parameters were kept as high voltage of 24kV, distance of 15 cm between needle to collector, flow rate of 8 μ l/min, temperature of 27 $^{\circ}$ C and 50% of relative humidity. Weight of PANi from the whole volume of the solution was taken as 0.5%, 1%, 2% to obtain PANi 0.5%, 1%,

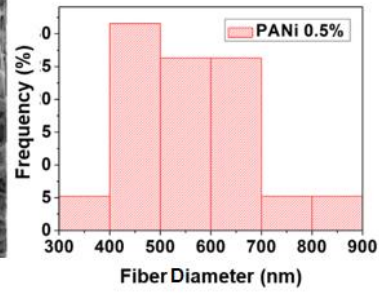
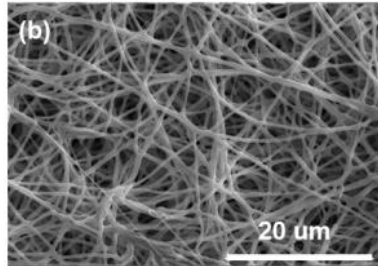
2% (w/v) samples. SEM images of Figure 4.6 illustrate fiber morphology and corresponding fiber diameter distribution of resultant electrospun PCL/PANi nanofibers with various concentrations of PANi-CSA. By increasing the PANi concentration, the average diameter (for 50 number of fibers) of nanofiber was decreased from 508 ± 225 nm to 352 ± 153 nm for PCL Pure to PANi 2%. Fiber diameter of PCL/PANi blended nanofibers was mentioned in the literature. There the content of PANi in PCL was increased as 1%, 2% and 3% (w/w). The fiber diameter was decreased as 525 ± 585 , 383 ± 154 , 343 ± 129 , 361 ± 122 nm for pure PCL, PANi 1%, PANi 2% and PANi 3%, respectively [101]. These fiber diameter values are closer to the values obtained in this study.

Mainly, in the electrospinning process, the conductivity and viscosity of the solution are two very important parameters, which can influence the electrospun nanofiber morphology. Literature gives evidences as to that of increasing the conductivity and decreasing the viscosity resulting in decreasing the average diameter of nanofibers [116]. Solutions with different amounts of PANi and PCL resulted in different viscosities. Since PANi is a dispersion, the viscosity of solution was reduced by decreasing the amount of PCL and replacing it with PANi. As shown in Figure 4.7 (e) PANi 4% solution did not produce any fibers. This is most likely due to the low viscosity of the solution. However, 0.5%, 1% and 2% PANi percentages resulted fiber formation.

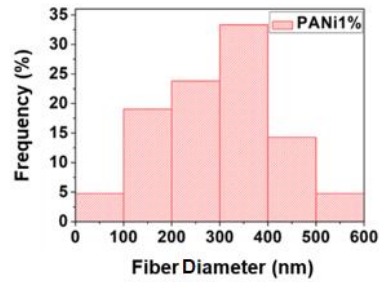
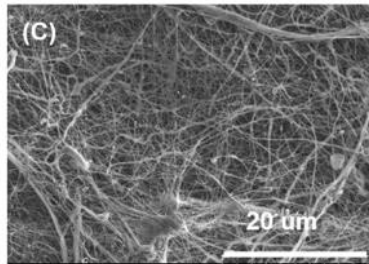
Average Diameter = 508 nm, SD = 225 nm



Average Diameter = 568 nm, SD = 121 nm



Average Diameter = 303 nm, SD = 142 nm



Average Diameter = 352 nm, SD = 153 nm

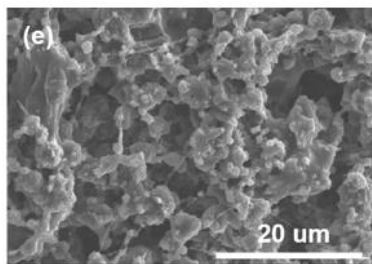
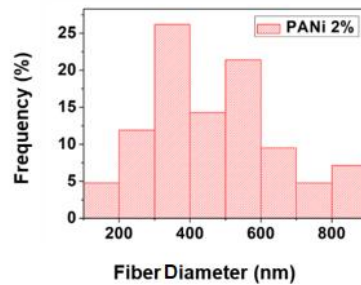
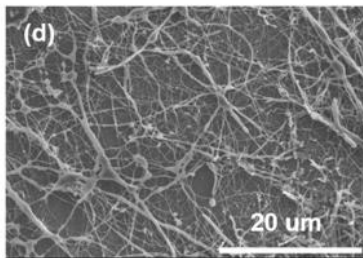


Figure 4.7: Morphology of nanofibers synthesized from different PANi concentrations and PCL. (a) pure PCL, (b) PANi 0.5%, (c) PANi 1%, (d) PANi 2%, (e) PANi 3%

4.3.2 Conductivity measurement

The electrical conductivity of these nanofiber structures can be varied by controlling the ratio of PCL and PANi. The effect of PANi amount on the electrical conductivity of the PCL/PANi nanofiber is illustrated in Figure 4.8 (a) and (b). Figure 4.8 (a) shows the raw data of supplied current against the measured voltage using four-probe technique. The gradient of the graph increased with increasing PANi content which represents the declining resistance which implies an increment of conductivity for material with the same dimensions of 20 x 20 x 0.05 mm. Figure 4.8 (b) demonstrates the calculated conductivity using the four-probe data. Table 4.2 illustrates resistivity values taken from four-probe methods and two-probe methods. Here, the volume resistivity and resistance per unit length were reported for a yarn with diameter of ~0.8mm. The average resistance over a 10 mm distance was measured as demonstrated in section 3.6. The resistivity values taken from four-probe method were higher when compared to the measurements taken from the two-probes of ohmmeter. Although the four probe-method was used for measuring the electrical conductivity of sheath resistance of thin films, it might not be suitable for measuring the electrical conductivity of nanofibers because of the inhomogeneity of the nanofiber mats as macroscopic mater [117]. Also, the random distribution, irregularity of thickness, and orientation of fiber can be considered as the reasons for variations of conductivity measurements of these two methods [118]. On the other hand, the resistance of PANi 0.5% sample cannot be measured from the ohmmeter, most likely due to the internal resistance of the ohmmeter.

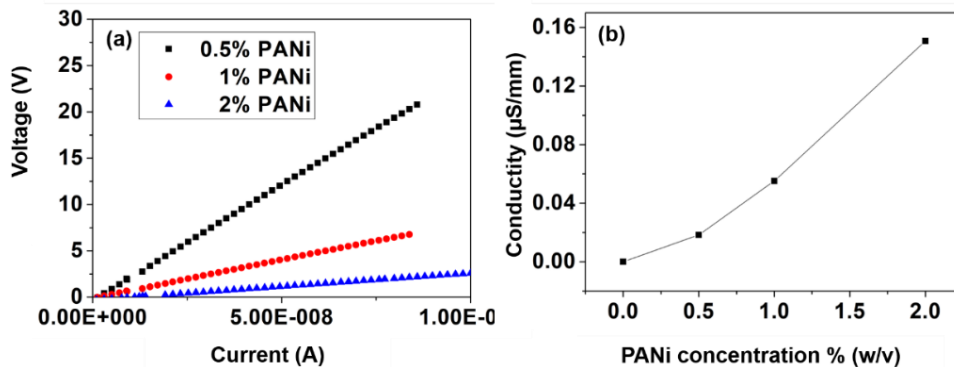


Figure 4.8: (a)The four probe V - I characteristics of PANi blended electrospun mats, (b) PANi concentration vs conductivity measured using four-probe method

However, it can be claimed from the results of both methods, the resistivity of the samples decreases with the increase of PANi content, the lowest electrical resistivity and highest conductivity increment result in when the PANi concentration is increased from 0.5 % to 2 %.

Table 4.2: Measuring resistivity by different methods.

Sample	Resistivity (4 probe, MΩmm)	Resistance per unit length (Ohmmeter, MΩ/cm)	Resistivity(Ohmmeter, MΩmm)
PANi 0.5%	54 ± 13	-	-
PANi 1%	18 ± 4	50 ± 8	2.51 ± 0.4
PANi2%	6 ± 0.1	10 ± 4	0.50 ± 0.2

Although there are hardly accessible literature about PCL/PANi blended CBNYS, there are some reported studies of development of PCL/PANi blended nanofiber mats [95, 101]. Among them the highest reported conductivity was 63.6 ± 6.6 mS/cm [101]. It was comparatively a higher value than the obtained result in this study that was 1.7 ± 0.1 μS/cm. In the mentioned study percentage of PANi in PCL was 3% (w/w) and mixture was dissolved in 1,1,1,3,3,3-Hexafluoro-2-propanol (HFIP). Here, purity of PANi and solubility of PANi might affected for varying the conductivity of nanofiber mat. Finally, it can be concluded that blending a conductive polymer to an insulator, PCL ($\sim 10^{-10}$ S/mm), is a promising method to increase the conductivity ($\sim 10^{-6}$ S/mm) and potentially useful for a possible application in the future.

4.3.3 Nanofibrous yarn formation

The conductive electrospun mats were prepared from PANi 2% solution using the modified electrospinning set up with a rotary collector (Figure 4.9). In order to form yarns, 5cm x 0.5cm stripes were cut from the mat and twisted onto a single yarn having a twist level of 30 twists per inch. The apparatus shown in Figure 4.9 (a) and (b) was

used to twist ribbons into yarns. To prepare single yarns one end of the ribbon was rotated while keeping the other end stationary. The basic self-twisting principle was utilized to twist two single yarns and assemble them together in a mechanical equilibrium position. Single yarns were twisted into s direction and such two yarns were assembled by twisting opposite Z direction to fabricate 2-ply yarn of 20 twists per inch. Three single-ply yarns were twisted into 3-ply yarn by giving Z twist with 10 twists per inch. SEM images of plied yarns are shown in Figure 4.9 (c-e).

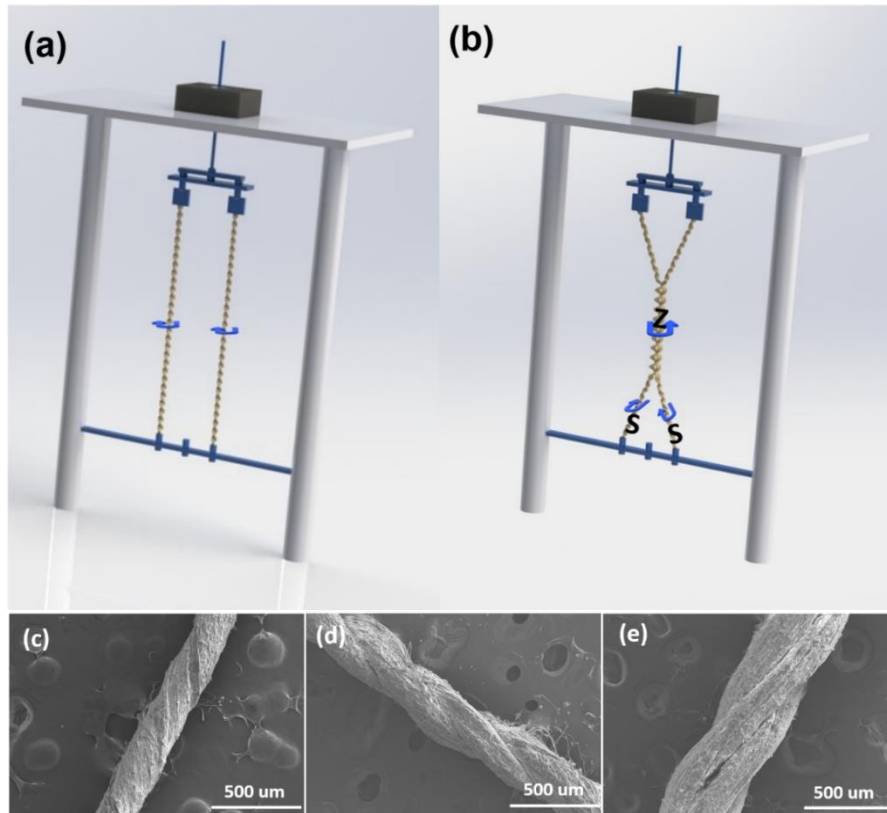


Figure 4.9: PANi 2% (a) Twisting single yarns, (b) twisting ply yarns, (c) PCL/PANi 1-ply yarn, (d) PCL/PANi 2-ply yarn, (e) PCL/PANi 3-ply yarn

The conductive properties of ply yarns were investigated by measuring resistance per unit length. According to the Equation (2) [119],

$$R = \frac{\rho l}{A} \quad (2)$$

Where, R = resistance, ρ = resistivity, l = length, A = area of the cross section, resistance can be decreased while area increases. Number of plies of a yarn is directly proportional to the diameter of the thread. As a result, resistance can decrease due increment of number of plies. This conclusion can be clearly shown in Figure 4.10.

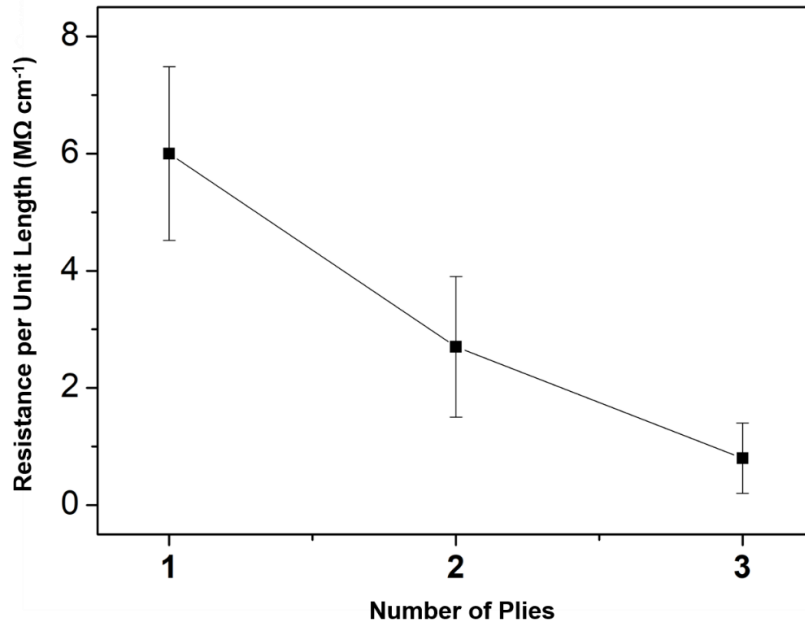


Figure 4.10: Effect of number of plies on resistance

4.3.4 Continuous yarn formation

A continuous yarn manufacturing unit was designed and developed. As shown in the Figure 4.11 (a) and (b), the green color PANi/PCL polymer jet ejected from the tip of the needle is assembled at the open end of the funnel and form a thin 3D nanofiber web. After the cone is formed, a nanofiber yarn (NY) was drawn and wound. The yarn was twisted by the rotation of the funnel.

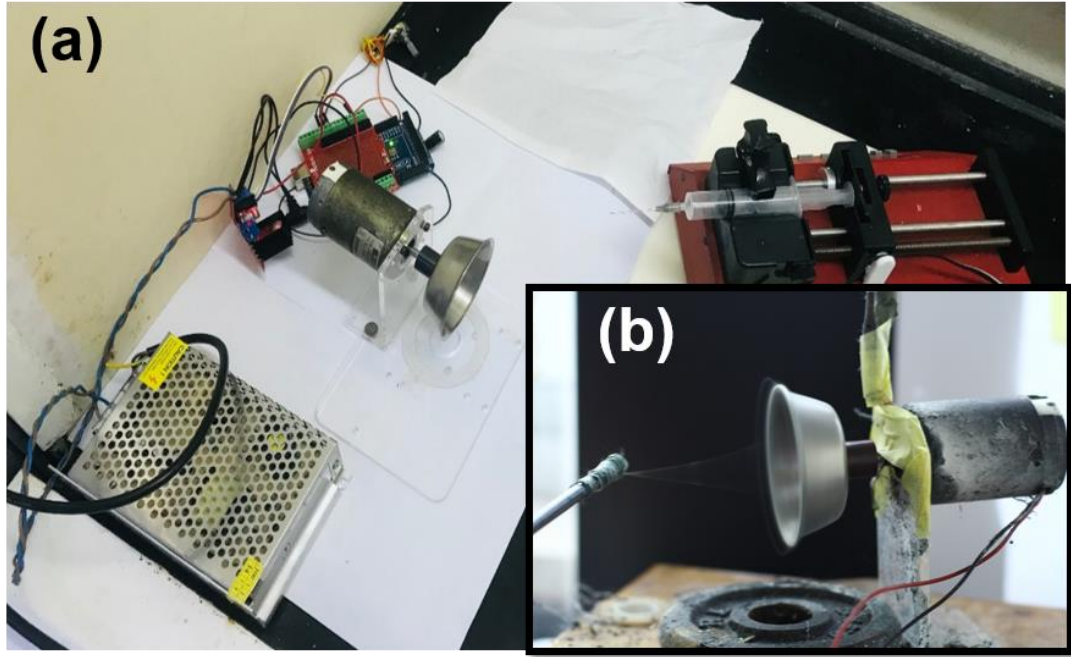


Figure 4.11: (a) Developed continuous yarn manufacturing unit, (b) 3D fibrous cone and twisted yarn

4.3.5 Effect of PANi concentration on mechanical properties of yarns

To investigate the influence of the content of PANi on the mechanical properties of PANi/PCL NYs the different PANi loaded PCL yarns were subjected to a series of tensile tests. Figure 4.12 (a) shows the stress-strain curves of NYs prepared from different polymer mixtures as pure PCL, PANi 0.5%, PANi 1%, PANi 2%.

The Young's modulus of pure PCL is 4.6 MPa which was enhanced as 5.4 MPa for 0.5%, 5.5 MPa for 1% and 5.9 MPa for 2% by increasing the PANi loading (Figure 4.12 (b)). Young's modulus of all nanofiber mats increased with addition of PANi indicating that PANi was efficient as a reinforcement nanofiller for PCL nanofiber matrix [120].

Before adding PANi, pure PCL exhibited the largest elongation-at-break (Figure 4.12 (a)), because of the movement of the PCL chains. After the addition of PANi, the elongation-at-break value become lower, which was attributed to the good dispersion of the PANi restricting the movement between polymer chains [121]. After the

addition of PANi, the tensile strength of the yarn was first increased from 3.92 MPa for pure PCL to 4.48 for PANi 0.5% due to the effect of PANi reinforcement on composite, and then decreased to 2.25 MPa for PANi 2% with increasing PANi loading. However, some papers have reported that the tensile strength of polymer/filler nanofiber is higher than that of polymer nanofibers only when the content of filler is lower than a critical value [122, 123]. When the content of filler is higher than the critical value, the tensile strength of polymer/filler nanofibers decreases gradually [121]. When increasing PANi content up to 2% (w/v), the modulus and the tensile strength has decreased than pure PCL. In addition to the reasons mentioned above, the hydrolysis of polymer chain in low pH due to increased amount of CSA may also be a factor to tensile strength reduction [124, 125].

The toughness is proportional to the absorbed energy at breakpoint for samples with similar dimensions. The Young's modules and energy at break value of pure PCL and PANi/PCL NYs are summarized in Figure 4.12 (b and c). Adding the PANi particles into the PCL polymer matrix would reduce the toughness of the NYs, but enhance Young's modulus of the yarns. These results show that the stiffness is improved by sacrificing the toughness. This was consistent with the results in many electrospun conductive nanofiber matrixes, epoxy nanocomposites and layered silicates/epoxy nanocomposites [121, 126, 127].

When comparing these results with studies in literature, reported study of preparation of conductive yarns by PCL and carbon nanotubes have not been mentioned about study of mechanical properties [14]. However, mechanical properties were studied for conductive nanofibrous mats of PCL/PANi [101]. The reported tensile strength was 10.5 ± 0.3 MPa and Young's modules was 55.2 ± 3.6 MPa for a nanofibrous mat with 3% (w/w) PANi in PCL [101]. These values were comparatively higher than obtained results of this study. In this study, HCl doped PANi and CSA was used while in the reported emeraldine base PANi and CSA was used. Therefore, in this study, HCl might be affected to mechanical property reduction of PANi/PCL yarns.

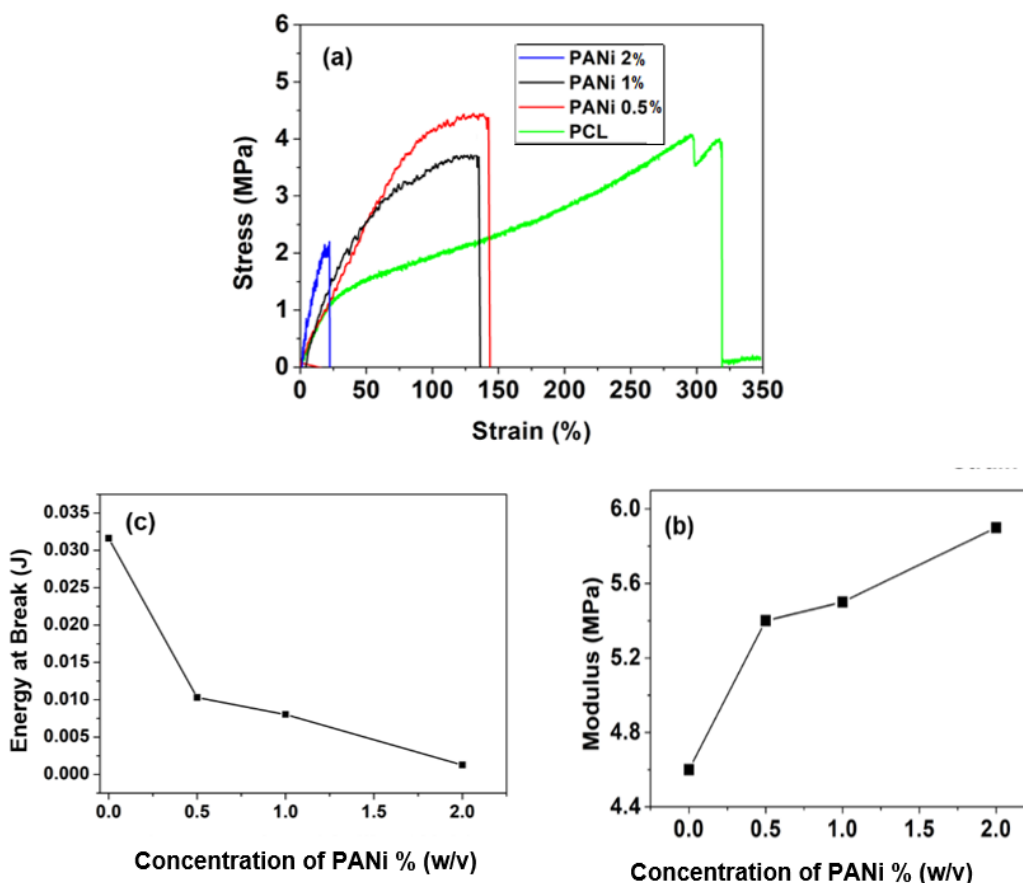


Figure 4.12: (a) The stress–strain curves of Pure PCL, PANi 0.5%, PANi 1%, PANi 2%, (b) effect of PANi concentration on energy at break value of yarns, (c) effect of PANi concentration on modulus of yarns

4.3.6 TGA analysis

According to TGA curve of polyaniline powder (Figure 4.13) pure polyaniline shows three major phases of weight loss. The first weight loss occurs due to loss of water, HCl and other volatile solvent between 0-120 °C. The second weight loss attributes to degradation of PANi which has an onset degradation temperature at ~195 °C (Table 4.3) that is shifted to 209.76 ± 4.63 °C for the blended fibers. The next main degradation occurs at onset temperature at ~381.32°C for PANi/PCL and ~378.73 °C for pure PCL which represents degradation of PCL.

At this stage, the mass loss is attributed to increased evaporation of HCl with increasing amounts of HCl doped PANi. The percentage of residue at 600 °C was also

increased with the increasing amount of PANI in the yarns, which may be attributed to remaining PANi degradation product [128]. Thermal stability analysis of PCL/PANi samples were carried out by reading the temperature as taking the temperature attributes to 95% residual weight of PCL as the thermal stable temperature.

Overall, it can be concluded that the amount of PANi in PANi/PCL yarn has a significant influence on thermal properties of PCL/PANi composite yarns and the thermal stability has decreased with increasing the PANi concentration.

Table 4.3: TGA data compilation for the tested fibers, including the first peak weight loss attributed to HCL, second onset and weight loss attributed to PANi, third onset and weight loss attributed to PCL and residual weight and thermal stability.

Sample	Peak (°C), Weight loss HCl (%)	Onset (°C) and weight loss PANi (%)	Onset (°C) and weight loss (%) of PCL	Residual weight (%)	Thermal stability (°C)
PANi powder	67, 12.82	194.35, 30.06	-	44.82	64.91
PANi 2%	64, 5.66	205.13, 26.86	381.32, 65.36	2.12	62.40
PANi 1%	60, 4.95	214.39, 18.20	378.26, 75.05	1.78	130.36
PCL pure	-	-	378.73, 94.43	1.78	356.27

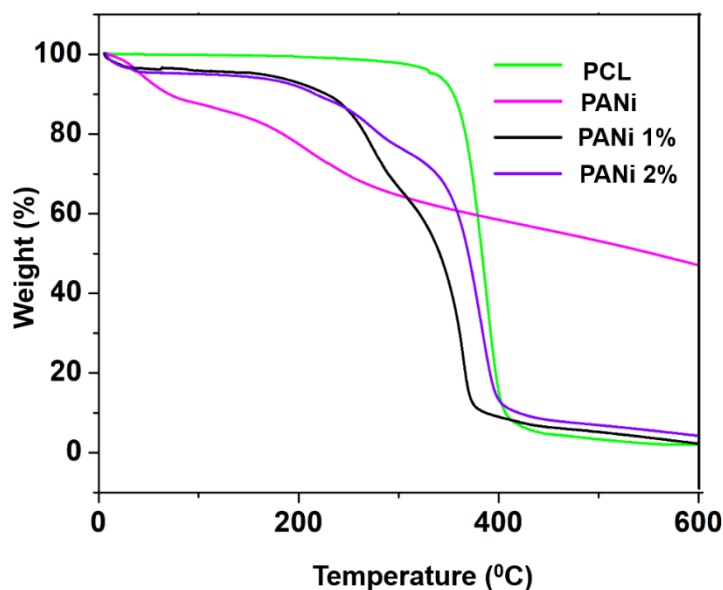


Figure 4.13: TGA profiles of pure PCL and conductive PANi/PCL yarns with different PCL to PANI ratio

4.3.7 DSC analysis

DSC thermal analysis curves for PANi powder, Pure PCL and PANi/PCL yarns are shown in Figure 4.14. DSC curve for PANi showed endothermic peak around 126°C. This endothermic transition is related to the excess water and HCL and it was dislocated with respect to TGA which indicated the weight loss to be between 55-100 °C. Water molecules between polymer chains, that was proven by DSC curve also a good indicator for conductivity, because water can be bound to the PANi lattice and change its conductivity [129]. Influence of water on the polymer crystal structure was also studied in literature [130]. A broad exothermic peak at 150-250 °C was due to exothermic reaction that resulted from crosslink reactions led by coupling of $\left[\text{C}_6\text{H}_4\text{-NH-C}_6\text{H}_4\text{-NH} \right]$ and $\left[\text{C}_6\text{H}_4\text{-N=C}_6\text{H}_4\text{=N} \right]$ through interaction of the N with its neighboring quinoid [131].

DSC curve of PCL nanofibers showed that the peak that represents melting temperature was at 60 °C with the melting enthalpy of 71.95 J/g (Table 4.4). This

melting enthalpy, melting temperature and percentage crystallinity of PCL is found to decrease from $\Delta H_m = 71.95 \text{ J/g}$, $T_m = 60.64 \text{ }^\circ\text{C}$ in pure PCL NYs to $\Delta H_m = 66.6 \text{ J/g}$, $T_m = 55.73 \text{ }^\circ\text{C}$ in PANi 2%. Also endothermic peak and exothermic peaks of PANi can also be observed around $135 \text{ }^\circ\text{C}$ and $150 \text{ }^\circ\text{C}$, respectively. These findings indicate that the crystallinity of PCL nanofibers has decreased due to the presence of PANi.

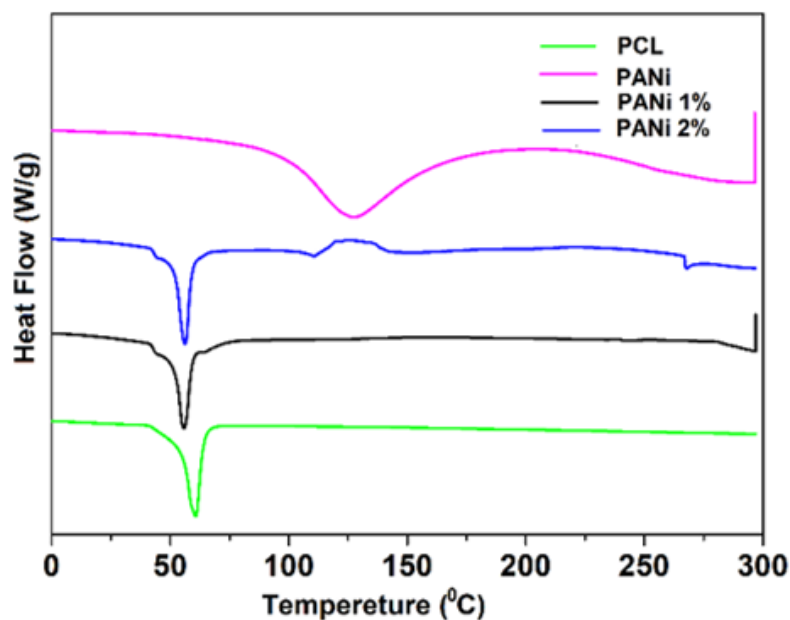


Figure 4.14: DSC profiles of pure PCL and conductive PANi/PCL yarns with different PCL to PANI ratio

Table 4.4: Melting temperature, melting enthalpy and percentage crystallinity of pure PCL and conductive PANi/PCL yarns with different PCL to PANI ratio

Sample Name	Melting Temperature of PCL (T_m , $^\circ\text{C}$)	Melting Enthalpy PCL (ΔH_m , J/g)	Percentage crystallinity (%)
PCL Pure	60.64	71.95	51.57
PANi 1%	56.18	70.13	50.27
PANi 2%	55.73	66.6	47.74

4.3.8 FTIR analysis

FTIR spectra for Pure PCL and PCL/PANi 2% were demonstrated in Figure 4.15. The characteristic peaks of PCL and PANi were as Table 4.5. Existing of PANi peaks provide an evidence for including of PANi in electrospun nanofibers.

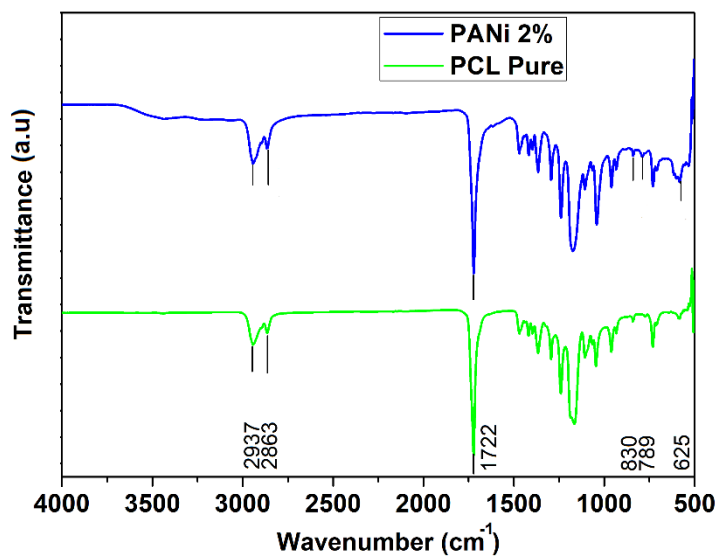


Figure 4.15: FTIR spectra of pure PCL and PANi 2%

Table 4.5: Characterization peaks of PCL and PANi 2%

Sample Name	Peak	Wave number(cm ⁻¹)
PCL [132]	-C-H ₂ - stretching	2937 and 2863
	Carbonyl groups	1722
PANi [96]	γ(C-H)	789
	Amine groups	652
	N-H bending	830

4.3.9 Optimizing PANi concentration

According to above results, PANi concentration has a significant impact on conductivity, fiber morphology, mechanical and material properties of PANi/PCL nanofiber yarns. Therefore, it is very important to optimize the concentrations PANi in order to achieve a conductive yarn with fibers in nano size range. Although the conductivity has increased with increasing the PANi concentration as per SEM images in Figure 4.7, nanofibers couldn't be obtained by PANi 3% solution. Therefore, PANi 2% solution was selected for further studies which has the highest conductivity level.

4.3.10 Electro-mechanical behavior of electro-conductive yarn

4.3.10.1 Effect of weaving and sewing on electrical resistance of the yarn

The twisted yarns were used for the demonstrating weaving and sewing. Figure 4.16 (a) shows a nanofibrous PCL/PANi conductive yarn on a piece of nylon fabric. The plied yarn was fed into a sewing needle and was stitched on the fabric. Figure 4.16 (b), the colored microscopic image of the CBNY on the nylon fabric which was taken by USB microscope (AmScope UBW500X02MP Digital 2MP USB Microscope, USA). It was proven that the yarn was mechanically strong enough to be sewn with a sewing needle. Similarly, woven fabric was woven manually (Figure 4.17 (a and b)) to confirm the ability of weaving of the yarn.

The PCL/PANi sewn conductive yarn with a diameter of ~ 0.8 mm and length of 40 mm has given a resistance value of ~ 40.5 M Ω . The calculated resistivity of the yarn was 0.50 M Ω mm which was equals to 0.50 M Ω mm for PANi 2% in section 4.3.2.

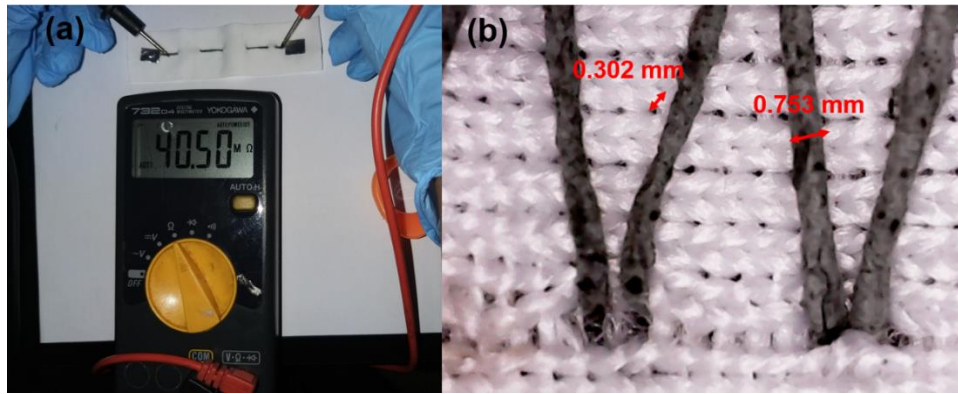


Figure 4.16: PCL/PANi 2% blended nanofibrous yarns. (a) Image of yarn stitched on a nylon fabric, (b) microscopic image of yarn stitched on the nylon fabric

Here, 2-ply conventional nylon yarns were used as weft in the woven structure (Figure 4.17 (a and b)), while the CBNYs were being used as the warp yarns. In the design of the fabric, resistance between the two ends (15 mm) of the fabric was $19.05 \text{ M}\Omega$ as demonstrated in Figure 4.17 (a). The calculated resistivity was recorded as $0.48 \text{ M}\Omega\text{mm}$ which was closer to $0.50 \text{ M}\Omega\text{mm}$ in section 1.4.2 of PANi 2%. Hence, it is clear that resistivity of the material has not changed by mechanical deformation of material during sewing and weaving. Figure 4.17 (c) shows a microscopic image of woven CBNYs.

Upon folding and unfolding, increasing and decreasing of resistance caused by disconnecting and connecting points of the yarns of the fabric (ex: point A and B in Figure 4.17 (d)). During fabric folding, the conductive paths may be short-circuited due to the contact points in bending such as A and B of the yarns. This leads to reduced resistance by four times the resistance of unfolded two ends. Figure 4.17 (e) illustrates the resistance change upon number of folding and unfolding cycles. Finally, the resistance of the yarn decreased by four times that can be seen from two resistance values ($19.05 \text{ }\Omega$ and $4.04 \text{ }\Omega$) of the multimeters in Figure 4.17 (a and b).

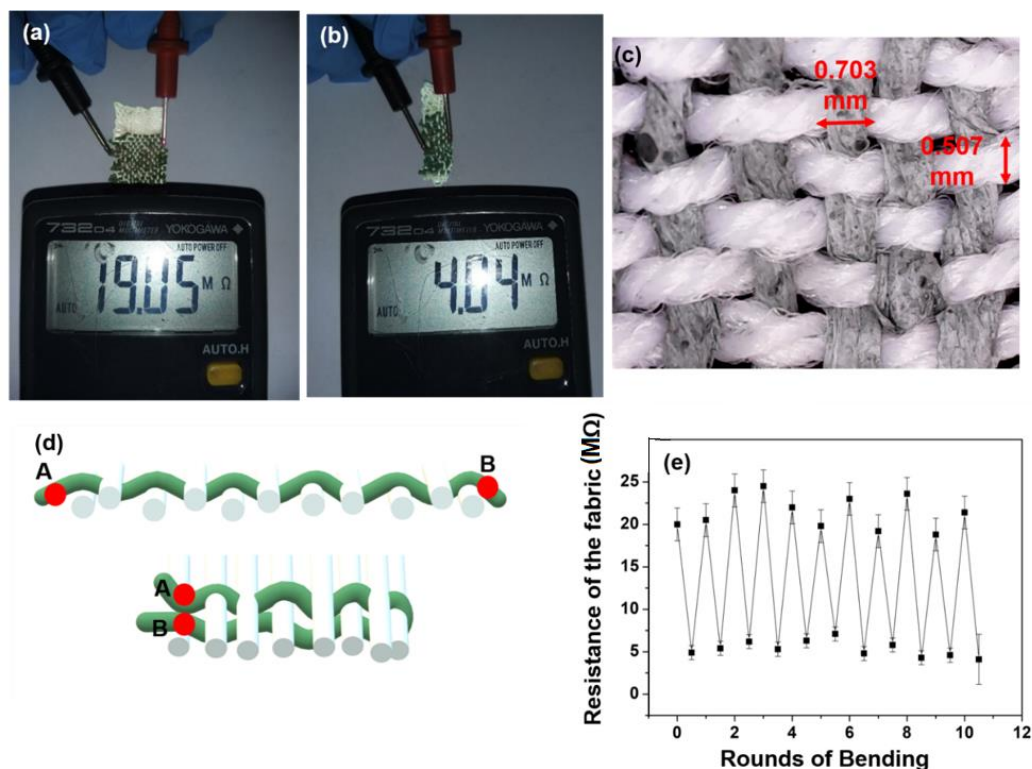


Figure 4.17: Fabric woven with PANi 2% blended nanofibrous yarns and 2-ply nylon yarns. (a) Conductivity measuring of unfolded fabric, (b) conductivity measuring of folded fabric, (c) microscopic image the fabric, (d) demonstrating yarn short circuiting by folding, (e) illustrating resistance change by number of folding cycles

4.3.10.2 Effect of strain on electrical resistance of the yarn

The relationship between conductivity and tensile strain was studied by measuring the resistance with respect to the extension of the yarn (Figure 4.18). Increasing displacement results in an increment of resistance between two ends of the yarn.

As the yarn strain increased, the distance between PANi particles might increase. As a result conductive pathway may be disturbed, however in some points there can't be seen a significant increment of resistance. When strain increased, compactness and alignment along the yarn axis can be increased with resulting in low resistance along the polymer chains. Therefore, the synergetic effect of increasing and decreasing resistance can be the reason behind the approximately similar resistance values in some points of the graph.

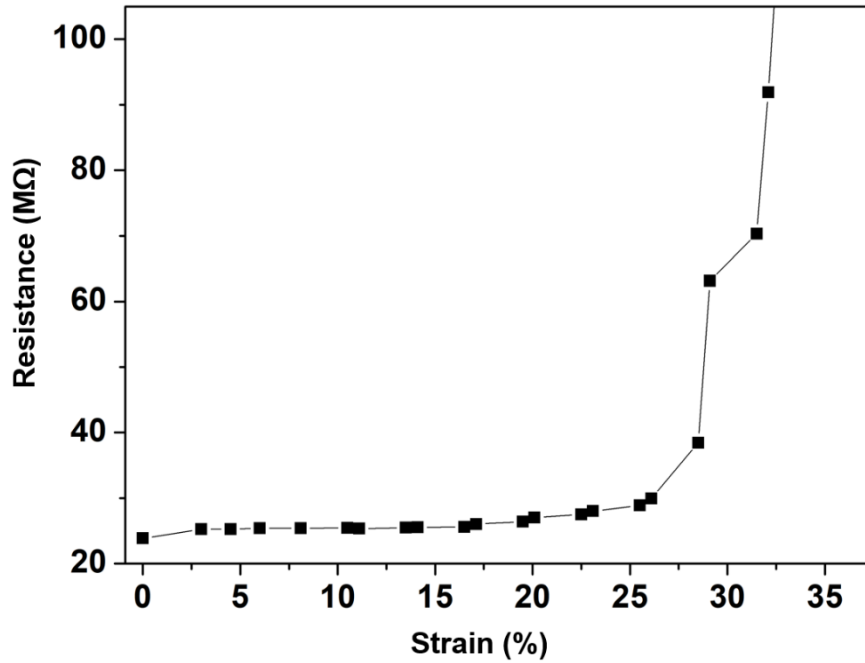


Figure 4.18: Effect of tensile strain on electrical resistance of PCL/PANi 2% blended yarn

4.3.10.3 Effect of twist on electrical resistance of the yarn

It had been reported that for most of conductive yarns as twist was increased, the resistance of ribbon was gradually decreased [133]. The resistance of the yarn before and after twisting was illustrated from Figure 4.19 (a and b). An inversely proportional relationship can be observed between yarn twist and resistance and results have been demonstrated in Figure 4.19 (c). Linear regression line can be fitted with all data. It was given from Figure 4.19 (c) that data points approximated to a linear trend attributed to higher R^2 value of 0.9894.

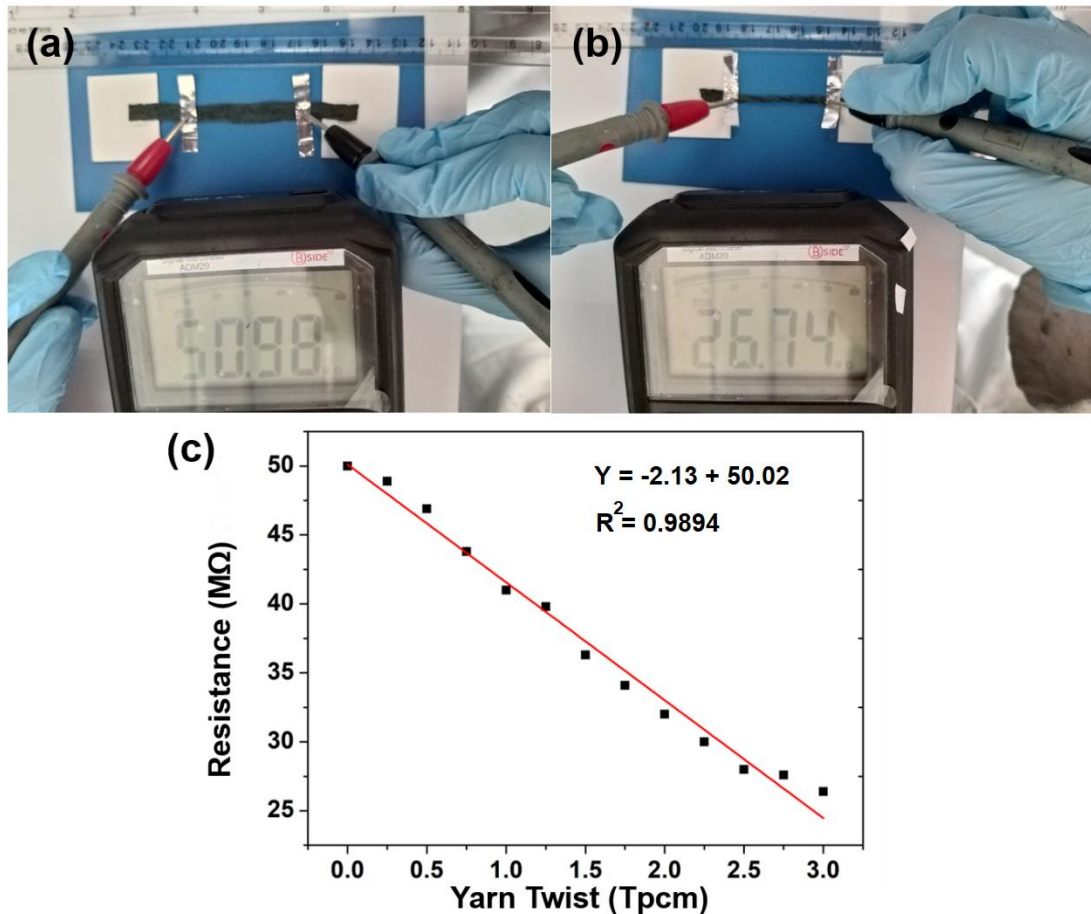


Figure 4.19: PANi 2% nanofibrous fiber ribbons (a) as made, (b) twisted and (c) effect of twist on electrical resistance

4.3.11 Biodegradability

Figure 4.20 shows the image of specimens recovered from compost soil at various level of degradation. Considering the biodegradable applications of yarns, composting is the most practical and preferable disposal route. Temperature and the humidity level affect the hydrolytic degradation of PCL. PCL is found to degrade gradually in a temperature of 58 °C and high humidity condition of 60%. The degradation process is consisted of steps as water absorption, hydrolysis of the ester linkages. As the first step of degradation of oligomer fractions, and diffusion of soluble oligomers by bacteria can take place in the polymer. It can be observed that PCL and PCL/PANi degradation have made the sample embrittled as early as two weeks. PCL/PANi has slower

degradation rate compare to pure PCL. The graph in the Figure 4.21 illustrates the residual weight percentage of compost as a function of time. A rapid increment in degradation can be detected after 14 days of time. Ultimately, it can be concluded that PCL/PANi composite is more susceptible to water, therefore it is considerably biodegradable.

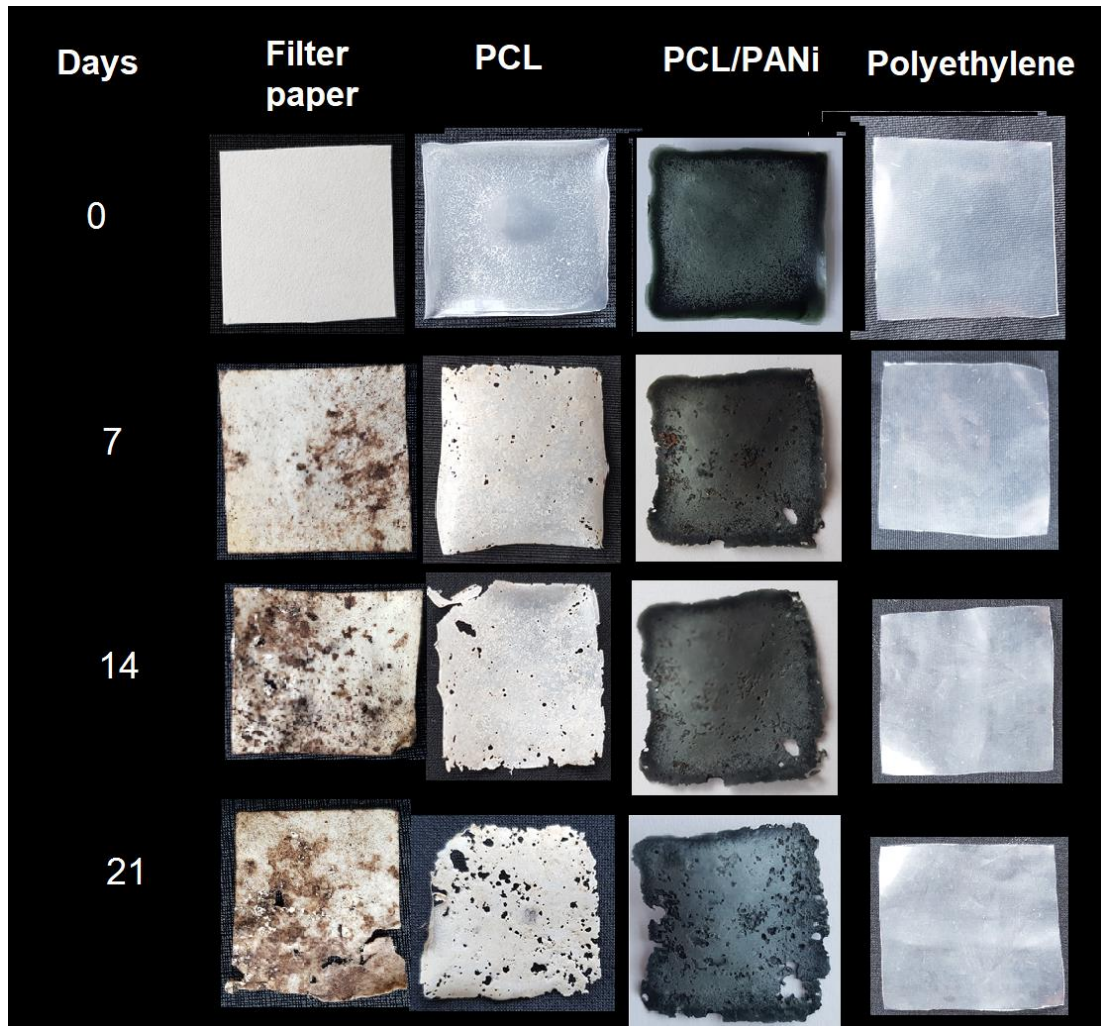


Figure 4.20: Physical appearance of different stages of biodegradation of cellulose filter paper, PCL, PCL/PANi, and polyethylene

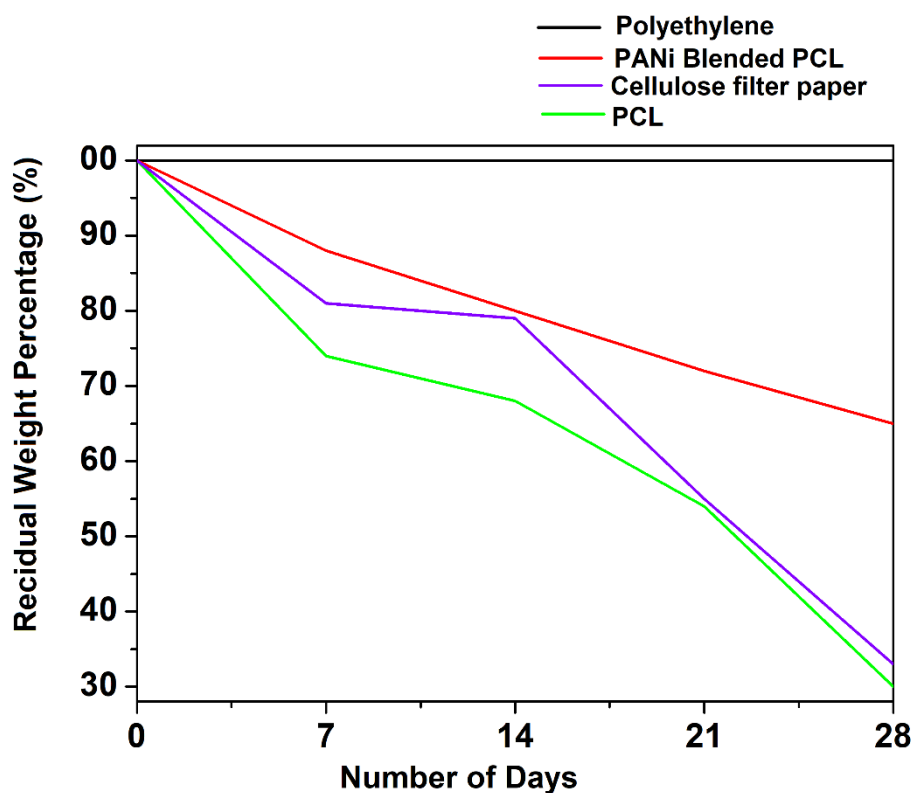


Figure 4.21: Residual weight percentages vs number of days in each stage of biodegradation

It can be seen that there was a correlation between the physical changes in surface morphology and weight loss percentage of casted films. Further, SEM images of nanofibrous degraded films showed more ruptures, grooves, pores, cavities, grooves of nanofibrous surface (Figure 4.22).

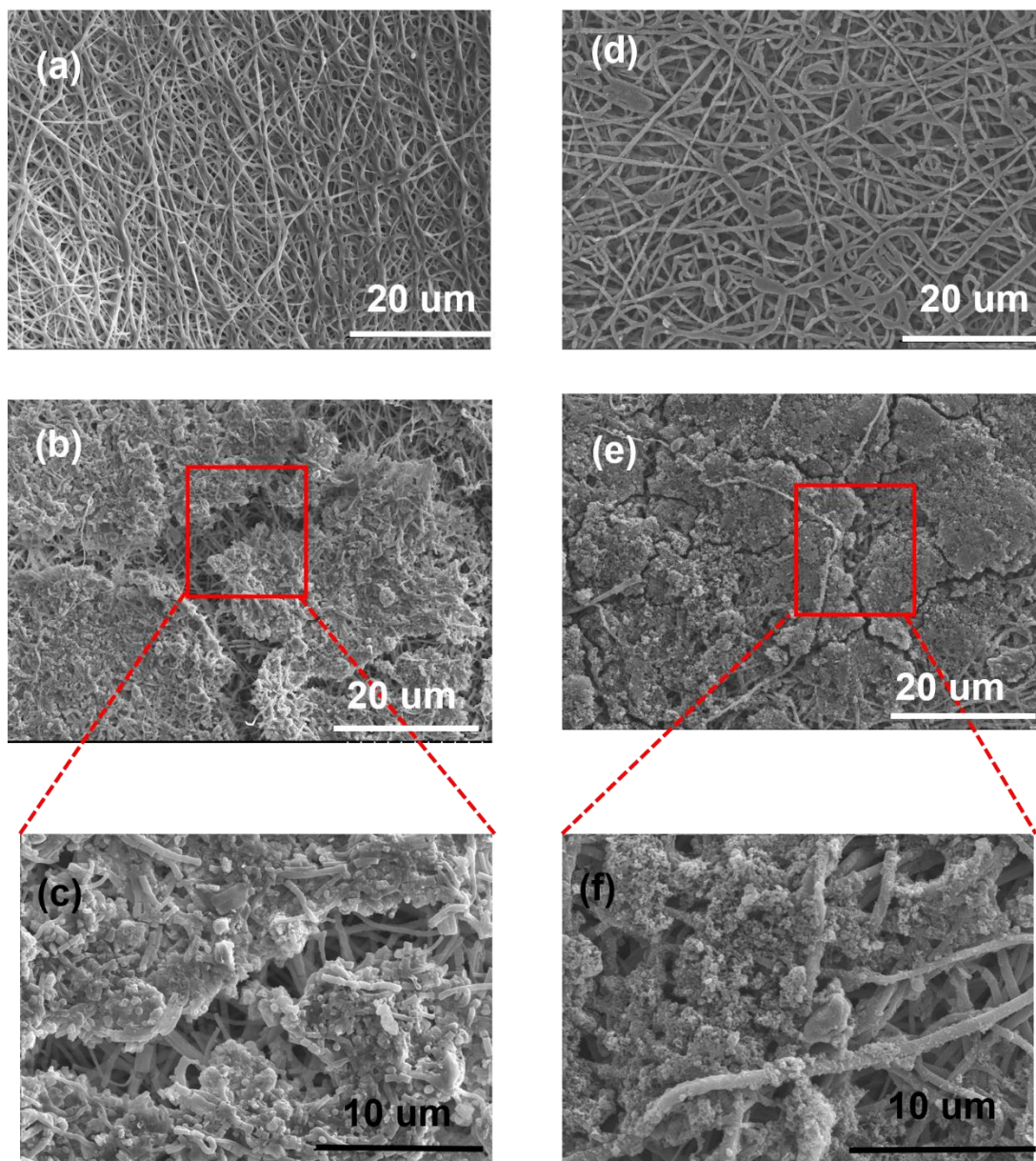


Figure 4.22: SEM images of (a) PCL before and (b) after degradation in soil and (c) magnified SEM image of after degradation in soil. (d) PCL/PANi blended fibres before and (e) after degradation in soil. (f) Magnified SEM image of after degradation in soil

4.4 PANi coated nanofibrous yarns

4.4.1 Effect of dip coating on PANi on fiber morphology, electrical and mechanical properties.

Figure 4.23 (a and b) shows the SEM images of dip coated nanofibers. The fiber mat dipped even in the lowest PANi concentration that was 10% (w/v), shows uneven deposition of PANi particles. It can be seen that the PANi particles have blocked the pores of nanofiber mat, instead of coating around nanofibers. The yarn prepared by these fiber ribbons has shown a resistance of ~ 500 k Ω /cm. The tensile strength of the yarn was also 50% less (2.1 MPa) compared to pure PCL yarn (Figure 4.23 (c)). This may be due to the hydrolysis of polymer by high amount of HCl and CSA in the solution. And the fiber ribbon may become very weak when increasing the PANi concentration up to 30%. Hence, PANi dip coated PCL yarns were found to be not suitable for textile applications. Therefore, the polymerization of aniline was investigated in order to obtain comparatively high conductivity and mechanical strength.

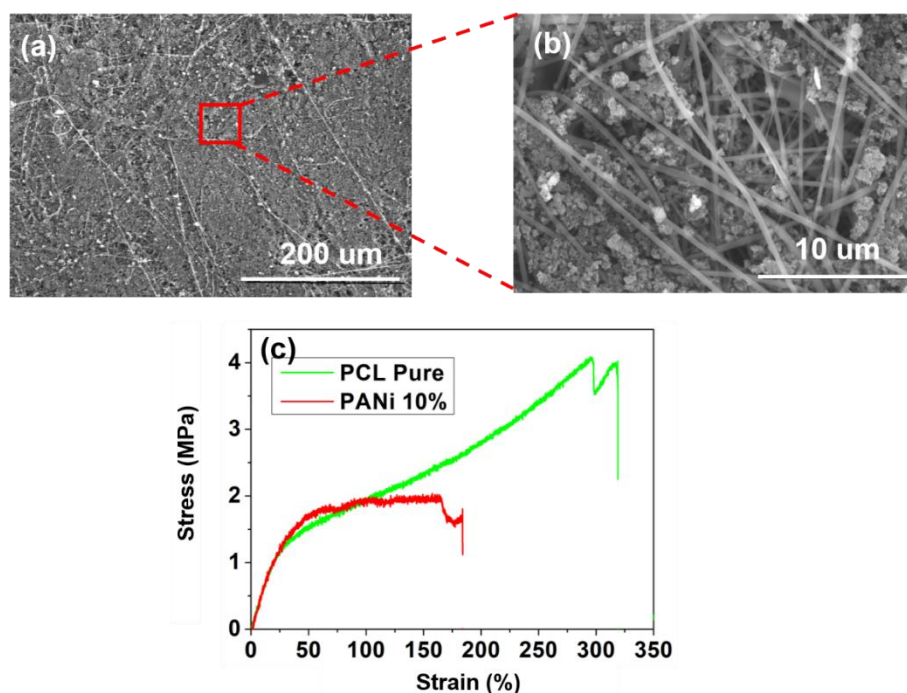


Figure 4.23: (a and b) SEM image and its magnified image of 10% PANi dip coated PCL nanofibers. (c) Stress- strain curve of PCL pure and PANi 10% dip coated nanofibrous yarns.

4.4.2 Studying PANi in-situ polymerization

4.4.2.1 Polymerization of aniline on PCL nanofibers

PANi/PCL CBNY yarns were prepared by a two-step method. First, PCL was electrospun as a partially aligned nanofiber mat using the set up with a rotational drum collector and using the customized electrospinning setup to prepare continuous yarns. The electrospinning parameters were kept as high voltage of 24kV, distance of 15 cm between needle to collector, flow rate of 8 μ l/min, temperature of 27 °C and 50% of relative humidity. Figure 4.24 (a) illustrates the schematic of the customized continuous electrospun yarn manufacturing unit. The rotational speed of the funnel and the take-up roller were maintained at 250 rpm and 2 mm/min, respectively. The twist of the yarn was inserted by rotation of the funnel. After the cone is formed (Figure 4.24 (a')), PCL NY can be drawn towards the take-up roller utilizing a plastic rod. Twisted nanofiber yarns were fabricated using modified continuous electrospinning unit as shown in Figure 4.24 (b). Scanning electron microscopy (SEM) revealed the twisted morphology of the fibers in the yarn and its magnified image revealed a good proportion of fibers aligning in the direction of twist (Figure 4.24 (c)). The yarn exhibited an average diameter of 150 μ m \pm 6. The fibers in the yarn were found to be comprised of fibers with an average diameter of 450 \pm 50 nm.

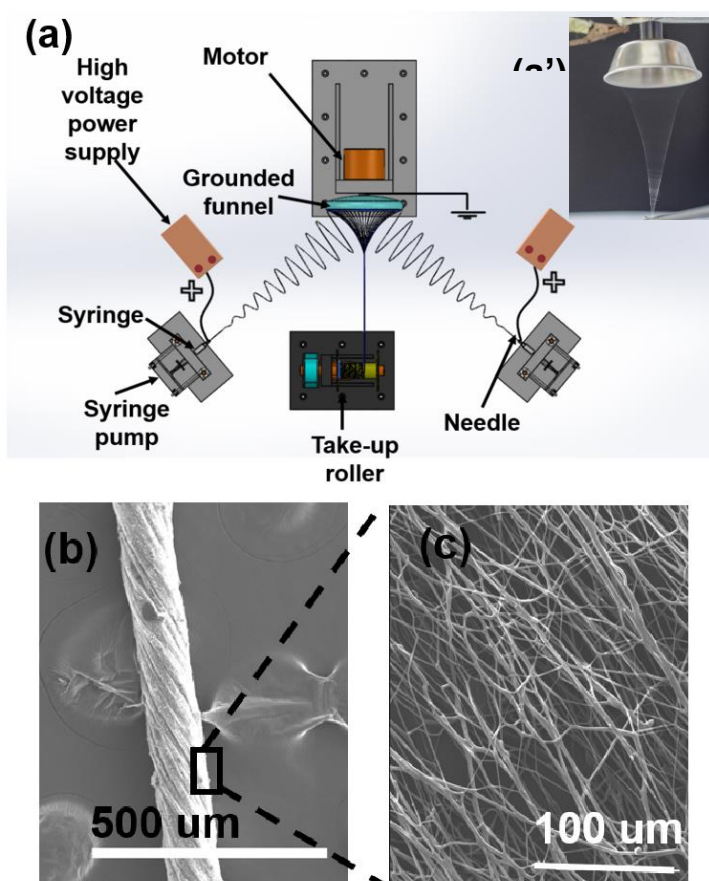


Figure 4.24: (a) Schematic of the apparatus for producing of continuous PCL twisted yarns. (a') The 3D nanofibrous cone drawing from collector. (b and c) SEM image of collected PCL nanofibrous twisted yarn and magnified image of aligned nanofibers.

As the second step, PANi layer was subsequently synthesized on the surface of PCL electrospun yarns by in-situ polymerization process. Briefly, around 0.1g of PCL yarn was wound on a nylon mesh to prepare PCL yarn skein and then this was immersed in 50 ml aniline/HCl solution and this solution was kept in a mechanical shaker with 100 rpm at room temperature for 15 min. Next, 50 ml of $(\text{NH}_4)_2\text{S}_2\text{O}_8$ (APS)/HCl mixture was added dropwise to the solution and agitated in the same conditions for 15 min. Subsequently, the yarn was washed with HCl, deionized water, ethanol and dried in a vacuum oven at 30 °C for 4 hours. $(\text{NH}_4)_2\text{S}_2\text{O}_8$ and aniline were mixed to HCl as shown in Table 4.6.

Table 4.6: Volume of aniline in aniline/HCl mixture and the weight of APS in APS/HCl mixture

Sample name	Aniline volume per 50 ml of HCl (μ l), HCl concentration (M)	APS weight per 50 ml of HCl (g), HCl concentration (M)
0.5% aniline	250, 0.5	0.775, 0.5
1% aniline	500, 1.0	1.550, 1.0
2% aniline	1000, 2.0	3.100, 2.0

This approach of decorating yarn with PANi by in-situ polymerization process is illustrated in Figure 4.25. Here, aniline monomers were converted to PANi through chemical oxidative polymerization [134]. The oxidation of monomer is achieved by using APS as the oxidizing agent. Steps of polymerization reaction are shown in Figure 4.25. The monomer and initiator were added in with 4:5 molar ratio as given in the equation in Figure 4.25.

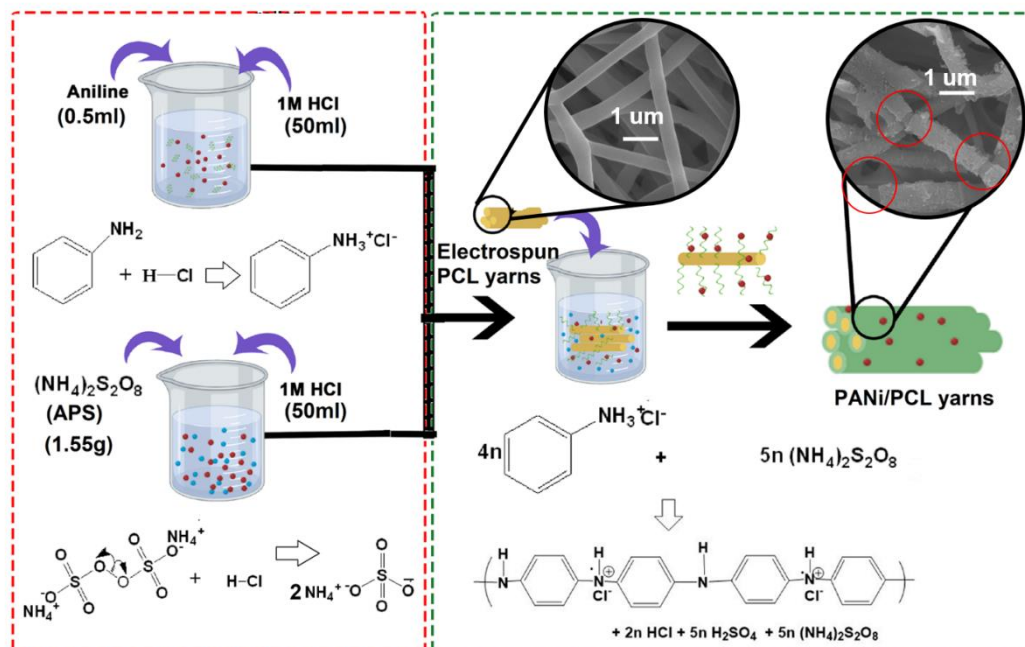


Figure 4.25: Sketch illustration of Fabrication of PANi decorated PCL nano-fibrous yarns

In this method, the formed polymer precipitates in the reaction medium and can be deposited in various non-conductive hydrophilic and hydrophobic surfaces [135]. As demonstrated in Figure 4.26 the starting colorless reaction solution (Figure 4.26 (a)) with the PCL yarn skein becomes pink in color (Figure 4.26 (b-c)). Then intensity of pink gradually reduced and turned into color violet (Figure 4.26 (d-e)) and was transformed to blue (Figure 4.26 (f)). After 4 min induction period, the homogeneous solution was transformed into heterogeneous dark blue precipitate (Figure 4.26 (g)) [136]. After 10 min of reaction time, the yarn skein and polyaniline precipitated in the solution to become dark green in color (Figure 4.26 (h)).

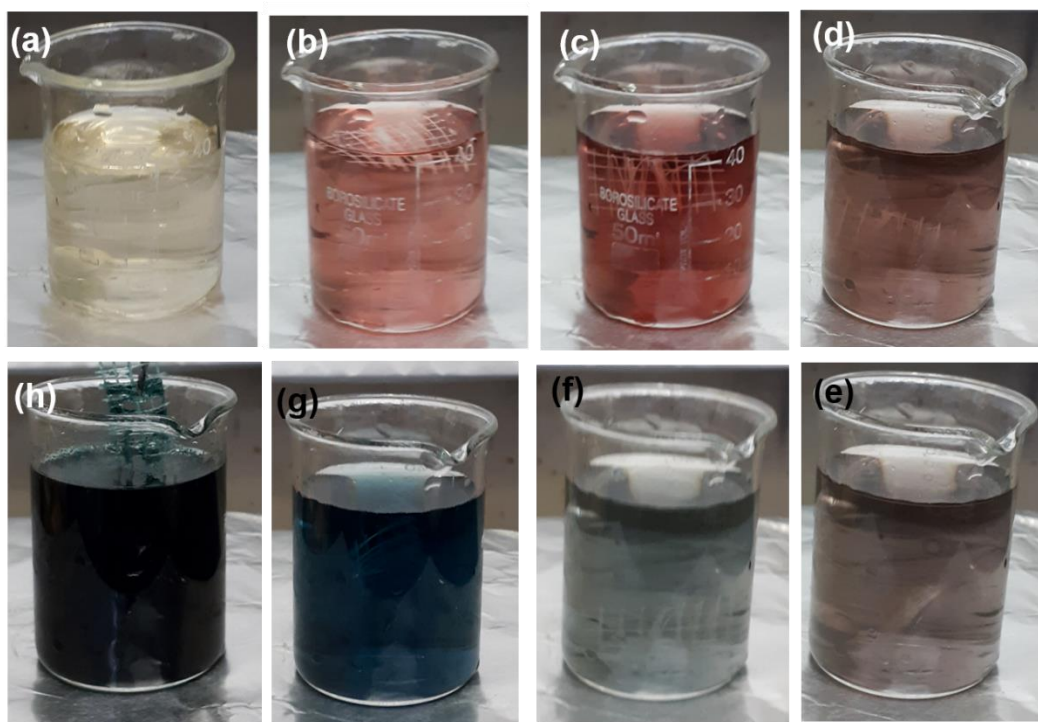


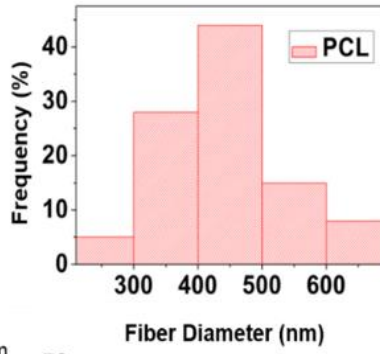
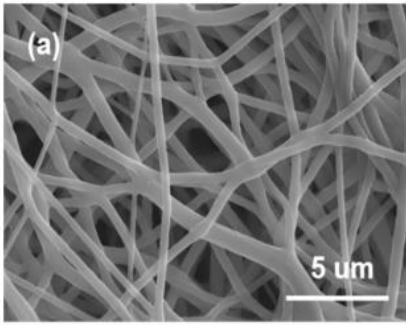
Figure 4.26: Color change of aniline reaction mixture by adding APS after (a) 60 s, (b) 90 s, (c) 120 s, (d) 150 s, (e) 180 s, (f) 220 s, (g) 260 s, (h) 10 min.

The higher conversion (~90%) of aniline to polyaniline can be obtained by keeping the reaction time for 30 min [137]. The monomer, unreacted initiator, and low-molecular-weight and water-soluble oligomers were removed by consecutive washing from 1 M HCl, deionized water, and ethanol. Even after several steps of washing, the PANi clusters were still retained on the PANi/PCL fiber surface [138, 139].

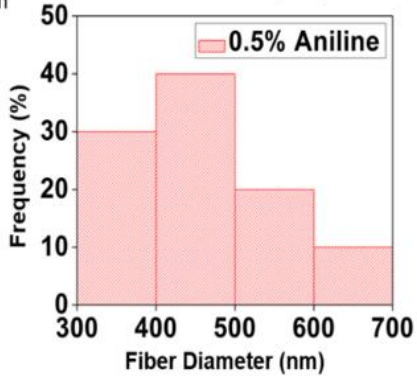
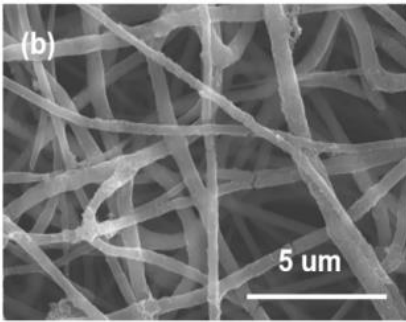
4.4.2.2 Effect of concentration of reaction mixture on fiber morphology

Aniline concentration was varied in the solution to determine the effect on fiber morphology (Figure 4.27 (a-d)). When the aniline concentration was increased, the average fiber diameter (for 50 number of fibers) of PANi decorated fibers were also increased to 443 ± 62 , 457 ± 83 , 468 ± 63 and 554 ± 73 nm, respectively. Previous reports have evidence of increasing of nanofiber diameter by in-situ polymerization of PANi layer on nanofiber surface. For an example polyacrylonitrile (PAN) nanofibers were decorated with PANi and the fiber diameter was increased from 557.6 nm for pure PAN to 667.0 nm for (PANi/PAN) [62]. In the lowest concentration (aniline 0.5%) of reaction mixture, a discontinuous thin layer of PANi sheath was formed on the surface of PCL fibers (figure 2b). Furthermore, the sporadic deposition of polyaniline on the surface of the fibers may have created gaps of conductive pathways. When the concentration of aniline in the reaction mixture was increased, a continuous layer of polyaniline was witnessed with the clusters of PANi self-assembling on the surface of the PANi nanolayer with an increase in the size and number of PANi particles (Figure 4.27 (c and d)). As shown in Figure 4.27(d), a thick layer of polyaniline entirely covered the PCL fiber surface with an increase of the aniline concentration. Here, a complete film of PANi was observed on the PCL fiber surface and the spaces of the fiber bundle were observed to be occupied by PANi. The average diameter of nanofibers has increased by about ~ 100 nm with the deposition of the PANi layer.

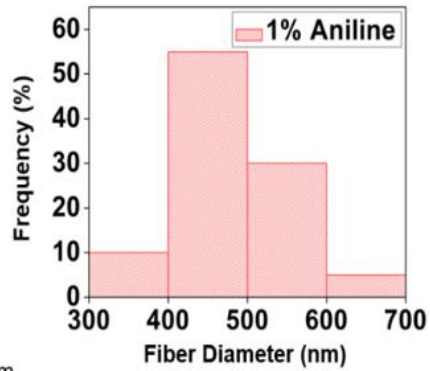
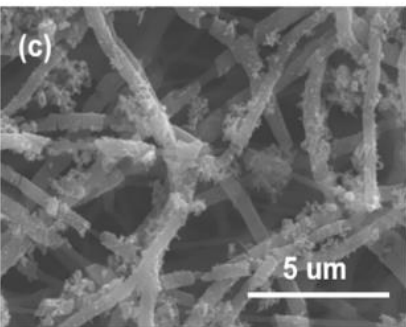
Average Diameter = 443 nm, SD = 62 nm



Average Diameter = 457 nm, SD = 83 nm



Average Diameter = 468 nm, SD = 63 nm



Average Diameter = 554 nm, SD = 73 nm

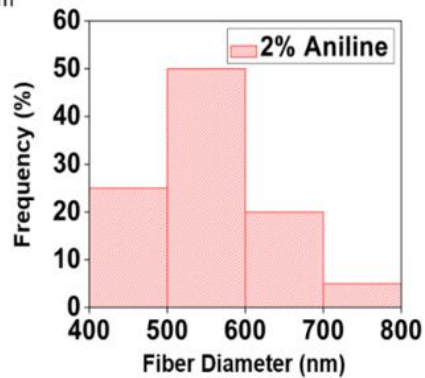
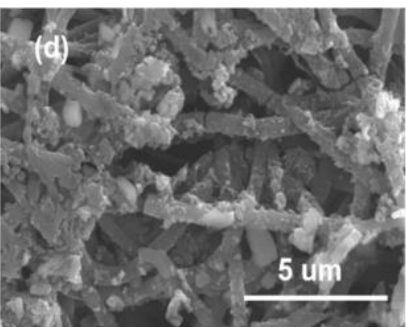


Figure 4.27: SEM images of (a) Pure PCL, (b) aniline 0.5%, (c) aniline 1% (d) aniline 2%.

4.4.3 Conductivity measurement

The effect of concentration of aniline on the resistivity of PANi/PCL core-shell yarns was investigated (Figure 4.28). The resistivity of the yarns was decreased as 162 ± 15 , 50 ± 8 and 6 ± 2 k Ω /cm for yarns coated by aniline concentrations of 0.5%, 1% and 2%, respectively. This decrease in resistivity could be attributed to the synthesizing of a continuous unbroken layer of polyaniline on the surface of the PCL fibers whereas only a discontinuous thin layer was observed for lower concentration of aniline resulting in higher resistivity. Furthermore, the resistivity values of core-shell fibers may be influenced by the degree of doping and the morphological structure of the polyaniline. Conductivity is found to increase proportionally with the amount of dopant used [42]. For low concentrations of aniline, the H⁺ dopant concentration was low resulting in polymerization of structured “tail–tail”, “head–head”, adducts, which could affect to decline in the electrical conductivity of Polyaniline. When the H⁺ concentration was high, the polymerization of aniline formed usually “head–tail” connections leading to lower resistivity values as observed in Figure 4.28 [140].

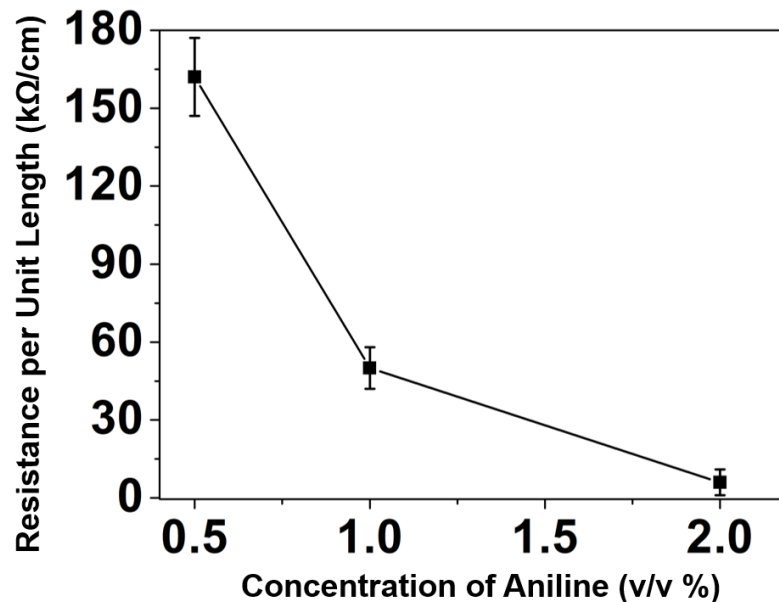


Figure 4.28: Resistance per unit length versus used aniline concentration in reaction mixture.

The second factor was the morphological structure of the PANi/PCL fiber surface. For low concentrations, although even thin films were created, the conductive pathways may be disturbed by discontinuity of the PANi layer. When the concentration was double from the minimum value, PANi particles on the surface of the fibers and space between fibers was increased further. This thick, uniform structure with dense structure enhanced the continuity of conductive pathways enabling the high conductivity as observed in our experiments. Furthermore, increasing the concentration of aniline caused agglomeration of PANi and adhered to the surface unevenly. Thereby, the structure was rough and the thickness was uneven. Moreover, PCL could be subjected to short-term degradation in 2M HCl due to hydrolysis of polymer backbone [125, 141]. Although, the average resistivity values were comparatively high, these structural defects hindered the traffic of electrons and a wide range of resistivity variation could be seen in the yarn coated from 2% aniline reaction mixture .

Figure 4.29 (a) shows the raw data of supplied current against measured voltage in four-probe technique. The gradient of the graph increased with increasing aniline content which represents the declining resistance for a material with same dimensions, 20 x 20 x 0.05 mm. Figure 4.29 (b) demonstrates the calculated conductivity for four-probe data. Table 4.7 illustrates resistivity values taken from four-probe methods and two-probe methods. Here, the volume resistivity and resistance per unit length were reported for a yarn with a diameter of ~0.8mm. The average resistance by 10 mm distance was taken from the method which was demonstrated in section 3.6. As similar, the conductivity data for PANi blended yarns, the resistivity values are taken from the four-probe method was higher compared to measurements taken from two probes of ohmmeter.

It was hard to find accessible literature on PANi in-situ polymerized PCL nanofibers. Across the literature, there are studies of development of PANi coated poly(L-lactic acid-co-3-caprolactone)/silk fibroin (PS) nanofibers [43]. The conductivity of PANi/PCL/PS nanofibers coated with 1.6% (w/v) PANi concentration was around 30.5 ± 3.1 mS/cm.

The value was comparatively higher than the conductivity level obtained in this study which was 3.3 ± 0.8 mS/cm for nanofibers obtained by aniline 2% solution. In the reported study, PANi was coated by coaxial spinning. Therefore, effective concentration was higher than in situ polymerization.

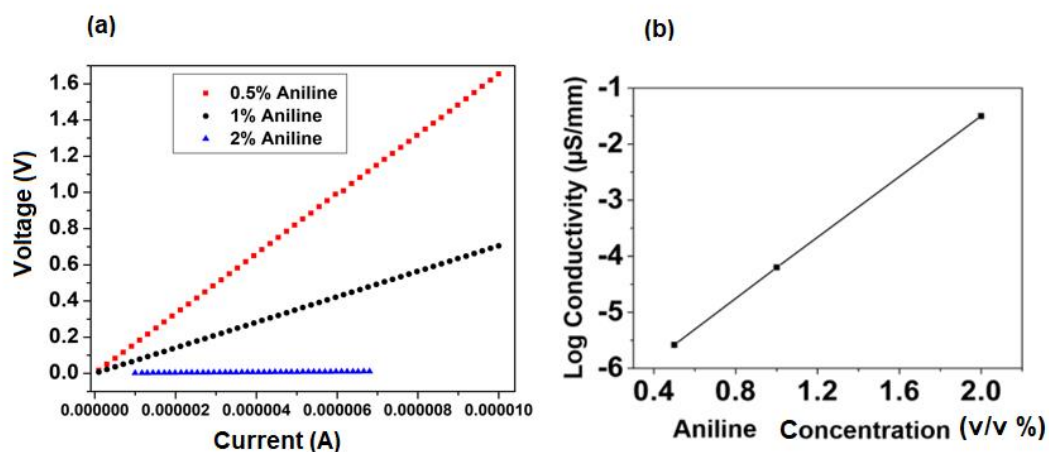


Figure 4.29: (a) The four probe V - I characteristics of PANi coated electrospun mats, (b) aniline concentration vs log value of conductivity measured from four probe

Table 4.7: Measuring resistivity by different methods

Sample	Resistivity(4 probe, $\text{k}\Omega\text{mm}$)	Resistance per unit length (Ohmmeter, $\text{k}\Omega/\text{cm}$)	Resistivity(Ohmmeter, $\text{k}\Omega\text{mm}$)
Aniline 0.5%	36.67 ± 4.5	162 ± 15	8.1 ± 2.25
Aniline 1%	15.70 ± 1.2	50 ± 8	2.47 ± 0.83
Aniline 2%	0.30 ± 0.12	6 ± 2	0.30 ± 0.1

4.4.4 Nanofibrous yarn formation

The conductive electrospun mats were coated from aniline 1% precursor solution. In order to form yarns, 5cm x 0.5cm stripes were cut from the mat and twisted onto a single yarn having a twist level of 30 twists per inch. 2 – ply and 3 –ply yarns were also produced using the same procedure as preparing PANi blended yarns. SEM images of ply yarns are shown in Figure 4.30.

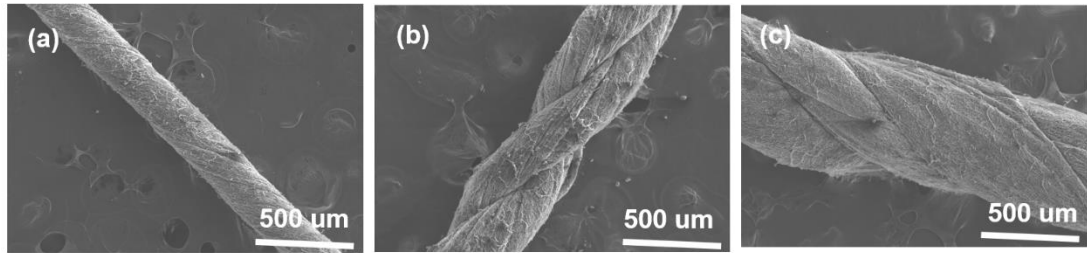


Figure 4.30: SEM images of (a) 1- ply yarn, (b) 2 – ply yarn and (c) 3 – ply yarn

The resistive properties of plied yarns were investigated by measuring the resistance per unit length. The increase of number of plies to 3 has resulted in a decrease in resistance (Figure 4.31). This reduction of resistance can be explained in terms of the increase of the cross sectional area using the same equation (Equation (2) in section 4.3.3).

The equation indicates that the, resistance is inversely proportional to the cross-sectional area. Number of plies of a yarn is directly proportional to the diameter of the thread (bundle of yarns) and thus the area, and therefore this will result in a reduction of resistance.

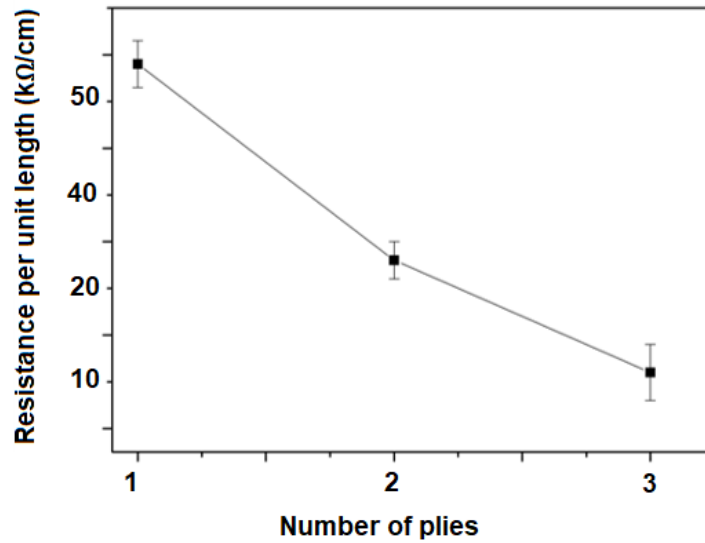


Figure 4.31: Effect of number of plies on resistance

4.4.5 Effect of aniline concentration on mechanical properties of yarns

The influence of content of aniline on the mechanical properties of PANi/PCL nanofiber yarns was investigated. Here, the different amounts of PANi coated yarn were subjected to a series of tensile tests. Figure 4.32 (a) shows the stress-strain curves of nanofiber yarns prepared from polymerized aniline content of 0.5 %, 1 %, 2 %. Figure 4.32 (b and c) represents the mechanical parameters of PANi coated PCL/PANi electrospun nanofibrous yarns, including the representative Young's modulus and energy at break. As shown in Figure 4.32, all samples exhibited a linear elastic behavior up to ~25% of strain. The tensile strength, modulus and energy at break decreased with increasing content of PANi on the fiber surface. For instance, the tensile strength decreased from 4.16 MPa for pure PCL to 2.76 MPa for 0.5 % aniline, 2.37 MPa for aniline 1% and 0.76 MPa for aniline 2%, respectively. The energy at break also decreased from 0.03 J for pure PCL to 0.018 J for aniline 0.5 %, 0.013 J for aniline 1% and 0.005 J for aniline 2%, respectively. The Young's modulus within the

elastic region was decreased from 4.6 MPa for pure PCL to 2.2 MPa for aniline 0.5 %, 2.14 MPa for aniline 1% and 0.15 MPa for aniline 2%, respectively.

The trend of these results with respect to the aniline concentration was similar to the trend of previously reported study about PANi coated core-sheath nanofibers [43]. In the reported study, PANi was coated on poly(L-lactic acid-co-3-caprolactone)/silk fibroin (PS) nanofibers through coaxial spinning. Tensile strength and Young's modulus were 5.7 ± 0.9 MPa and 7.2 ± 1.2 MPa, respectively for 1.6% (v/w) of PANi concentration. It can be observed that modulus and tensile strength value of this study were lower than the reported results. The reason was that the initial (before treating with PANi) tensile strength and Young's modulus of nanofibers were 13.7 ± 1.5 MPa and 7.2 ± 1.2 MPa that values are higher than the tensile strength and Young's modulus values obtained for pure PCL nanofibers in this study.

Although the elasticity decreased with increasing PANi, the nanofibrous yarns were still relatively elastic to be used for textile or biomedical applications. PANi coating have not supported an increment of modulus or tensile strength as the PANi particles which acted as fillers in PANi blended yarns. The hydrolysis of polymer chain at low pH was due to increasing concentration of HCl in the reaction mixtures that may also have affected a tensile strength reduction [124, 125].

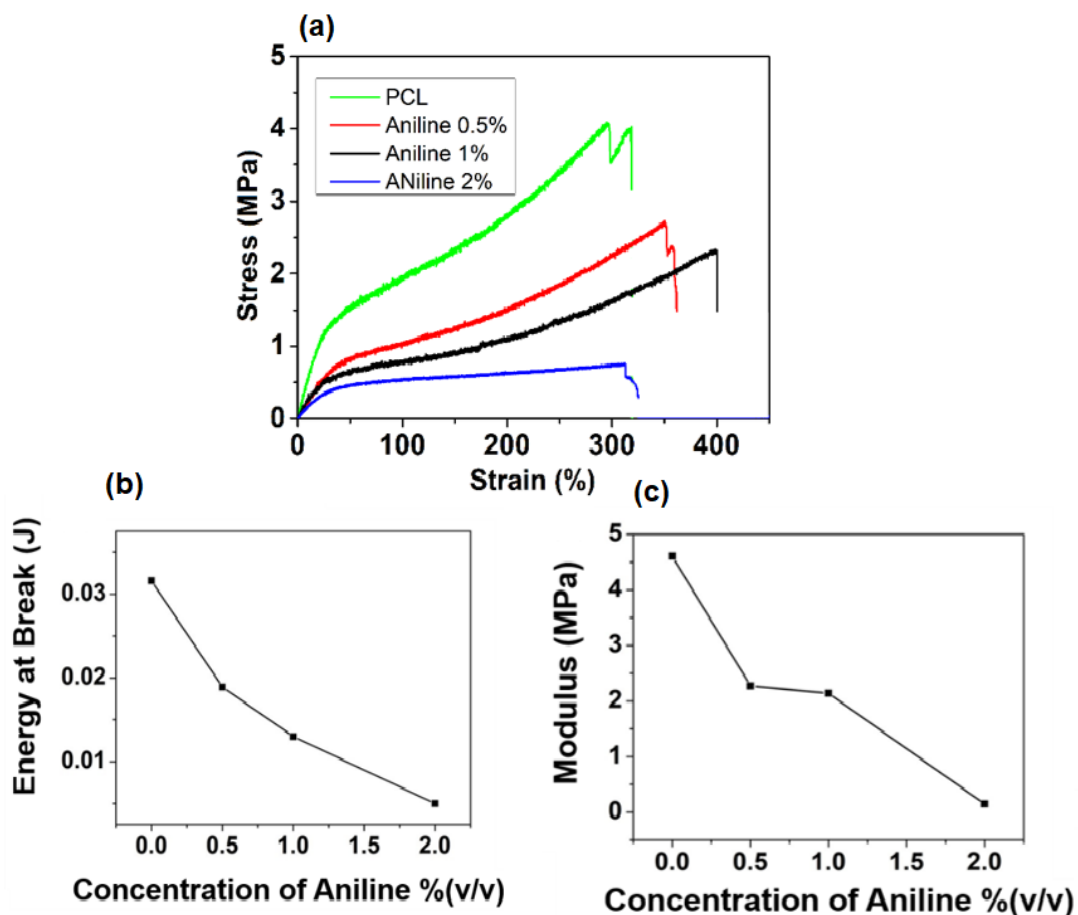


Figure 4.32: (a) The stress–strain curves of Pure PCL, aniline 0.5%, aniline 1%, aniline 2%, (b) effect of aniline concentration on energy at break value of yarns, (c) effect of aniline concentration on modulus of yarns

4.4.6 TGA analysis

According to TGA curves in Figure 4.33 a pattern can be seen in weight loss occurring due to loss of water, HCl and other volatile solvents between 0-120 °C [142], onset temperature and weight loss attribute to PCL degradation, and residual weight at 600 °C. The weight loss is attributed to evaporation of HCl, water and other volatile compounds that were increased with increasing the PANi content. This is due to water molecules interacting to form hydrogen bonds with doped PANi during the polymerization [143]. Therefore, first weight loss is a good indication for content of PANi in PANi/PCL yarns.

The next main degradation event occurs at an onset temperature between 375 °C – 385 °C (see Table 4.8) which is attributed to the degradation of PCL. The onset temperature of PCL degradation is found to be decreased from 385.85 °C for pure PCL to 374.23 °C for aniline 2% which represents degradation of PCL. Thermal stability analysis of PCL/PANi samples were carried out by reading the temperature as taking the temperature attributes to 95% residual weight of PCL as the thermal stable temperature. Thermal stable temperature was reduced with increasing the aniline concentration. The PANi coted PCL composites revealed a higher amount of residue with the increase the content of PANi in the composite. This indicated that coating PANi acted as a protective barrier on the surface of PCL against thermal degradation in PANi/PCL composite membranes [144].

Table 4.8: TGA data compilation for the tested fibers, including weight loss attributed to HCL and water, second third onset, weight loss attributed to PCL, residual weight and thermal stability

Sample	Weight loss HCl (%),	Onset PCL (°C)	Weight loss PCL (%)	Residual weight (%)	Thermal stability (°C)
PANi powder	67, 12.82	-	-	44.82	64.91
Aniline 2%	15.80	374.23	53.88	30.32	95.76
Aniline 1%	7.22	378.28	89.04	3.76	187.72
Aniline 0.5%	2.78	389.04	95.80	1.33	251.55
PCL pure	-	385.85	97.53	2.47	356.27

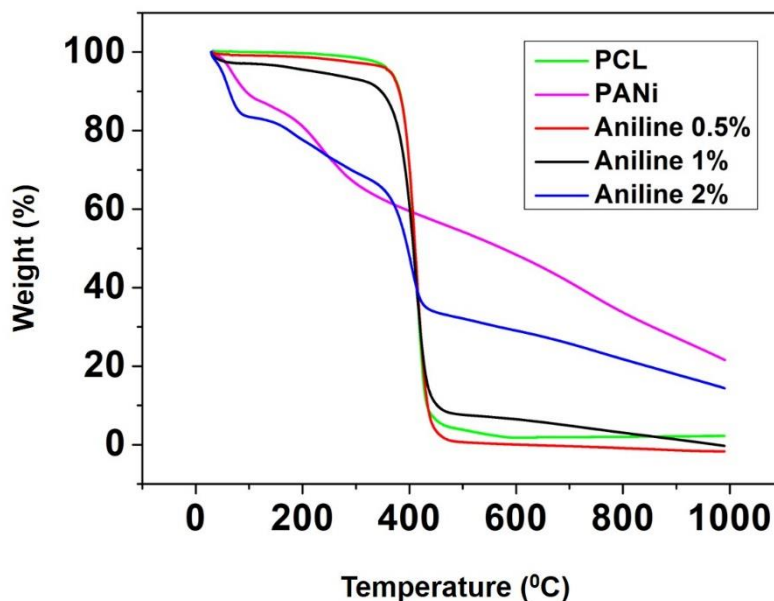


Figure 4.33: TGA profiles of pure PCL, aniline 0.5%, aniline 1%, aniline 2%

4.4.7 DSC analysis

Thermal properties of PANI/PCL yarn were investigated using Differential Scanning Calorimetry (DSC) analysis as shown in Figure 4.34. Melting temperature (T_m) and melting enthalpy (ΔH_m) were determined from the DSC heating thermograms of PCL/PANI yarns. Two endothermic peaks at $\sim 126^\circ\text{C}$ and a broad exothermic peak at $150\text{-}250^\circ\text{C}$ were observed for pure polyaniline. The endothermic peak at around 100°C could be attributed to the evaporation of water bound to the PANi crystal lattice [129]. A reduction of weight was exhibited in the TGA curves further supporting this observation (Figure 4.34). The exothermic reaction has resulted from crosslink

reactions led by coupling of $\left[\text{C}_6\text{H}_4\text{-NH-C}_6\text{H}_4\text{-NH} \right]$ and $\left[\text{C}_6\text{H}_4\text{-N=C}_6\text{H}_4\text{=N} \right]$ through the interaction of the N with its neighboring quinoid [131].

The DSC thermogram of PCL nanofiber yarns (Figure 4.34) showed a peak corresponding at 60°C that is attributed to the melting point with an enthalpy of 71.75 J/g . This melting enthalpy of PCL is found to decrease from $\Delta H_m=71.75\text{ J/g}$ for neat PCL yarn to $\Delta H_m=51.50\text{ J/g}$ for PCL/PANi yarns made from 1% aniline concentration. The melting enthalpy of the PCL/PANi yarns from 2% aniline concentration was

further reduced to the lowest levels which may be attributed to the disturbances to the crystal structure of PCL when more PANI molecules are formed on the surface. Interestingly, another broad peak at $\sim 80^\circ\text{C}$ has emerged next to the melting peak for the PCL/PANi yarns made from the highest concentration of aniline. This peak could resemble the endothermic peak of PANi itself which has shifted downward from the position observed for pure PANi. Furthermore, the T_m of PCL decreased from 60.64°C for pure PCL to 58.48°C for PANI/PCL NY. This reduction of PCL melting temperature, thermal stable temperature (Table 4.8) and percentage of crystallinity (Table 4.9) were further supports the idea that in presence of PANi and HCl, either the size of PCL crystals has been reduced (Table 4.9) or creation of crystal defect due to the hydrolysis of PCL.

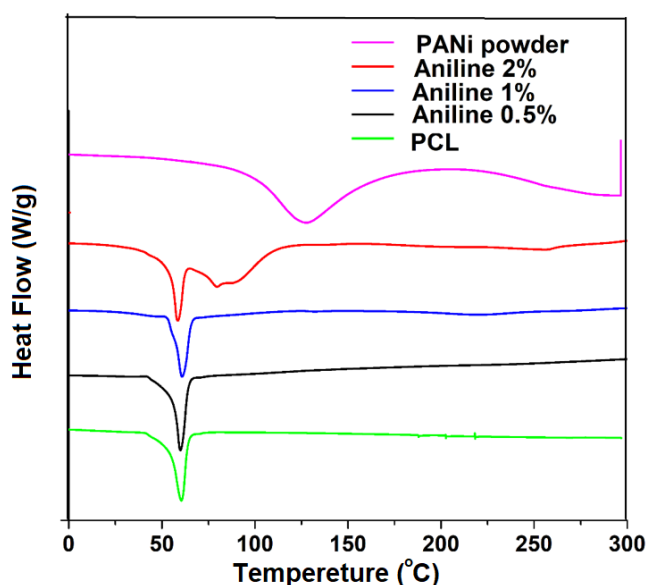


Figure 4.34: DSC profile of pure PCL, aniline 0.5%, aniline 1%, aniline 2%

Table 4.9. Melting temperature, melting enthalpy and percentage crystallinity of pure PCL, aniline 0.5%, aniline 1%, aniline 2%

Sample Ref.	Melting Temperature of PCL (T_m , °C)	Melting Enthalpy PCL (ΔH_m , J/g)	Percentage crystallinity (%)
PCL Pure	60.64	71.95	51.57
Aniline 0.5%	59.96	68.87	48.74
Aniline 1%	60.81	51.50	36.55
Aniline 2%	58.48	254.80	182.07

4.4.8 FTIR analysis

FTIR spectra for Pure PCL and aniline 1% were demonstrated in Figure 4.35. The characteristic peaks of PCL and PANi was given in the Table 4.10.

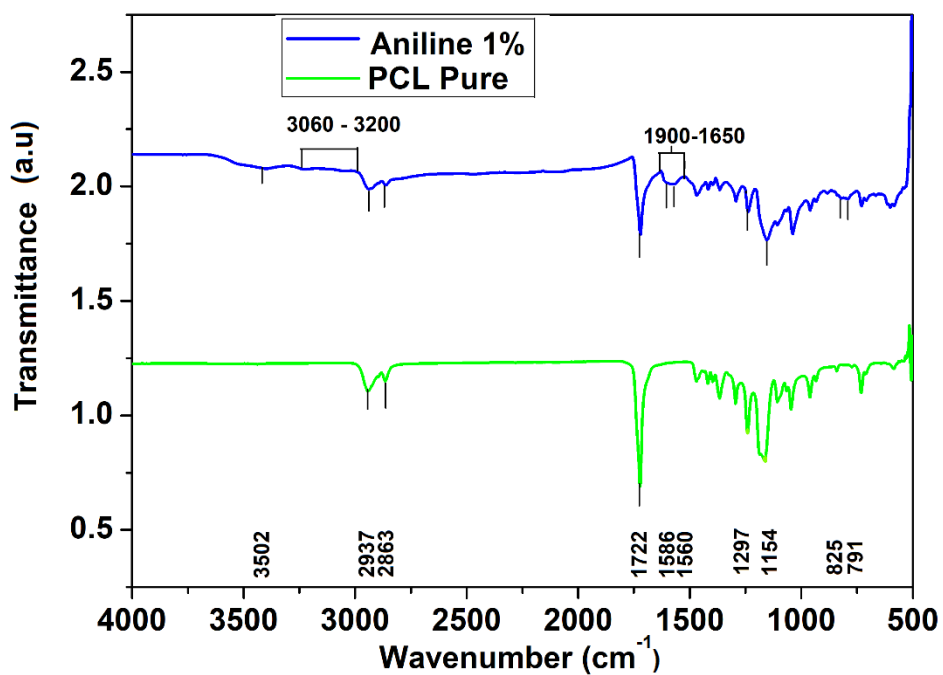


Figure 4.35: FTIR spectra of pure PCL and aniline 1%

Table 4.10. Characterization peaks of PCL and PANi for aniline 1% nanofibers

Sample Name	Peak	Wave number(cm ⁻¹)
PCL [132]	-C-H ₂ - stretching	2937 and 2863
	Carbonyl groups	1722
PANi [96]	γ(C-H) aromatic ring	791
	Vibration mode of quinoid ring	1154
	Stretching vibration of C-N	1297
	N-H stretching vibration	3502
	stretching vibration of the C=C in the benzenoid units	1560
	Weak aromatic overtone and combination bands	1650 to 1900
	Stretching vibrations of aromatic C-H	3060–3200
	Stretching vibration of N-quinoid ring	1586
	N-H bending	830

4.4.9 Electro-mechanical behaviour of electro-conductive yarn

4.4.9.1 Effect of weaving and sewing on electrical resistance of the yarn

The plied yarn was fed into a sewing needle and was stitched onto a polyamide fabric successfully (Figure 4.36 (a)). Figure 4.36 (b) and (c) show microscopic and SEM images of sewn yarn respectively. It was verified that the yarn was mechanically strong enough to be sewn with a sewing needle. The PCL/PANi conductive yarn with a diameter of ~ 0.8 mm sewn into fabric with a length of 40 mm has indicated a resistance of 197.9 k Ω . The calculated resistance per unit length was ~ 50 k Ω /cm and volume resistivity was 2.47 k Ω mm which is equal to the calculated resistivity in section 4.4.3 for aniline 1%.

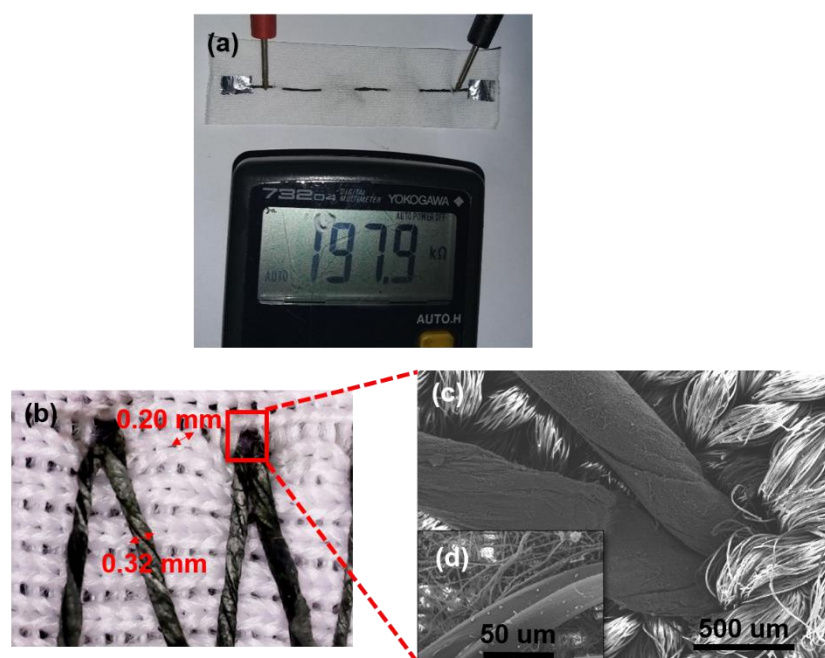


Figure 4.36: Aniline 1% coated nanofibrous yarns. (a) Image of yarn stitched on a nylon fabric, (b) microscopic image of yarn stitched on the nylon fabric.

To demonstrate the ability to incorporate this yarn into fabrics, weaving was successfully performed as shown in (Figure 4.37 (a-d)). In the design of the fabric, 2-ply conventional polyamide yarns were used as weft in the woven structure while the CBNYs were being used as the warp yarns. The resistance of the two ends of a warp yarn with 1.5 cm length and ~ 0.8 mm diameter in the fabric was 80.1 k Ω . The

calculated volume resistivity was $2.68 \text{ k}\Omega\text{mm}$ which is closer to calculated resistivity, $2.47 \text{ k}\Omega\text{mm}$ in section 1.4.2 for aniline 1%. For both sewn and woven yarn. Hence, it is clear that resistivity of the material does not change with mechanical deformation of material during sewing and weaving.

Upon folding and unfolding, increasing and decreasing resistance caused by disconnecting and connecting points of the yarns of the fabric (ex: point A and B in Figure 4.37 (e)). The resistance of the yarn decreased by approximately four times that can be seen from two resistance values ($80.1 \text{ k}\Omega$ and $14.1 \text{ k}\Omega$) of multimeter in Figure 4.37 (a, b and f). The reason is that length is reduced by 50% and the width is increased by two times as described in section 4.3.10.

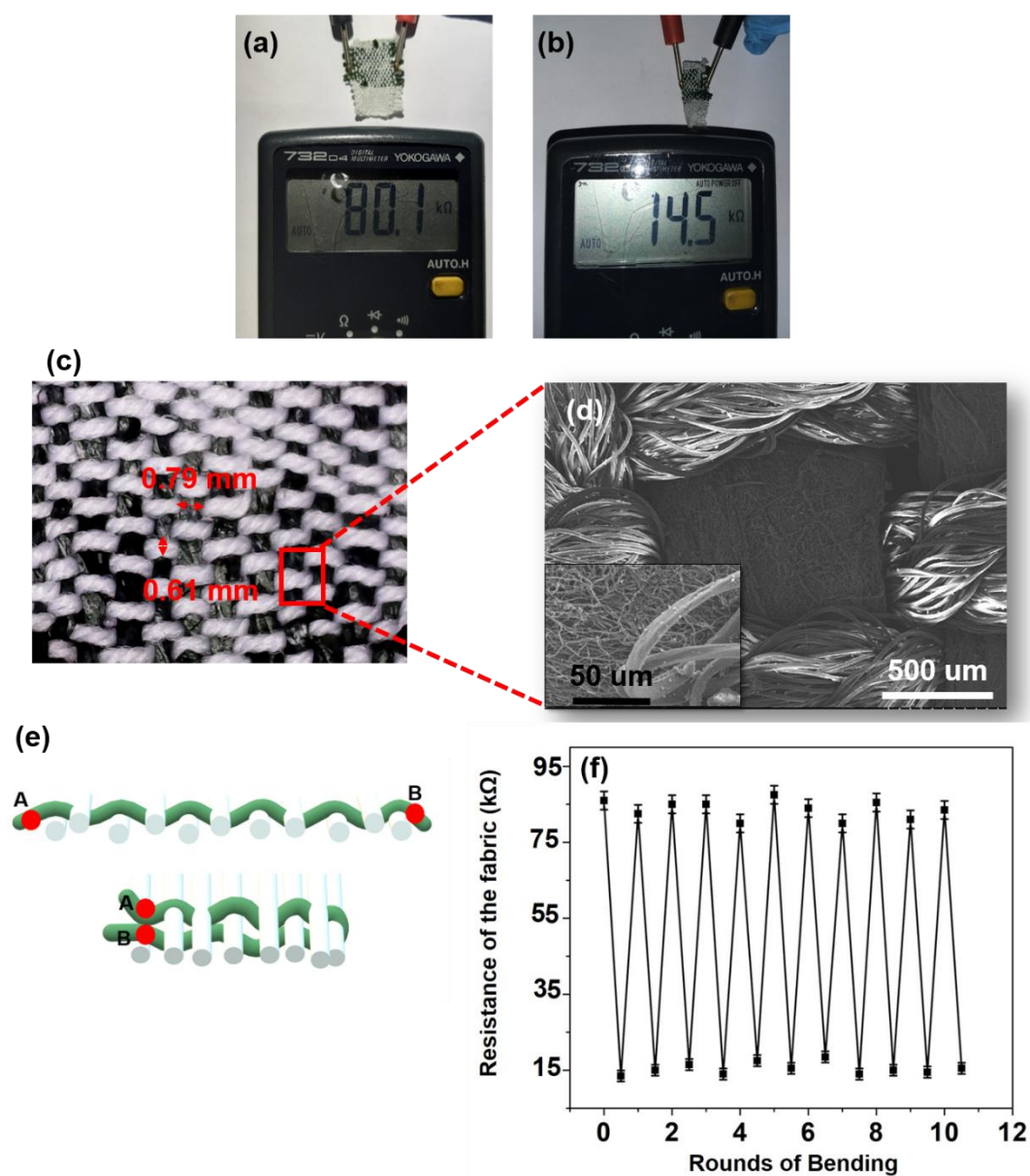


Figure 4.37: Fabric woven with aniline 1% coated nanofibrous yarns and 2-ply nylon yarns. (a) Conductivity measuring of unfolded fabric, (b) conductivity measuring of folded fabric, (c) microscopic image the fabric, (d) SEM image of the fabric (e) demonstrating yarn short circuiting by folding, (f) illustrating resistance change by number of folding cycles.

4.4.9.2 Effect of tensile strain on electrical resistance of the yarn

The relationship between the electrical resistance and the applied strain to the yarn was investigated to support the intended wearable applications of this yarn (Figure 4.38). The electrical resistance increased exponentially with the applied strain on yarn. This can be attributed to the break-down of conductive regions of the PANi polymer with applied strain making it difficult for the intermolecular charge transfer to take place.

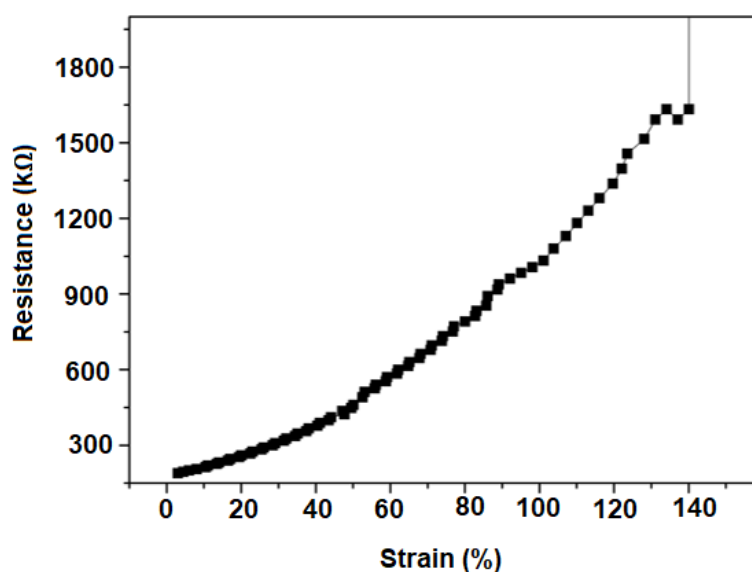


Figure 4.38: Effect of tensile strain on electrical resistance of yarn.

Wearable applications envisaged for this yarn is subjected to constant stretch and recovery cycles arising from body movements. The electrical resistance of PCL/PANI yarn for seven repeated stretch-recovery cycles was measured (Figure 4.39). The yarns were subjected to 20% strain and released at a displacement rate of 0.16 cm/s. The yarns exhibited an increase and decrease of resistance corresponding to stretch and recovery, respectively. The rate of increase and decrease was observed to be consistent for all stretch-recovery cycles demonstrating the repeatability of this process. This can be attributed to the continuous coverage of the PCL fiber surface by polyaniline ensuring that the conductive pathways are not easily disturbed at 20% strain. Interestingly, the resistance changes almost instantaneously with the stretch for multiple stretch and recovery cycles. This rapid and sensitive response to mechanical

loading and unloading is promising to validate the possibility of the applications of PCL/PANi conductive yarns as strain sensors for human motion monitoring

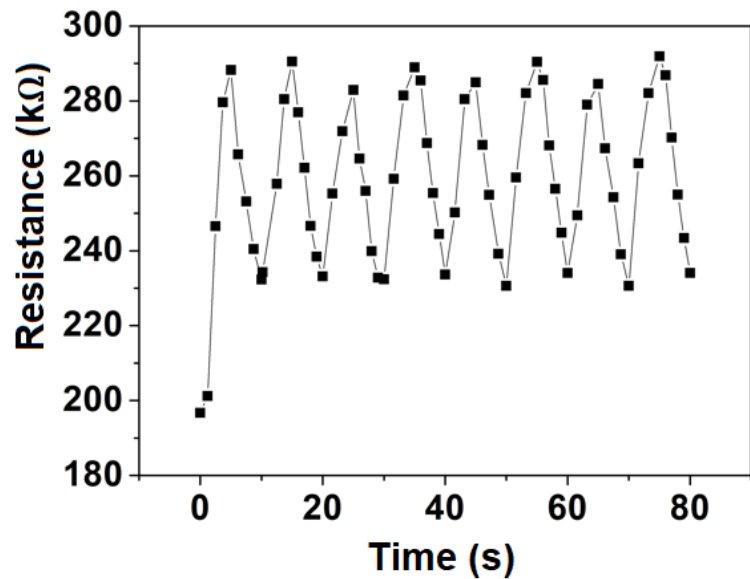


Figure 4.39: Time-dependent normalized resistance change of the yarn under maximum strains of 20%.

4.4.9.3 Effect of twist on electrical resistance of the yarn

The resistance of the yarn was reduced after twisting of the electrospun mat. This can be seen in Figure 4.40 (a and b). An inversely proportional relationship was found between yarn twist and the resistance and results have been demonstrated in Figure 4.40 (c). Linear regression line can be fitted to all the data showing a linear inverse relationship between the yarn twist and the resistance. It was given from Figure 4.40 (d) that data points approximated to a linear trend attributed to higher R^2 value of $R^2 = 0.9936$ that is closer to $R^2 = 1$.

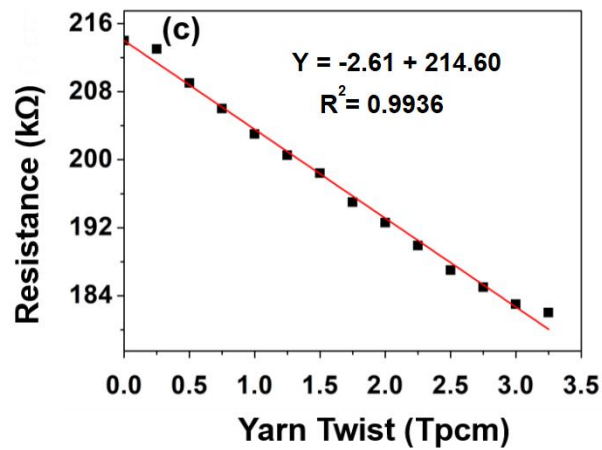
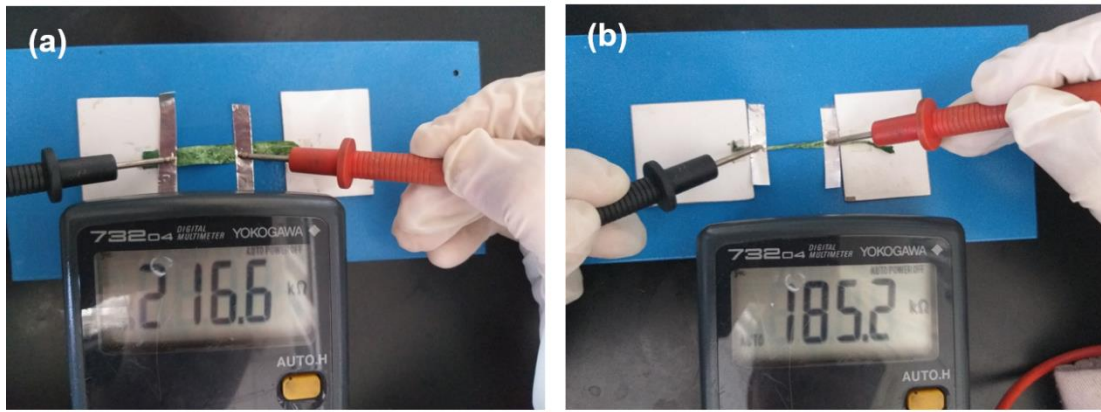


Figure 4.40: Aniline 1% nanofibrous fiber ribbons (a) as made, (b) twisted, (c) effect of twist on electrical resistance

4.4.10 Biodegradability

Degradation of PCL may take place in various ecosystems such as water, soil, and compost due to the action of aerobic and anaerobic microorganisms [145]. The degradation process has consisted of steps as water absorption, hydrolysis of the ester linkages and [77].

It can be observed that PCL and PCL/PANi degradation were started by sample embrittlement as early as one week. PCL/PANi exhibited a slower degradation rate compared to pure PCL. As illustrated in Figure 4.41, a rapid increment in degradation can be detected after 21 days of time due to the removal of PANi layer (Figure 4.42).

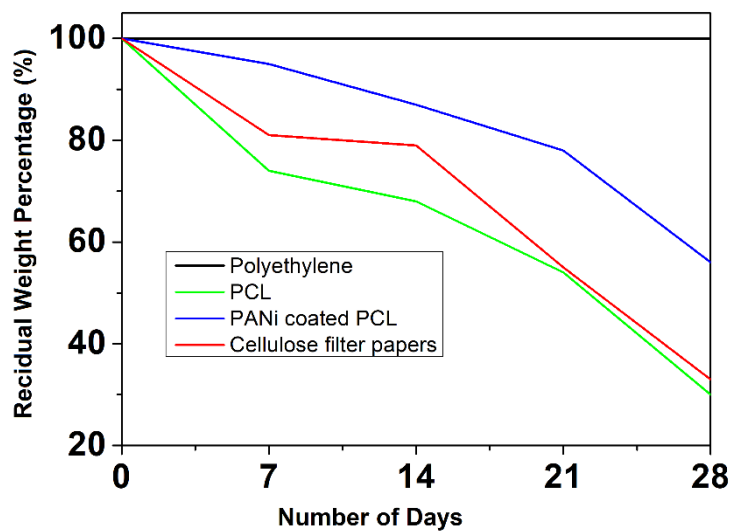


Figure 4.41: Residual weight percentage versus number of days in each stage of biodegradation.

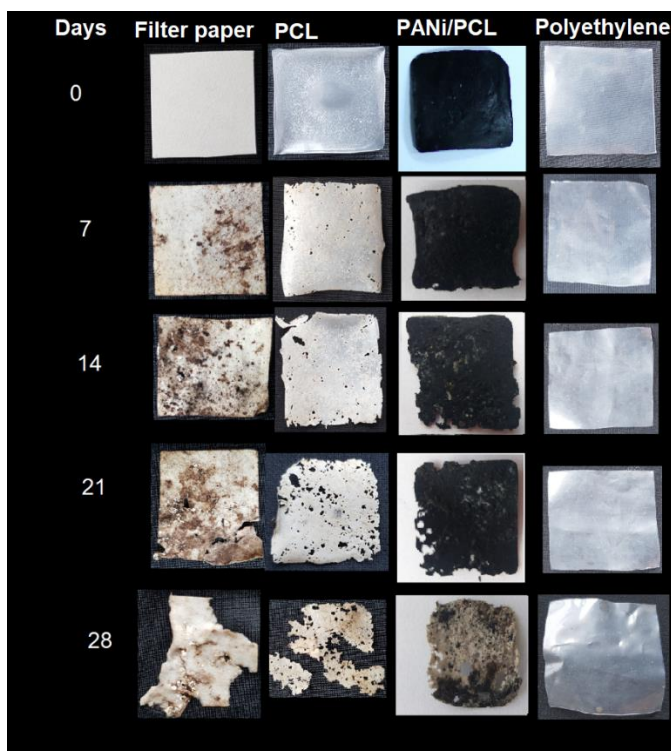


Figure 4.42: Physical appearance of different stages of biodegradation of cellulose filter paper, PCL, PCL/PANi and polyethylene

Although PANi is a non-biodegradable polymer, the ultrathin coating of PANi was observed to be detaching from PCL core with the degradation of PCL in Figure 4.43. It can be seen that there was a correlation between the physical changes in surface morphology and weight loss percentage of films. The degraded films showed more ruptures, grooves, pores, cavities, grooves of nanofibrous surface (Figure 4.43). Finally, it can be concluded that flexible electronic devices prepared from PANi coated PCL composite is an ideal replacement to address the problem of uncontrollable e-waste.

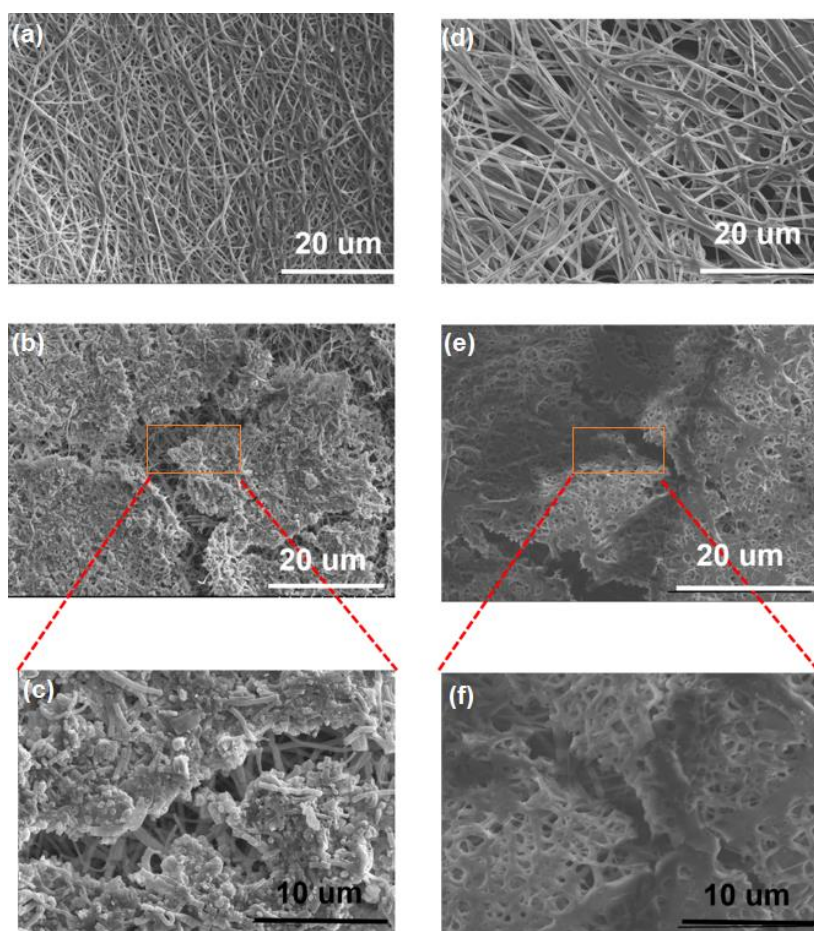


Figure 4.43: SEM images of PCL nanofiber (a) before degradation and (b-c) after degradation in soil. PANi/PCL nanofibers (d) before degradation and (e-f) after degradation in soil.

4.5 Comparison of PANi blended and coated yarns and potential applications

As shown in SEM images of the PANi blended yarns, the fiber diameter was decreased with increasing PANi content. On the other hand, PANi coated yarns have exhibited an increase of fiber diameter with increasing aniline percentage of the reaction mixture. The fiber diameter distribution was broader in PANi blended nanofibers than PANi coated nanofibers. For the optimized material concentrations, yarns with a diameter of ~ 0.8 mm had a resistivity of 10 ± 4 M Ω /cm for PANi blended yarns and 50 ± 8 k Ω /cm for PANi coated yarns. Tensile strength for PANi blended yarn with PANi 2% was 1.4 MPa and for PANi coated yarn with aniline 1% was 2.37 MPa. When increasing the PANi concentration of blended fibers, the modulus of the yarn was increased while in the PANi coated yarns, it was decreased with increasing the concentration of reaction mixture. PANi coated yarns have given reproducible resistance values for cycles of stretch and recovery. However, the PANi blended yarns were not recovered within the region of 20% strain.

During first three weeks, degradation rate of PANi coated composite was lower than PANi blended composite. The rapid degradation of PANi coated composite only started after detachment of coating.

Comparing conductive and mechanical properties PANi coated yarns have higher conductivity and excellent mechanical properties which can be used for consumer textile applications. On the other hand, PANi blended yarns have exhibited low tensile strength, elasticity and conductivity. The conductivity in semiconductor range (10^{-5} - 10^{-7} S cm $^{-1}$) might be adequate to pass a micro-current for stimulating cell proliferation and differentiation because the micro-current intensity in the human body is very low [146, 147]. Although the elasticity decreased with increasing PANi, the hybrid nanofibers were still relatively elastic and suitable for tissue engineering [43].

Therefore, at the end of the studies applicability of PANi blended and coated yarns were validated by demonstrating a capacitive sensor for PANi coated yarn and testing biocompatibility for PANi blended yarns.

4.5.1 Capacitive sensor

As a proof-of-concept, a capacitive sensing device was fabricated by sewing the PANi coated PCL/PANi yarn into a fabric as an electrode for capacitive sensing (Figure 4.44). A LED bulb was connected to the circuit to observe the signal output. The LED bulb can be turned ON by one touch and turned OFF by a consecutive another touch. Likewise, the LED bulb can be turned ON and OFF by touching the flexible fabric electrode.

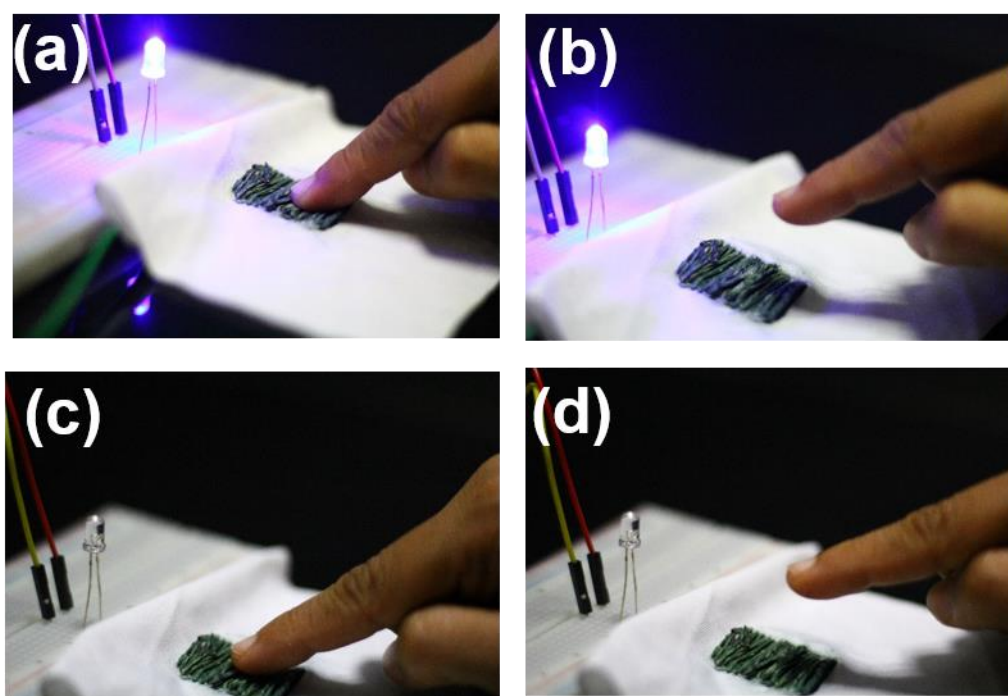


Figure 4.44: Illustration of the electrical conductivity nature for the prepared PANi coated PANi /PCL yarns with application of flexible capacitive sensor for operation of LED (a) ON by touching, (b) unchanged by releasing, (c) OFF and (d) unchanged by releasing.

4.5.2 Biocompatibility

4.5.2.1 Cytotoxic effects of the PANi blended nanofibers.

The cytotoxic effects of Pure PCL nanofibers and PANi blended PCL nanofibers on Vero cells (green monkey kidney cell line) was studied by means of the MTT (3-(4,5-dimethylthiazol-2-yl)-2,5-diphenyltetrazolium bromide) assay. The results show that the PCL nanofibers or PANi blended PCL nanofibers were not able to induce cytotoxicity in Vero cells (Figure 4.45)

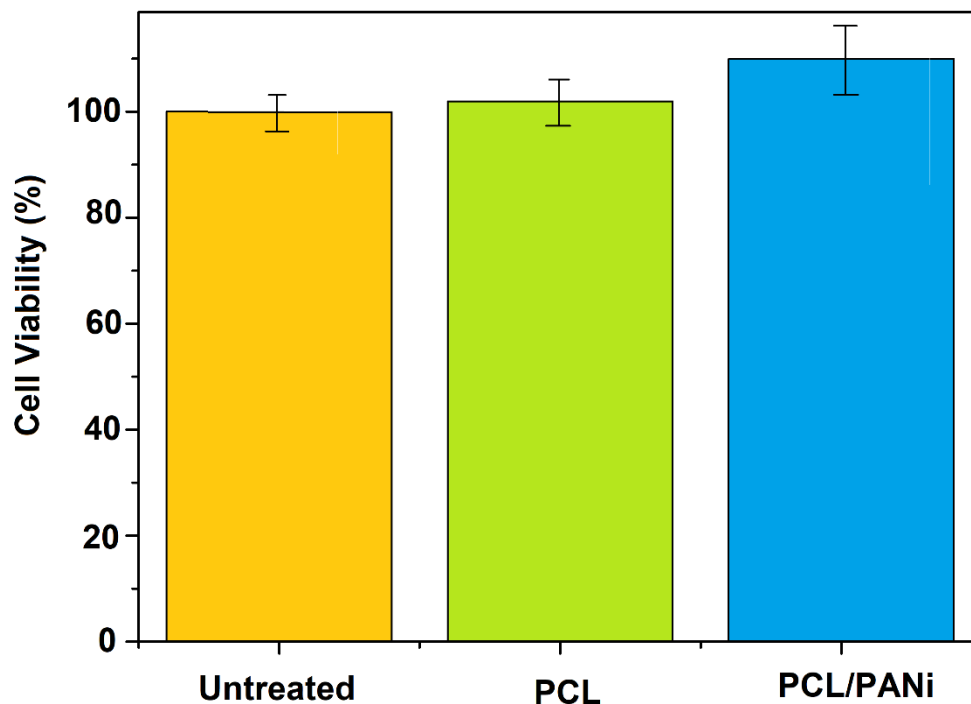


Figure 4.45: In-vitro cytotoxicity effects of the PCL and PANi/PCL electrospun nanofibers on Vero cells (green monkey kidney)

4.5.2.2 Cell morphology study

It is recognized that cellular adhesion and growing behavior were very crucial parameters for investigating the biocompatibility of a biomaterial. The reason is that they may directly affect the reproduction quality of cells. Figure 4.46 shows the SEM images of the Vero cells (green monkey kidney cell line) on PCL and PANi/PCL blended nanofibers. The SEM images show that Vero cells have good cellular adhesion

to both PCL and PCL/PANi nanofibers. As shown in SEM images (Figure 4.46), PANi/PCL nanofibers facilitate more active sites for the live cells to expand, and spread with a high initial cell seeding density.

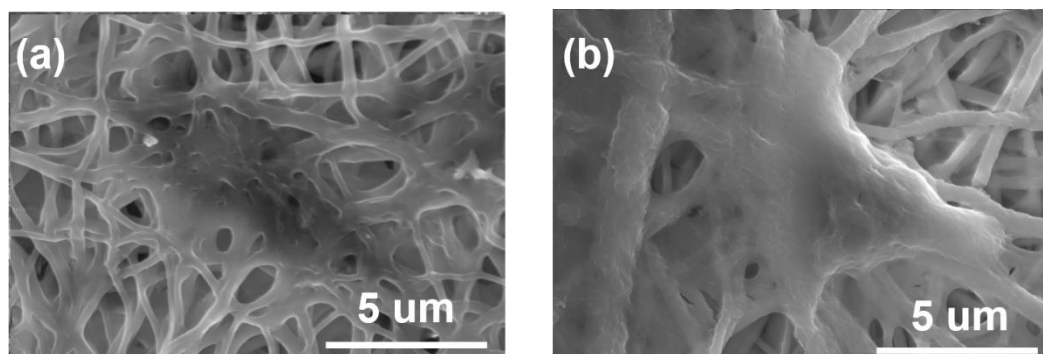


Figure 4.46: SEM images of (a) Vero cells seeded PCL nanofibers and (b) PCL/PANi nanofibers.

4.5.2.3 In-vitro degradability

The scaffolds may ideally be made out of biodegradable, biocompatible polymers, which should slowly degrade when cells begin to regenerate to avoid subsequent surgical removal. Also it should not be toxic to the cells in the initial and degraded forms [148]. Therefore, the in-vitro degradability of the PCL, and PANi blended PCL nanofibers were investigated by evaluating the gravimetric measurements and morphological changes. The nanofibers were soaked in (PBS; pH 7.4; Invitrogen, CA, USA) at 38 °C.

As seen in Figure 4.47, both PCL and PANi/PCL nanofibers have a high rate of mass loss up to 4 weeks. The mass loss rate of PCL was higher than PANi/PCL. After 4 weeks period total mass loss was calculated to be 70.3% and 40.1% for PCL and PANi/PCL, respectively. In addition, SEM images provide an evidence on the in vitro degradability (Figure 4.48). The samples were soaked in PBS for 20 days and dried in order to take SEM images. It can be seen that swelling, rupturing and other morphological changes of fibers occur during degradation.

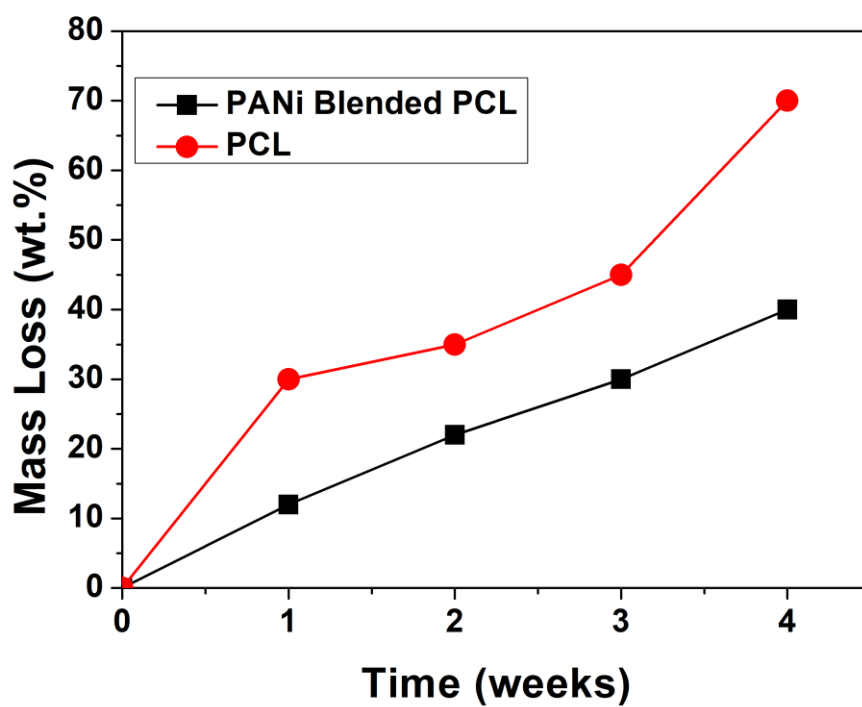


Figure 4.47: Degradation profile of the PCL, and PANi blended PCL electrospun nanofibers.

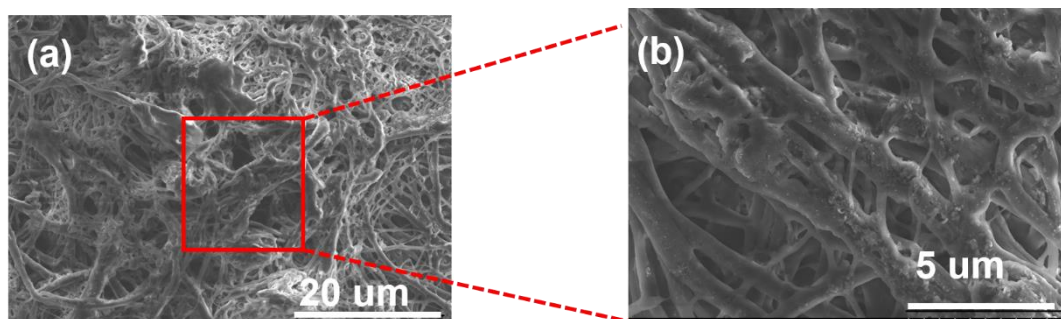


Figure 4.48: SEM images of the (a) PANi/PCL electrospun nanofibers after 20 days soaking in PBS and (b) magnified SEM image

4.6 Summary

This chapter discussed the results of the fabrication and characterization of nanofibrous yarns, which were obtained in line with the methodology. Developed conductive and biodegradable nanofibrous yarns were analyzed quantitatively using results obtained from SEM, FTIR, TGA, DSC, Instron tensile tester, Keithley SMU, and Fluke multimeter. Fiber morphology was studied from SEM images. FTIR, TGA, and DSC confirmed the presence of PANi. High amount of HCl resulted in hydrolysis of polymer chains confirmed by SEM images, DSC and tensile tests.

Further, mechanical and electro-mechanical properties of yarns were studied. The ability to sew and weave the yarn without changing the conductive properties of the yarn was also studied. Finally, the applicability of yarns for biomedical applications and smart textile applications was demonstrated.

CHAPTER 05

5. CONCLUSIONS AND RECOMMENDATIONS

5.1 Introduction

The main driving force for carrying out this research is to take a new approach for developing conductive yarns, in order to add value to wearable and biodegradable electronic devices . An expansive literature survey was performed to identify the background of the study and the knowledge gap, which this research seeks to address. Thus, after identifying the requirement for incorporating conductivity to biodegradable nanofibrous yarns, conductive and biodegradable yarns were synthesized and fabricated using electrospinning.

5.2 Key conclusions

The proposed research aimed to develop conductive and biodegradable nanofibrous yarns. Nanofibers were electrospun into nanofiber mats as well as continuous nanofiber yarns using two modified electrospinning setups with drum collector and funnel collector. The conductivity was incorporated into nanofibers by two approaches; first, blending in PANi with the PCL solution for electrospinning of nanofibers and secondly, in-situ polymerization of aniline on electrospun nanofibers. Newly developed yarns were comprehensively analyzed quantitatively using results obtained from SEM, DSC, TGA, FTIR, Instron tensile tester, Keithley SMU 2456 Instrument and multimeter. Table 5.1 shows summarized data for PANi blended and coated yarns.

Table 5.1: Summary of important results of the study

Property	PANi blended		PANi coated	
Fiber diameter (nm)	PANi 0.5%	568 ± 121	Aniline 0.5%	457 ± 83
	PANi 1%	303 ± 142	Aniline 1%	468 ± 63
	PANi 2%	353 ± 153	Aniline 2%	554 ± 73
Conductivity	PANi 0.5%	-	Aniline 0.5% (kΩ)	162 ± 15
	PANi 1% (MΩ)	50 ± 8	Aniline 1% (kΩ)	50 ± 8
	PANi 2% (MΩ)	10 ± 4	Aniline 2% (kΩ)	6 ± 2
Modulus (MPa)	PANi 0.5%	5.4	Aniline 0.5%	2.2
	PANi 1%	5.5	Aniline 1%	2.14
	PANi 2%	5.9	Aniline 2%	0.15
Optimum concentrations	PANi 2%		Aniline 1%	
Thermal stability (°C)	PANi 1%	130.34	Aniline 1%	187.72
	PANi 2%	62.40	Aniline 2%	95.76
Crystallinity (%)	PANi 1%	50.27	Aniline 0.5%	48.74
	PANi 2%	47.74	Aniline 1%	36.55

The change of resistance of yarns was demonstrated under different applications including ply yarns, woven fabrics, sewn yarns where yarn can be subjected to various degrees of mechanical deformations. In PANi coated yarns, the resistance changes were almost instantaneously with the stretch for multiple stretch and recovery cycles with 20% maximum strain and this behavior is very desirable for the production of highly sensitive strain sensors. Additionally, the application of the PANi coated yarn was demonstrated by operating as a flexible capacitor. Furthermore, the application of the PANi blended yarn as a biomaterial was demonstrated by studying the morphology of cells and cell viability.

Biodegradability of PCL/PANi hybrid systems were investigated using relevant testing protocols. It was found that the developed PANi coated and blended yarns can serve as short life cycle substitutes for the components of an electronic device addressing the issue of e-waste.

5.3 Recommendations

There are two main recommendations from this study.

A. Continuous electrospinning of conductive and biodegradable nanofibrous yarns have the potential to be scaled up to industrial level.

B. This can be used for many applications such as organic supercapacitors, gas sensors, pH sensors, visible-light photocatalytic degradation, field-effect transistors can be obtained by altering the desirable functional materials (further research).

Reference list

- [1] R. Salvado, C. Loss, R. Gonçalves, and P. Pinho, "Textile materials for the design of wearable antennas: a survey," *Sensors*, vol. 12, pp. 15841-15857, 2012.
- [2] C. Cochrane, V. Koncar, M. Lewandowski, and C. Dufour, "Design and development of a flexible strain sensor for textile structures based on a conductive polymer composite," *Sensors*, vol. 7, pp. 473-492, 2007.
- [3] H. Chen, K. Lee, J. Lin, and M. Koch, "Comparison of electromagnetic shielding effectiveness properties of diverse conductive textiles via various measurement techniques," *Journal of Materials Processing Technology*, vol. 192, pp. 549-554, 2007.
- [4] F. Dabirian and S. Hosseini, "Novel method for nanofibre yarn production using two differently charged nozzles," *Fibres Text. East. Eur.*, vol. 17, pp. 45-47, 2009.
- [5] M. Yousefzadeh, M. Latifi, W. E. Teo, M. Amani-Tehran, and S. Ramakrishna, "Producing continuous twisted yarn from well-aligned nanofibers by water vortex," *Polymer Engineering & Science*, vol. 51, pp. 323-329, 2011.
- [6] B. Wu, B. Zhang, J. Wu, Z. Wang, H. Ma, M. Yu, *et al.*, "Electrical switchability and dry-wash durability of conductive textiles," *Scientific reports*, vol. 5, p. 11255, 2015.
- [7] B. Kim, V. Koncar, and C. Dufour, "Polyaniline-coated PET conductive yarns: Study of electrical, mechanical, and electro-mechanical properties," *Journal of Applied Polymer Science*, vol. 101, pp. 1252-1256, 2006.
- [8] V. Beachley and X. Wen, "Polymer nanofibrous structures: Fabrication, biofunctionalization, and cell interactions," *Progress in polymer science*, vol. 35, pp. 868-892, 2010.
- [9] A. Subramanian, U. M. Krishnan, and S. Sethuraman, "Axially aligned electrically conducting biodegradable nanofibers for neural regeneration," *Journal of Materials Science: Materials in Medicine*, vol. 23, pp. 1797-1809, 2012.
- [10] R. Sarvari, B. Massoumi, M. Jaymand, Y. Beygi-Khosrowshahi, and M. Abdollahi, "Novel three-dimensional, conducting, biocompatible, porous, and elastic polyaniline-based scaffolds for regenerative therapies," *RSC Advances*, vol. 6, pp. 19437-19451, 2016.
- [11] M. Montazer and Z. K. Nia, "Conductive nylon fabric through in situ synthesis of nano-silver: Preparation and characterization," *Materials Science and Engineering: C*, vol. 56, pp. 341-347, 2015.

- [12] T. Linz, C. Kallmayer, R. Aschenbrenner, and H. Reichl, "Embroidering electrical interconnects with conductive yarn for the integration of flexible electronic modules into fabric," in *Ninth IEEE International Symposium on Wearable Computers (ISWC'05)*, 2005, pp. 86-89.
- [13] T. Dias, *Electronic textiles: Smart fabrics and wearable technology*: Woodhead Publishing, 2015.
- [14] Y. Wu, L. Wang, B. Guo, and P. X. Ma, "Interwoven aligned conductive nanofiber yarn/hydrogel composite scaffolds for engineered 3D cardiac anisotropy," *Acs Nano*, vol. 11, pp. 5646-5659, 2017.
- [15] L. A. Buechley, "An investigation of computational textiles with applications to education and design," University of Colorado at Boulder, 2007.
- [16] G.-S. Chung, D.-h. Lee, and J. S. An, "Process and system for producing digital yarns using metal filaments for info-communications and digital yarns produced by said process," ed: Google Patents, 2010.
- [17] A. Schwarz, I. Kazani, L. Cuny, C. Hertleer, F. Ghekiere, G. De Clercq, *et al.*, "Electro-conductive and elastic hybrid yarns—The effects of stretching, cyclic straining and washing on their electro-conductive properties," *Materials & Design*, vol. 32, pp. 4247-4256, 2011.
- [18] X. Cai, M. Peng, X. Yu, Y. Fu, and D. Zou, "Flexible planar/fiber-architected supercapacitors for wearable energy storage," *Journal of Materials Chemistry C*, vol. 2, pp. 1184-1200, 2014.
- [19] D. De Rossi, A. Della Santa, and A. Mazzoldi, "Dressware: wearable hardware," *Materials Science and Engineering: C*, vol. 7, pp. 31-35, 1999.
- [20] Y. Huang, H. Hu, Y. Huang, M. Zhu, W. Meng, C. Liu, *et al.*, "From industrially weavable and knittable highly conductive yarns to large wearable energy storage textiles," *ACS nano*, vol. 9, pp. 4766-4775, 2015.
- [21] D. Yu, S. Mu, L. Liu, and W. Wang, "Preparation of electroless silver plating on aramid fiber with good conductivity and adhesion strength," *Colloids and Surfaces A: Physicochemical and Engineering Aspects*, vol. 483, pp. 53-59, 2015.
- [22] G. S. Sandhu and T. T. Doan, "Pulsed plasma enhanced CVD of metal silicide conductive films such as TiSi₂," ed: Google Patents, 1994.
- [23] Y. Dietzel, W. Przyborowski, G. Nocke, P. Offermann, F. Hollstein, and J. Meinhardt, "Investigation of PVD arc coatings on polyamide fabrics," *Surface and Coatings Technology*, vol. 135, pp. 75-81, 2000.

- [24] S. Schaefer, L. Rast, and A. Stanishevsky, "Electroless silver plating on spin-coated silver nanoparticle seed layers," *Materials Letters*, vol. 60, pp. 706-709, 2006.
- [25] B. Adhikari and S. Majumdar, "Polymers in sensor applications," *Progress in polymer science*, vol. 29, pp. 699-766, 2004.
- [26] H. Bai and G. Shi, "Gas sensors based on conducting polymers," *Sensors*, vol. 7, pp. 267-307, 2007.
- [27] S. Roth, H. Bleier, and W. Pukacki, "Charge transport in conducting polymers," *Faraday Discussions of the Chemical Society*, vol. 88, pp. 223-233, 1989.
- [28] D. Kumar and R. Sharma, "Advances in conductive polymers," *European polymer journal*, vol. 34, pp. 1053-1060, 1998.
- [29] K. M. Molapo, P. M. Ndangili, R. F. Ajayi, G. Mbambisa, S. M. Mailu, N. Njomo, *et al.*, "Electronics of conjugated polymers (I): polyaniline," *International Journal of Electrochemical Science*, vol. 7, pp. 11859-11875, 2012.
- [30] U. Salzner, J. Lagowski, P. Pickup, and R. Poirier, "Comparison of geometries and electronic structures of polyacetylene, polyborole, polycyclopentadiene, polypyrrole, polyfuran, polysilole, polyphosphole, polythiophene, polyselenophene and polytellurophene," *Synthetic Metals*, vol. 96, pp. 177-189, 1998.
- [31] Y.-J. Cheng, S.-H. Yang, and C.-S. Hsu, "Synthesis of conjugated polymers for organic solar cell applications," *Chemical reviews*, vol. 109, pp. 5868-5923, 2009.
- [32] A. Hassan, T. Iqbal, M. Tahir, and S. Afsheen, "A review on copper vanadate-based nanostructures for photocatalysis energy production," *International Journal of Energy Research*, vol. 43, pp. 9-28, 2019.
- [33] K. Mahesh, S. Karpagam, and K. Pandian, "How to Design Donor–Acceptor Based Heterocyclic Conjugated Polymers for Applications from Organic Electronics to Sensors," *Topics in Current Chemistry*, vol. 377, p. 12, 2019.
- [34] N. Yamazoe, "Toward innovations of gas sensor technology," *Sensors and Actuators B: Chemical*, vol. 108, pp. 2-14, 2005.
- [35] P. Harrey, B. Ramsey, P. Evans, and D. Harrison, "Capacitive-type humidity sensors fabricated using the offset lithographic printing process," *Sensors and Actuators B: Chemical*, vol. 87, pp. 226-232, 2002.
- [36] S. Yun and S. T. Oyama, "Correlations in palladium membranes for hydrogen separation: a review," *Journal of membrane science*, vol. 375, pp. 28-45, 2011.

- [37] L. Ghasemi-Mobarakeh, M. P. Prabhakaran, M. Morshed, M. H. Nasr-Esfahani, H. Baharvand, S. Kiani, *et al.*, "Application of conductive polymers, scaffolds and electrical stimulation for nerve tissue engineering," *Journal of tissue engineering and regenerative medicine*, vol. 5, pp. e17-e35, 2011.
- [38] N. K. Guimard, N. Gomez, and C. E. Schmidt, "Conducting polymers in biomedical engineering," *Progress in polymer science*, vol. 32, pp. 876-921, 2007.
- [39] D. D. Zhou, X. T. Cui, A. Hines, and R. J. Greenberg, "Conducting polymers in neural stimulation applications," in *Implantable Neural Prostheses 2*, ed: Springer, 2009, pp. 217-252.
- [40] R. Ravichandran, S. Sundarrajan, J. R. Venugopal, S. Mukherjee, and S. Ramakrishna, "Applications of conducting polymers and their issues in biomedical engineering," *Journal of the Royal Society Interface*, vol. 7, pp. S559-S579, 2010.
- [41] L. Ghasemi-Mobarakeh, M. P. Prabhakaran, M. Morshed, M. H. Nasr-Esfahani, and S. Ramakrishna, "Electrical stimulation of nerve cells using conductive nanofibrous scaffolds for nerve tissue engineering," *Tissue Engineering Part A*, vol. 15, pp. 3605-3619, 2009.
- [42] A. Kaynak, L. Rintoul, and G. A. George, "Change of mechanical and electrical properties of polypyrrole films with dopant concentration and oxidative aging," *Materials Research Bulletin*, vol. 35, pp. 813-824, 2000.
- [43] J. Zhang, K. Qiu, B. Sun, J. Fang, K. Zhang, E.-H. Hany, *et al.*, "The aligned core-sheath nanofibers with electrical conductivity for neural tissue engineering," *Journal of Materials Chemistry B*, vol. 2, pp. 7945-7954, 2014.
- [44] M. T. Cortés and J. C. Moreno, "Artificial muscles based on conducting polymers," *e-Polymers*, vol. 3, 2003.
- [45] J. Y. Wong, R. Langer, and D. E. Ingber, "Electrically conducting polymers can noninvasively control the shape and growth of mammalian cells," *Proceedings of the National Academy of Sciences*, vol. 91, pp. 3201-3204, 1994.
- [46] X. Liu, K. J. Gilmore, S. E. Moulton, and G. G. Wallace, "Electrical stimulation promotes nerve cell differentiation on polypyrrole/poly (2-methoxy-5 aniline sulfonic acid) composites," *Journal of neural engineering*, vol. 6, p. 065002, 2009.
- [47] G. Shi, M. Rouabhia, Z. Wang, L. H. Dao, and Z. Zhang, "A novel electrically conductive and biodegradable composite made of polypyrrole nanoparticles and polylactide," *Biomaterials*, vol. 25, pp. 2477-2488, 2004.

- [48] G. Wallace and G. Spinks, "Conducting polymers—bridging the bionic interface," *Soft Matter*, vol. 3, pp. 665-671, 2007.
- [49] J. Pelto, S. Haimi, E. Puukilainen, P. G. Whitten, G. M. Spinks, M. Bahrami-Samani, *et al.*, "Electroactivity and biocompatibility of polypyrrole-hyaluronic acid multi-walled carbon nanotube composite," *Journal of Biomedical Materials Research Part A: An Official Journal of The Society for Biomaterials, The Japanese Society for Biomaterials, and The Australian Society for Biomaterials and the Korean Society for Biomaterials*, vol. 93, pp. 1056-1067, 2010.
- [50] V. Gilja, K. Novaković, J. Travas-Sejdic, Z. Hrnjak-Murgić, M. Kraljić Roković, and M. Žic, "Stability and synergistic effect of polyaniline/TiO₂ photocatalysts in degradation of azo dye in wastewater," *Nanomaterials*, vol. 7, p. 412, 2017.
- [51] W. E. Teo and S. Ramakrishna, "A review on electrospinning design and nanofibre assemblies," *Nanotechnology*, vol. 17, p. R89, 2006.
- [52] J. F. Cooley, "Apparatus for electrically dispersing fluids," ed: Google Patents, 1902.
- [53] J.-H. He, Y. Liu, and L. Xu, "Apparatus for preparing electrospun nanofibres: a comparative review," *Materials Science and Technology*, vol. 26, pp. 1275-1287, 2010.
- [54] A. M. Afifi, S. Nakano, H. Yamane, and Y. Kimura, "Electrospinning of continuous aligning yarns with a 'funnel' target," *Macromolecular Materials and Engineering*, vol. 295, pp. 660-665, 2010.
- [55] U. Ali, Y. Zhou, X. Wang, and T. Lin, "Direct electrospinning of highly twisted, continuous nanofiber yarns," *Journal of the Textile Institute*, vol. 103, pp. 80-88, 2012.
- [56] Z. Xie, H. Niu, and T. Lin, "Continuous polyacrylonitrile nanofiber yarns: preparation and dry-drawing treatment for carbon nanofiber production," *RSC Advances*, vol. 5, pp. 15147-15153, 2015.
- [57] E. Yang, Z. Xu, L. K. Chur, A. Behroozfar, M. Baniasadi, S. Moreno, *et al.*, "Nanofibrous smart fabrics from twisted yarns of electrospun piezopolymer," *ACS applied materials & interfaces*, vol. 9, pp. 24220-24229, 2017.
- [58] L. Fan, Q. Ma, J. Tian, D. Li, X. Xi, X. Dong, *et al.*, "Novel nanofiber yarns synchronously endowed with tri-functional performance of superparamagnetism, electrical conductivity and enhanced fluorescence prepared by conjugate electrospinning," *RSC Advances*, vol. 7, pp. 48702-48711, 2017.

- [59] L. Chen, D. Li, L. Chen, P. Si, J. Feng, L. Zhang, *et al.*, "Core-shell structured carbon nanofibers yarn@ polypyrrole@ graphene for high performance all-solid-state fiber supercapacitors," *Carbon*, vol. 138, pp. 264-270, 2018.
- [60] T. Yan, Z. Wang, Y.-Q. Wang, and Z.-J. Pan, "Carbon/graphene composite nanofiber yarns for highly sensitive strain sensors," *Materials & Design*, vol. 143, pp. 214-223, 2018.
- [61] J. Li, L. Tian, N. Pan, and Z. j. Pan, "Mechanical and electrical properties of the PA6/SWNTs nanofiber yarn by electrospinning," *Polymer Engineering & Science*, vol. 54, pp. 1618-1624, 2014.
- [62] S. Wu, P. Liu, Y. Zhang, H. Zhang, and X. Qin, "Flexible and conductive nanofiber-structured single yarn sensor for smart wearable devices," *Sensors and Actuators B: Chemical*, vol. 252, pp. 697-705, 2017.
- [63] X. Wang, H. Hu, Z. Yang, L. He, Y. Kong, B. Fei, *et al.*, "Smart hydrogel-functionalized textile system with moisture management property for skin application," *Smart materials and structures*, vol. 23, p. 125027, 2014.
- [64] A. Lendlein and R. Langer, "Biodegradable, elastic shape-memory polymers for potential biomedical applications," *Science*, vol. 296, pp. 1673-1676, 2002.
- [65] X. Kang, J. Wang, H. Wu, I. A. Aksay, J. Liu, and Y. Lin, "Glucose oxidase–graphene–chitosan modified electrode for direct electrochemistry and glucose sensing," *Biosensors and Bioelectronics*, vol. 25, pp. 901-905, 2009.
- [66] Q. Meng, J. Hu, K. Ho, F. Ji, and S. Chen, "The shape memory properties of biodegradable chitosan/poly (L-lactide) composites," *Journal of Polymers and the Environment*, vol. 17, p. 212, 2009.
- [67] A. Sugunan, C. Thanachayanont, J. Dutta, and J. Hilborn, "Heavy-metal ion sensors using chitosan-capped gold nanoparticles," *Science and Technology of Advanced Materials*, vol. 6, p. 335, 2005.
- [68] A. Kaushik, P. R. Solanki, A. A. Ansari, G. Sumana, S. Ahmad, and B. D. Malhotra, "Iron oxide-chitosan nanobiocomposite for urea sensor," *Sensors and Actuators B: Chemical*, vol. 138, pp. 572-580, 2009.
- [69] L. H. Chen, T. Li, C. C. Chan, R. Menon, P. Balamurali, M. Shailender, *et al.*, "Chitosan based fiber-optic Fabry–Perot humidity sensor," *Sensors and Actuators B: Chemical*, vol. 169, pp. 167-172, 2012.
- [70] J. Zeng, X. Xu, X. Chen, Q. Liang, X. Bian, L. Yang, *et al.*, "Biodegradable electrospun fibers for drug delivery," *Journal of controlled release*, vol. 92, pp. 227-231, 2003.

- [71] H. Yoshimoto, Y. Shin, H. Terai, and J. Vacanti, "A biodegradable nanofiber scaffold by electrospinning and its potential for bone tissue engineering," *Biomaterials*, vol. 24, pp. 2077-2082, 2003.
- [72] Y. Z. Cai, G. R. Zhang, L. L. Wang, Y. Z. Jiang, H. W. Ouyang, and X. H. Zou, "Novel biodegradable three-dimensional macroporous scaffold using aligned electrospun nanofibrous yarns for bone tissue engineering," *Journal of Biomedical Materials Research Part A*, vol. 100, pp. 1187-1194, 2012.
- [73] Y. Tokiwa and T. Suzuki, "Hydrolysis of polyesters by lipases," *Nature*, vol. 270, p. 76, 1977.
- [74] M. A. Woodruff and D. W. Hutmacher, "The return of a forgotten polymer—Polycaprolactone in the 21st century," *Progress in polymer science*, vol. 35, pp. 1217-1256, 2010.
- [75] V. Sinha, K. Bansal, R. Kaushik, R. Kumria, and A. Trehan, "Poly- ϵ -caprolactone microspheres and nanospheres: an overview," *International journal of pharmaceutics*, vol. 278, pp. 1-23, 2004.
- [76] A. A. Shah, F. Hasan, A. Hameed, and S. Ahmed, "Biological degradation of plastics: a comprehensive review," *Biotechnology advances*, vol. 26, pp. 246-265, 2008.
- [77] T.-K. Chua, M. Tseng, and M.-K. Yang, "Degradation of Poly (ϵ -caprolactone) by thermophilic *Streptomyces thermoviolaceus* subsp. *thermoviolaceus* 76T-2," *AMB Express*, vol. 3, p. 8, 2013.
- [78] C. V. Benedict, J. Cameron, and S. J. Huang, "Polycaprolactone degradation by mixed and pure cultures of bacteria and a yeast," *Journal of Applied Polymer Science*, vol. 28, pp. 335-342, 1983.
- [79] J. G. Sanchez, A. Tsuchii, and Y. Tokiwa, "Degradation of polycaprolactone at 50° C by a thermotolerant *Aspergillus* sp.," *Biotechnology Letters*, vol. 22, pp. 849-853, 2000.
- [80] D.-M. Abou-Zeid, R.-J. Müller, and W.-D. Deckwer, "Degradation of natural and synthetic polyesters under anaerobic conditions," *Journal of biotechnology*, vol. 86, pp. 113-126, 2001.
- [81] D.-M. Abou-Zeid, R.-J. Müller, and W.-D. Deckwer, "Biodegradation of aliphatic homopolyesters and aliphatic–aromatic copolyesters by anaerobic microorganisms," *Biomacromolecules*, vol. 5, pp. 1687-1697, 2004.
- [82] K.-E. Jaeger and F. Rosenau, "Overexpression and secretion of *Pseudomonas* lipases," in *Pseudomonas*, ed: Springer, 2004, pp. 491-508.

- [83] Y. Tokiwa, B. P. Calabia, C. U. Ugwu, and S. Aiba, "Biodegradability of plastics," *International journal of molecular sciences*, vol. 10, pp. 3722-3742, 2009.
- [84] D. H. Reneker and I. Chun, "Nanometre diameter fibres of polymer, produced by electrospinning," *Nanotechnology*, vol. 7, p. 216, 1996.
- [85] N. Bhardwaj and S. C. Kundu, "Electrospinning: a fascinating fiber fabrication technique," *Biotechnology advances*, vol. 28, pp. 325-347, 2010.
- [86] S. Shao, S. Zhou, L. Li, J. Li, C. Luo, J. Wang, *et al.*, "Osteoblast function on electrically conductive electrospun PLA/MWCNTs nanofibers," *Biomaterials*, vol. 32, pp. 2821-2833, 2011.
- [87] F. Yang, R. Murugan, S. Wang, and S. Ramakrishna, "Electrospinning of nano/micro scale poly (L-lactic acid) aligned fibers and their potential in neural tissue engineering," *Biomaterials*, vol. 26, pp. 2603-2610, 2005.
- [88] X. Ma, J. Ge, Y. Li, B. Guo, and P. X. Ma, "Nanofibrous electroactive scaffolds from a chitosan-grafted-aniline tetramer by electrospinning for tissue engineering," *Rsc Advances*, vol. 4, pp. 13652-13661, 2014.
- [89] M. Li, Y. Guo, Y. Wei, A. G. MacDiarmid, and P. I. Lelkes, "Electrospinning polyaniline-contained gelatin nanofibers for tissue engineering applications," *Biomaterials*, vol. 27, pp. 2705-2715, 2006.
- [90] S. H. Bhang, S. I. Jeong, T. J. Lee, I. Jun, Y. B. Lee, B. S. Kim, *et al.*, "Electroactive Electrospun Polyaniline/Poly [(L-lactide)-co-(ϵ -caprolactone)] Fibers for Control of Neural Cell Function," *Macromolecular bioscience*, vol. 12, pp. 402-411, 2012.
- [91] S. Aznar-Cervantes, M. I. Roca, J. G. Martinez, L. Meseguer-Olmo, J. L. Cenis, J. M. Moraleda, *et al.*, "Fabrication of conductive electrospun silk fibroin scaffolds by coating with polypyrrole for biomedical applications," *Bioelectrochemistry*, vol. 85, pp. 36-43, 2012.
- [92] T. J. Rivers, T. W. Hudson, and C. E. Schmidt, "Synthesis of a novel, biodegradable electrically conducting polymer for biomedical applications," *Advanced Functional Materials*, vol. 12, pp. 33-37, 2002.
- [93] N. Li, Q. Zhang, S. Gao, Q. Song, R. Huang, L. Wang, *et al.*, "Three-dimensional graphene foam as a biocompatible and conductive scaffold for neural stem cells," *Scientific reports*, vol. 3, p. 1604, 2013.
- [94] A. Kotwal and C. E. Schmidt, "Electrical stimulation alters protein adsorption and nerve cell interactions with electrically conducting biomaterials," *Biomaterials*, vol. 22, pp. 1055-1064, 2001.

- [95] S. H. Ku, S. H. Lee, and C. B. Park, "Synergic effects of nanofiber alignment and electroactivity on myoblast differentiation," *Biomaterials*, vol. 33, pp. 6098-6104, 2012.
- [96] K. Low, N. Chartuprayoon, C. Echeverria, C. Li, W. Bosze, N. V. Myung, *et al.*, "Polyaniline/poly (ϵ -caprolactone) composite electrospun nanofiber-based gas sensors: optimization of sensing properties by dopants and doping concentration," *Nanotechnology*, vol. 25, p. 115501, 2014.
- [97] Y. Li, X. Li, R. Zhao, C. Wang, F. Qiu, B. Sun, *et al.*, "Enhanced adhesion and proliferation of human umbilical vein endothelial cells on conductive PANI-PCL fiber scaffold by electrical stimulation," *Materials Science and Engineering: C*, vol. 72, pp. 106-112, 2017.
- [98] S. Chung, A. K. Moghe, G. A. Montero, S. H. Kim, and M. W. King, "Nanofibrous scaffolds electrospun from elastomeric biodegradable poly (L-lactide-co- ϵ -caprolactone) copolymer," *Biomedical Materials*, vol. 4, p. 015019, 2009.
- [99] D. Kai, M. P. Prabhakaran, G. Jin, and S. Ramakrishna, "Polypyrrole-contained electrospun conductive nanofibrous membranes for cardiac tissue engineering," *Journal of biomedical materials research Part A*, vol. 99, pp. 376-385, 2011.
- [100] J. Y. Lee, C. A. Bashur, A. S. Goldstein, and C. E. Schmidt, "Polypyrrole-coated electrospun PLGA nanofibers for neural tissue applications," *Biomaterials*, vol. 30, pp. 4325-4335, 2009.
- [101] M.-C. Chen, Y.-C. Sun, and Y.-H. Chen, "Electrically conductive nanofibers with highly oriented structures and their potential application in skeletal muscle tissue engineering," *Acta biomaterialia*, vol. 9, pp. 5562-5572, 2013.
- [102] Y. Liu, H. Cui, X. Zhuang, Y. Wei, and X. Chen, "Electrospinning of aniline pentamer-graft-gelatin/PLLA nanofibers for bone tissue engineering," *Acta biomaterialia*, vol. 10, pp. 5074-5080, 2014.
- [103] L. Wang, Y. Wu, B. Guo, and P. X. Ma, "Nanofiber yarn/hydrogel core-shell scaffolds mimicking native skeletal muscle tissue for guiding 3D myoblast alignment, elongation, and differentiation," *ACS nano*, vol. 9, pp. 9167-9179, 2015.
- [104] A. Uhlir Jr, "The potentials of infinite systems of sources and numerical solutions of problems in semiconductor engineering," *Bell System Technical Journal*, vol. 34, pp. 105-128, 1955.

- [105] J. Greene, "Biodegradation of Biodegradable and Compostable Plastics under Industrial Compost, Marine and Anaerobic Digestion," *Ecology, Pollution and Environmental science*, vol. 1(1): 13-18, 2018.
- [106] S. M. Willerth and S. E. Sakiyama-Elbert, "Approaches to neural tissue engineering using scaffolds for drug delivery," *Advanced drug delivery reviews*, vol. 59, pp. 325-338, 2007.
- [107] L. Huang, X. Zhuang, J. Hu, L. Lang, P. Zhang, Y. Wang, *et al.*, "Synthesis of biodegradable and electroactive multiblock polylactide and aniline pentamer copolymer for tissue engineering applications," *Biomacromolecules*, vol. 9, pp. 850-858, 2008.
- [108] V. Ka, "I, M. Eskandani, Y. Omid, H. Nazamiyeh and J. Barar," *RSC Adv*, vol. 5, pp. 18041-18051, 2015.
- [109] S. Agarwal, J. H. Wendorff, and A. Greiner, "Chemistry on electrospun polymeric nanofibers: merely routine chemistry or a real challenge?," *Macromolecular rapid communications*, vol. 31, pp. 1317-1331, 2010.
- [110] X. Qi, X. Yao, S. Deng, T. Zhou, and Q. Fu, "Water-induced shape memory effect of graphene oxide reinforced polyvinyl alcohol nanocomposites," *Journal of Materials Chemistry A*, vol. 2, pp. 2240-2249, 2014.
- [111] S. T. McGovern, G. M. Spinks, and G. G. Wallace, "Micro-humidity sensors based on a processable polyaniline blend," *Sensors and Actuators B: Chemical*, vol. 107, pp. 657-665, 2005.
- [112] V. G. Kulkarni, "Processing of polyanilines," in *Intrinsically conducting polymers: an emerging technology*, ed: Springer, 1993, pp. 45-50.
- [113] S. Bhandari, "Polyaniline: Structure and Properties Relationship," in *Polyaniline Blends, Composites, and Nanocomposites*, ed: Elsevier, 2018, pp. 23-60.
- [114] J. Santos Jr, J. Malmonge, A. C. Silva, A. d. J. Motheo, Y. P. Mascarenhas, and L. Mattoso, "Characteristics of polyaniline electropolymerized in camphor sulfonic acid," *Synthetic Metals*, vol. 69, pp. 141-142, 1995.
- [115] F. Cataldo and P. Maltese, "Preparation of polyaniline conductive composites with diene-rubber or polyphenylacetylene," *Polymers for Advanced Technologies*, vol. 12, pp. 293-299, 2001.
- [116] G. Eda, "Effects of solution rheology on electrospinning of polystyrene," 2006.
- [117] P. H. Picciani, E. S. Medeiros, Z. Pan, W. J. Orts, L. H. Mattoso, and B. G. Soares, "Development of conducting polyaniline/poly (lactic acid) nanofibers by electrospinning," *Journal of Applied Polymer Science*, vol. 112, pp. 744-753, 2009.

- [118] E. Tavakkol, H. Tavanai, A. Abdolmaleki, and M. Morshed, "Production of conductive electrospun polypyrrole/poly (vinyl pyrrolidone) nanofibers," *Synthetic Metals*, vol. 231, pp. 95-106, 2017.
- [119] W. Lowrie and A. Fichtner, *Fundamentals of geophysics*: Cambridge university press, 2019.
- [120] J. Han, K. Lu, Y. Yue, C. Mei, C. Huang, Q. Wu, *et al.*, "Nanocellulose-templated assembly of polyaniline in natural rubber-based hybrid elastomers toward flexible electronic conductors," *Industrial crops and products*, vol. 128, pp. 94-107, 2019.
- [121] S. Yao, Y. Li, Z. Zhou, and H. Yan, "Graphene oxide-assisted preparation of poly (vinyl alcohol)/carbon nanotube/reduced graphene oxide nanofibers with high carbon content by electrospinning technology," *RSC Advances*, vol. 5, pp. 91878-91887, 2015.
- [122] Y. Qi, Z. Tai, D. Sun, J. Chen, H. Ma, X. Yan, *et al.*, "Fabrication and characterization of poly (vinyl alcohol)/graphene oxide nanofibrous biocomposite scaffolds," *Journal of applied polymer science*, vol. 127, pp. 1885-1894, 2013.
- [123] Y. Liu, M. Park, H. K. Shin, B. Pant, J. Choi, Y. W. Park, *et al.*, "Facile preparation and characterization of poly (vinyl alcohol)/chitosan/graphene oxide biocomposite nanofibers," *Journal of Industrial and Engineering Chemistry*, vol. 20, pp. 4415-4420, 2014.
- [124] A. R. Hernández, O. C. Contreras, J. C. Acevedo, and L. G. N. Moreno, "Poly (ϵ -caprolactone) degradation under acidic and alkaline conditions," *Am. J. Polym. Sci*, vol. 3, p. 70, 2013.
- [125] A. Haryńska, J. Kucinska-Lipka, A. Sulowska, I. Gubanska, M. Kostrzewa, and H. Janik, "Medical-Grade PCL Based Polyurethane System for FDM 3D Printing—Characterization and Fabrication," *Materials*, vol. 12, p. 887, 2019.
- [126] Y. Wang, Z. Iqbal, and S. Mitra, "Rapidly functionalized, water-dispersed carbon nanotubes at high concentration," *Journal of the American Chemical Society*, vol. 128, pp. 95-99, 2006.
- [127] M. J. Kim, J. Lee, D. Jung, and S. E. Shim, "Electrospun poly (vinyl alcohol) nanofibers incorporating PEGylated multi-wall carbon nanotube," *Synthetic Metals*, vol. 160, pp. 1410-1414, 2010.
- [128] F. F. Garrudo, C. A. Chapman, P. R. Hoffman, R. W. Udangawa, J. C. Silva, P. E. Mikael, *et al.*, "Polyaniline-polycaprolactone blended nanofibers for neural cell culture," *European Polymer Journal*, vol. 117, pp. 28-37, 2019.

- [129] B. Lubentsov, O. Timofeeva, S. Saratovskikh, V. Krinichnyi, A. Pelekh, V. Dmitrenko, *et al.*, "The study of conducting polymer interaction with gaseous substances IV. The water content influence on polyaniline crystal structure and conductivity," *Synthetic Metals*, vol. 47, pp. 187-192, 1992.
- [130] P. S. d. Freitas, "Síntese da polianilina em escala piloto e seu processamento," 2000.
- [131] E. Scherr, A. MacDiarmid, S. Manohar, J. Masters, Y. Sun, X. Tang, *et al.*, "Polyaniline: oriented films and fibers," *Synthetic Metals*, vol. 41, pp. 735-738, 1991.
- [132] B. Massoumi, M. Ramezani, M. Jaymand, and M. Ahmadinejad, "Multi-walled carbon nanotubes-g-[poly (ethylene glycol)-b-poly (ϵ -caprolactone)]: synthesis, characterization, and properties," *Journal of Polymer Research*, vol. 22, p. 214, 2015.
- [133] S. Maity and A. Chatterjee, "Preparation and characterization of electro-conductive rotor yarn by in situ chemical polymerization of pyrrole," *Fibers and Polymers*, vol. 14, pp. 1407-1413, 2013.
- [134] H. Higashimura, K. Fujisawa, S. Namekawa, M. Kubota, A. Shiga, Y. Morooka, *et al.*, "Coupling selectivity in the radical-controlled oxidative polymerization of 4-phenoxyphenol catalyzed by (1, 4, 7-triisopropyl-1, 4, 7-triazacyclononane) copper (II) complex," *Journal of Polymer Science Part A: Polymer Chemistry*, vol. 38, pp. 4792-4804, 2000.
- [135] S. Fedorova and J. Stejskal, "Surface and precipitation polymerization of aniline," *Langmuir*, vol. 18, pp. 5630-5632, 2002.
- [136] G. Odian, "Principles of Polymerization, John Wiley & Sons," *Inc.: Hoboken, NJ*, 2004.
- [137] N. Y. Abu-Thabit, "Chemical oxidative polymerization of polyaniline: A practical approach for preparation of smart conductive textiles," *Journal of Chemical Education*, vol. 93, pp. 1606-1611, 2016.
- [138] H. Bai, L. Zhao, C. Lu, C. Li, and G. Shi, "Composite nanofibers of conducting polymers and hydrophobic insulating polymers: preparation and sensing applications," *Polymer*, vol. 50, pp. 3292-3301, 2009.
- [139] H.-D. Zhang, C.-C. Tang, Y.-Z. Long, J.-C. Zhang, R. Huang, J.-J. Li, *et al.*, "High-sensitivity gas sensors based on arranged polyaniline/PMMA composite fibers," *Sensors and Actuators A: Physical*, vol. 219, pp. 123-127, 2014.
- [140] J. Hong, Z. Pan, M. Yao, and X. Zhang, "Preparation and properties of continuously produced conductive UHMWPE/PANI composite yarns based on in-situ polymerization," *Synthetic Metals*, vol. 193, pp. 117-124, 2014.

- [141] A. R. Hernández, O. C. Contreras, J. C. Acevedo, and L. Moreno, "Poly (ϵ -caprolactone) degradation under acidic and alkaline conditions," *Am. J. Polym. Sci.*, vol. 3, p. 70, 2013.
- [142] M. A. C. Mazzeu, L. K. Faria, A. d. M. Cardoso, A. M. Gama, M. R. Baldan, and E. S. Gonçalves, "Structural and morphological characteristics of polyaniline synthesized in pilot scale," *Journal of Aerospace Technology and Management*, vol. 9, pp. 39-47, 2017.
- [143] W. Łużny and K. Piwowarczyk, "Hydrogen bonds in camphorsulfonic acid doped polyaniline," *Polimery*, vol. 56, pp. 652-656, 2011.
- [144] L. Yue, Y. Xie, Y. Zheng, W. He, S. Guo, Y. Sun, *et al.*, "Sulfonated bacterial cellulose/polyaniline composite membrane for use as gel polymer electrolyte," *Composites Science and Technology*, vol. 145, pp. 122-131, 2017.
- [145] F. Lefebvre, C. David, and C. Vander Wauven, "Biodegradation of polycaprolactone by micro-organisms from an industrial compost of household refuse," *Polymer degradation and stability*, vol. 45, pp. 347-353, 1994.
- [146] L. Huang, J. Hu, L. Lang, X. Wang, P. Zhang, X. Jing, *et al.*, "Synthesis and characterization of electroactive and biodegradable ABA block copolymer of polylactide and aniline pentamer," *Biomaterials*, vol. 28, pp. 1741-1751, 2007.
- [147] T. H. Qazi, R. Rai, and A. R. Boccaccini, "Tissue engineering of electrically responsive tissues using polyaniline based polymers: A review," *Biomaterials*, vol. 35, pp. 9068-9086, 2014.
- [148] S. Agarwal, J. H. Wendorff, and A. Greiner, "Progress in the field of electrospinning for tissue engineering applications," *Advanced Materials*, vol. 21, pp. 3343-3351, 2009.

Appendix A: Arduino code linked with cap sense library

```
#include <CapacitiveSensor.h>

/*
 * CapitiveSense Library Demo Sketch
 * Paul Badger 2008
 * Uses a high value resistor e.g. 10M between send pin and receive pin
 * Resistor effects sensitivity, experiment with values, 50K - 50M. Larger
 * Receive pin is the sensor pin - try different amounts of foil/metal on this pin
 */
int trigger=0;//define the trigger control to the led
int capvalue=400;
int preVar = 0;
int curVar = 0;
CapacitiveSensor cs_2_6 = CapacitiveSensor(2,7);

void setup()
{
  //cs_2_3.set_CS_Autocal_Millis(0xFFFFFFFF);
  // turn off autocalibrate on channel 1 - just as an example

  Serial.begin(9600);
  pinMode(13, OUTPUT);
}

void loop()

{
  // long start = millis();
  long totall = cs_2_6.capacitiveSensor(30); // right up
  |
  curVar = totall;

  //
  if (curVar - preVar >= capvalue){
    if(trigger == 0){
      digitalWrite(13, HIGH);//turning the light on
      trigger = 1;
      Serial.println("Turning The Light ON");
    }else if (trigger == 1){
      digitalWrite(13, LOW);//turning the light on
      trigger = 0;
      Serial.println("Turning The Light OFF");
    }
  }
  int sensorValue = analogRead(A0);
  float voltage= sensorValue*(5000 / 1023.0);
  Serial.print(voltage);
  Serial.print(",");
  //Serial.println(totall+4500);
  Serial.println(totall);

  preVar = curVar;
  delay(200);
}
```

Appendix B: Publications on this study

- A. P. V. T. Weerasinghe, Nandula D. Wanasekara, Geetha Dissanayake, H.M.Ravindu T. Banadara, N.D.Tissera, R.N.Wijesena, K.M.N.de Silva, Anushanth Karalasingam "All Organic, Conductive Nanofibrous Twisted Yarns," *2019 IEEE 14th International Conference on Nano/Micro Engineered and Molecular Systems (NEMS)*, Bangkok, Thailand, 2019, pp. 308-311.
- B. S. B. Y. Abeywardena, S. Perera, P. V. T. Weerasinghe, K. M. N. D. Silva, S. Walpalage, M. C. W. Somaratne, N. M. Hettiarachchi, and S. Jeyasakthy, "Shape memory clay flaps assisted body cooling fabrics," *IOP Conference Series: Materials Science and Engineering*, vol. 459, p. 012027, Jul. 2018
- C. P. V. Thilini Weerasinghe, Nandula D. Wanasekara, D.G. Kanchana Dissanayake, W. Pamoda Thavish D. Perera, Nadeeka Tissera, Ruchira N. Wijesena "All-organic, conductive and biodegradable yarns from coreshell nanofibers through electrospinning" *ACS Macro letters*.(under review)